Periodical Part, Report, Published Version

Bülow, Katharina; Ganske, Anette; Heinrich, Hartmut; Hüttl-Kabus, Sabine; Klein, Birgit; Klein, Holger; Möller, Jens; Rosenhagen, Gudrun; Schade, Nils; Tinz, Birger

Comparing meteorological fields of the ENSEMBLES regional climate models with ERA-40-data over the North Sea

KLIWAS Schriftenreihe

KLIWAS
Klima . Wasser . Schifffahrt

KLIWAS Schriftenreihe
KLIWAS-21/2013

Comparing meteorological fields of the ENSEMBLES regional climate models with ERA-40-data over the North Sea

Koblenz, im Oktober 2013

BUNDESAMT FÜR SEESCHIFFFAHRT UND HYDROGRAPHIE

DWD


KLIWAS

KLIWAS Schriftenreihe KLIWAS-21/2013

Comparing meteorological fields of the ENSEMBLES regional climate models with ERA-40-data over the North Sea

KLIWAS-Sea Author Team:

Katharina Bülow
Anette Ganske
Hartmut Heinrich
Sabine Hüttl-Kabus
Birgit Klein
Holger Klein
Jens Möller
Gudrun Rosenhagen
Nils Schade
Birger Tinz

DOI:
10.5675/Kliwas_21.2013_ERA40data

Page Chapter

Contents

Page Table

List of tables

Page Figure

List of figures

Summary

The KLIWAS Project 1.03 analysed atmospheric near sea surface fields over the North Sea originating from the EU ENSEMBLES hindcast simulations forced with ERA-40 data. Since these atmospheric fields are used as boundary conditions for ocean models, these atmospheric parameters have great impact on the ocean state. Since these regional models are also used to predict the future oceanographic status of the North Sea, e.g. the water temperature and circulation patterns, it is therefore important to assess their bandwidths and possible impacts on the development of appropriate practical adaptation measures.

This report presents the results of a comprehensive assessment of a variety of relevant atmospheric parameters in comparison to the ERA-40 reanalysis data. A comparison against in-situ observations was not possible because of insufficient homogeneity of the long-term observational datasets of the North Sea.
Seven meteorological parameters from 12 regional models were investigated, such as sea level pressure, wind speed and direction, air temperature, global radiation, cloud cover and precipitation. The comparisons were restricted to grid points at sea using the land-sea masks provided by the data base. For the whole North Sea climatological means and their standard deviations have been computed and plotted for the period 1971-2000 as well as the differences between model results and ERA-40 for the annual mean, January and July. Frequency distributions have been constructed as well. For the latter two purposes the North Sea was divided into four subregions.

Sea level pressure: The deviations between the pressure fields of the regional climate models and ERA-40 show a variety of different patterns. The annual cycles for the four North Sea subregions demonstrate good agreement of the ENSEMBLES RCMs with ERA-40 and, the ensemble mean reflects the ERA-40 picture very well. Only one RCM shows a permanent positive bias. The regional climate models thus follow to a great extent their driving model ERA-40.

Wind speed: The differences between the monthly mean wind speed of ERA-40 and the RCMs show no systematic behaviour. There are no differences in the seasonal cycle and, there are positive as well as negative deviations. All of the selected RCMs agreed with ERA-40 considering the huge inherent variability of ERA-40 wind fields over the North Sea.

Wind direction: For all subregions in all wind speed and wind direction classes the frequencies of RCM wind directions differ from those of ERA-40. However, the largest deviations of the wind direction frequencies of all RCMs from those of ERA-40 are smaller than 7.6 %. Most RCMs agree with ERA-40 in southwest being the prevailing and northeast the least frequent wind direction.

Air temperature: Differences in temperature between all RCMs and ERA-40 are relatively small over the North Sea. For the annual means as well as for January and July nearly all regional models show a smaller variability than ERA-40. The RCMs are consistently warmer than ERA-40 in winter but colder in July. The fact that, along the coasts nearly all RCMs are warmer in winter and colder in summer than ERA-40 possibly depends on a continental influence onto the coastal grid points. Since comparisons with in-situ observations show similar results, it can be assumed, that the regional models are closer to the reality, mainly because of their higher spatial resolution.

Global radiation: All models show an increase of global radiation from north to south for the North Sea area. However, there are big differences in the gradients and the absolute range. Temporal variability at each grid point is much larger in the RCMs than in ERA-40. The RCMs can basically be divided into two groups, those which overestimate the annual cycle of global radiation and those that underestimate it. All models share the tendency for growing differences to ERA-40 during the summer maximum, i.e. those which overestimate simulate a stronger seasonal cycle and those which underestimate a weaker seasonal cycle.

Cloud cover: All RCMs simulate similar spatial patterns in cloud cover over the North Sea with an NW/SE oriented decrease but the differences to the ERA-40 cloud cover vary strongly between the models. Basically the same separation of the RCMs as in the simulation of global radiation exists for cloud cover. Models in which overestimation of global radiation was detected underestimate cloud cover; however, there are some exemptions. The annual cycles in the RCM vary in time and amplitude compared to ERA-40. The long-term standard deviations of the majority of the RCMs are larger than that of ERA-40.

Precipitation: In the RCMs precipitation shows a similar pattern as ERA-40. During the entire year the RCMs simulate much more precipitation than ERA-40. The standard deviations of the RCM for the annual mean show higher variability than ERA-40, while in summer the variability is higher than that of ERA-40 and lower in winter. Therefore, the annual cycle is more pronounced in ERA-40 than in the RCMs.

Some general conclusions can be drawn from the analyses: A higher resolving grid is favourable close to the coasts. Distant from the coasts on the open sea there is hardly a difference to models with a lower spatial resolution.

1 Motivation

Shipping and other economic uses of the oceans, protection of the coasts and coastal infrastructures as well as biogeochemical processes in the ocean are vulnerable to climate change. In order to provide the basic physical parameters that are relevant for the development of adaptation measures for the North and the Baltic Sea, the possible evolution of the future oceanographic and meteorological status of these two seas needs to be known.

Global climate models that were used in the Fourth Assessment Report of the Intergovernmental Panel on Climate Change (Solomon et al. 2007) had rather coarse spatial resolution and were thus not ideally suited to identify climate change signals in regional seas like the North and the Baltic Sea. Therefore, dynamical downscaling of climate model output is required to incorporate physical processes important on regional and local scale and to obtain high resolution output.

The European ENSEMBLES project (van den Linden and Mitchel 2009) carried out a comprehensive downscaling exercise for the European region using 15 different regional atmospheric models from different research institutions. However, the primary target of ENSEMBLES was the atmosphere over land areas and not over the adjacent seas and oceans. In addition, most validation studies have focused on land areas only (e.g. Déqué 2011, Jacob 2007, Nikulin 2010, Räisänen 2012). Therefore, the KLIWAS research programme of the German Federal Ministry of Transport, Building and Urban Development (BMVBS) within its marine work packages 1.03[1] and 2.01[2] has investigated the spread of ENSEMBLES climate projections in the North Sea area (read more at www.kliwas.de).

Within KLIWAS as a first step the atmospheric fields close to the sea surface from the ENSEMBLES hindcast simulations forced with ERA-40 data were validated. Since these atmospheric fields are used as boundary conditions for ocean models, these atmospheric parameters have great impacts on the ocean model results and their bandwidth of future prediction of the possible oceanographic status of the North Sea, e.g. on the water temperature and circulation patterns and, subsequently on the development of appropriate practical adaptation measures.

This report presents the results of a comprehensive assessment of a variety of relevant atmospheric parameters in comparison to the ERA-40 reanalysis that is used as forc-

[1] WP 1.03: Atmospheric and Oceanic Reference Data and Climate Projections for Coastal and Open Sea Areas

[2] WP 2.01: Climate Change Scenarios for the Maritime Area and their Parametrisation

ing for the ENSEMBLES modelling exercise. A comparison against observations was rejected because of the lack of a homogeneous observational dataset of the North Sea.

2 Data and Methods

Regional ocean models require data as forcing inputs both at their boundaries to the atmosphere and at their geographical boundaries. These so-called boundary conditions for the lateral ocean boundaries are provided by a global ocean model and, for the interface with the atmosphere by the output of a down-scaled atmospheric model. The atmospheric forcing plays a crucial role for the resulting oceanic circulation pattern, since the oceanic circulation of shelf seas like the North Sea and the Baltic Sea is mainly wind-driven.

2.1 ENSEMBLES Regional Climate Models for the North Sea

The aim of the ENSEMBLES climate change project, initiated by the European Commission is to run multiple regional climate models (van der Linden and Mitchell 2009).

For the following analysis the ENSEMBLES data set is used. The official ENSEMBLES data base at http://www.ensembles-eu.org/ has been updated occasionally and in this analysis data from the latest updates have been used (see Table 1). One exception is the DMI dataset for 10 m wind, which we obtained directly from DMI (Ole Bossing Christensen, pers. communication). For a fair comparison only datasets that were interpolated on the common ENSEMBLES spatial grid were used.

Table 1: The calendar dates of the downloads from the ENSEMBLES database (http://www.ensembles-eu.org/)

Model	Air temperature	Sea level pressure	10 m wind	Global radiation	Cloud cover	Precipitation
C4I	17.09.2009	17.09.2009	15.10.2009	15.10.2009	15.10.2009	15.10.2009
CNRM	17.09.2009	17.09.2009	17.09.2009	17.09.2009	17.09.2009	17.09.2009
DMI	18.09.2009	18.09.2009	01.10.2010	18.09.2009	18.09.2009	18.09.2009
ETHZ	20.10.2009	30.09.2009	30.09.2009	20.10.2009	30.09.2009	30.09.2009
HC3Q0	30.09.2009	30.09.2009	30.09.2009	30.09.2009	30.09.2009	30.09.2009
HC3Q3	21.10.2009	01.10.2009	01.10.2009	01.10.2009	01.10.2009	01.10.2009
HC3Q16	01.10.2009	01.10.2009	01.10.2009	01.10.2009	01.10.2009	01.10.2009
ICTP	01.10.2009	01.10.2009	01.10.2009	01.10.2009	No data	01.10.2009
KNMI	01.10.2009	01.10.2009	01.10.2009	01.10.2009	01.10.2009	01.10.2009
METNO	01.10.2009	01.10.2009	01.10.2009	01.10.2009	01.10.2009	01.10.2009
MPI	02.10.2009	02.10.2009	02.10.2009	02.10.2009	02.10.2009	02.10.2009
SMHI	30.06.2010	29.06.2010	01.07.2010	29.06.2010	30.06.2010	29.06.2010

The analysis focuses on the following parameters, which are commonly used to calculate the boundary conditions of oceanic climate models: sea level pressure, wind speed and direction, air temperature, global radiation, cloud cover and precipitation. All the data are daily means/sums, except for the wind data of DMI, which has a resolution of one hour.

For the comparison of the regional climate models the 30 year period 1971-2000 is used in this study. All models are driven with boundary conditions of the reanalysis ERA-40 (see section 2.2). The data of the different models were interpolated on a common grid with a horizontal resolution of 25 km x 25 km (see Fig. 1).

2.2 ERA-40 Reanalysis

Global reanalysis are often used for climatological studies and for the validation of global and regional climate models. Another application is nesting regional climate models in reanalysis.

Reanalysis is a scientific method for developing a comprehensive record of the state of the atmosphere (or the ocean; see http://reanalyses.org) using assimilation of data into models. This is chosen because of the lack of homogeneous observational data base spanning an extended historical period with the required spatial resolution. Available observations for the atmosphere come from different sources, e.g. classical land based observatories, voluntary observing ships, buoys, radiosondes, aircraft observations and satellites are used as input of an assimilation scheme of a numerical weather prediction model (NWP). The reprocessing for a long time period of several decades results in a three-dimensional globally gridded meteorological dataset for the atmosphere, a tool ideally qualified for subsequent climatological studies.

The ERA-40 reanalysis is developed by the European Centre for Medium-Range Weather Forecasts (ECMWF); see Uppala et al. (2005). It uses a “frozen” version of the Integrated Forecasting System (IFS). ERA-40 covers the 45 year period from September 1957 to August 2002. The model data has a horizontal resolution of 1.125° (T159, about 125 km) and 60 vertical levels. http://www.ecmwf.int/research/era/do/get/era-40). Data is available six-hourly, i.e. for the following hours: 00, 06, 12 and 18 UTC. Conventional observations used for the assimilation come from different sources; an overview is given in Uppala et al. (2005). Satellite data are assimilated since 1972; cloud motion winds are included since 1979.

The quality of ERA-40 data is evaluated by ECMWF (http://www.ecmwf.int/research/era/ERA-40/Performance/index.html). A significant improvement in comparison with the former ERA15 reanalysis is found, but some deficiencies e.g. in radiation or water cycle (Bengtsson et al. 2004) still occur.

2.3 Methods of Data Processing

In this report the output of the ENSEMBLES regional climate models (RCMs) hindcasts using ERA-40 boundary conditions is compared to the original ERA-40 fields for the meteorological parameters listed in section 2.1. All comparisons are restricted to grid points at sea using the land-sea masks provided by the data base. In order to compare the data sets climatological means and standard deviations have been computed for the commonly used base period from 1971-2000 (Arguez and Vose 2011).

Three different types of analysis will be presented:

- Spatial maps for the whole North Sea region,
- Annual cycles in four subregions
- Frequency distributions in these subregions.

The following evaluations were done for the whole North Sea region:

1a) Model means (1971-2000), plots for annual, January and July values.

1b) Plots of mean differences between RCMs and ERA-40 fields, annual, January, and July values. RCM fields are interpolated to the coarser ERA-40 grid, differences are calculated for each ERA-40 grid point over sea.

For the analysis of annual cycles and frequency distributions the North Sea is divided into four subregions (see Fig. 1). The division into these areas was carried out with regard to comparability of the climate and the ratios of open sea-to-coastal areas and a comparable number of data points in each subregion. For each subregion of the North Sea the following three properties were calculated:

2a) Annual cycles of monthly means and corresponding standard deviations. For the calculations of the annual cycles first spatial means for all grid points in each subregion were evaluated, afterwards monthly means and standard deviations.

2b) Differences of annual cycles of mean monthly RCM and ERA-40 data.

3) Frequency distributions, concatenated over all time steps and all grid points in each subregion.

Details of the results for each parameter will be given in the next chapters.

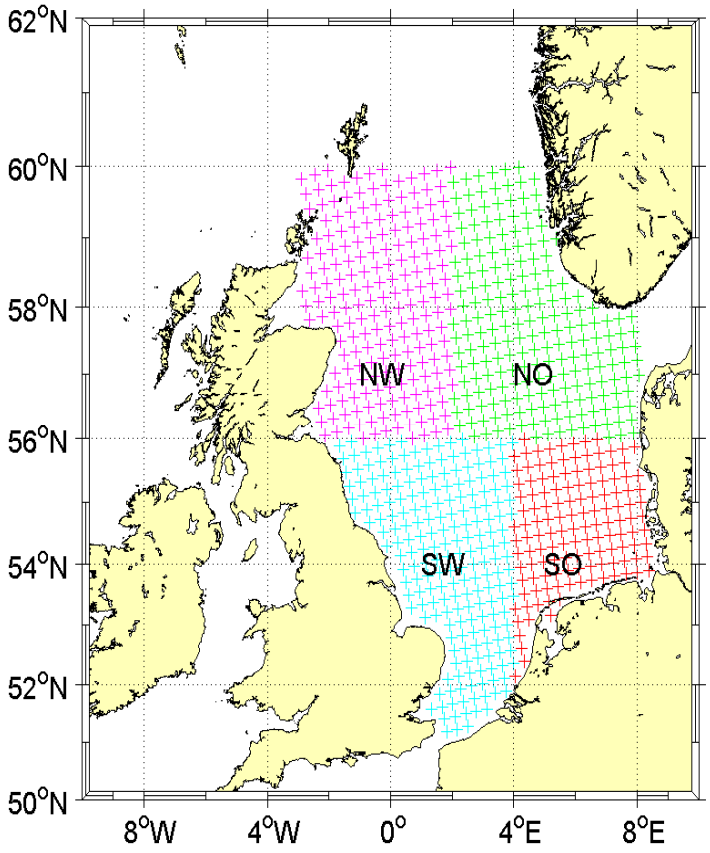

Figure 1: Location of data points in the four subregions of the North Sea: common ENSEMBLE-grid northwest (NW), northeast (NE), southwest (SW), southeast (SE)

3 Comparison of ENSEMBLES Regional Climate Models results to ERA-40 reanalysis data

3.1 Overview

Seven meteorological parameters, such as sea level pressure, wind speed and direction, air temperature, global radiation, cloud cover and precipitation of 12 regional models are compared to ERA-40 data. We investigate only meteorological elements with the scheme described in chapter 2.3. All mini pictures show absolute values and anomalies over the 30 years time period 1971-2000. Starting with the most prominent parameter “sea level pressure”, we point out the similarities and differences between each of the different RCMs and between the RCMs and ERA-40.

3.2 Sea Level Pressure

Air pressure is a basic atmospheric parameter. As the air pressure decreases with increasing altitude, reduced data to sea level height - the sea level pressure (SLP) - is commonly used in meteorology. Sea level pressure varies widely on Earth, and these changes are of utmost importance in studying weather and climate. Changes in sea level pressure can cause subsequent changes in other parameters, e.g. atmospheric circulation and sea level. Thus, influences on the pressure fields by the regionalization models compared to ERA-40 values are of utmost interest.

Fig. 3.2.1 shows the annual mean values of sea level pressure of the ERA-40 reanalysis and the ENSEMBLES RCMs for the period 1971-2000. A clear zonal structure can be seen in all model results with higher values in the SSE and lower values in the NNW. The deviations between the pressure fields of the regional climate models and the mother model (ERA-40) show a variety of different patterns. They can be classified into two characteristic types (see Fig. 3.2.2): Those with a nearly constant offset (positive and negative) and others with dominating differences in the pressure gradient field.

In winter (see Fig. 3.2.3, January), the zonal gradient is most pronounced and the curvature of the isobars prevailingly cyclonic. In summer (see Figs. 3.2.5 and 3.2.6, July) the pressure is higher than in winter and more evenly distributed. The isobars show anticyclonic curvatures. As in winter there are still considerable differences between the model fields.

Figs. 3.2.7, 3.2.9 and 3.2.11 display the fields of the standard deviations of the sea level pressure: An increased variability over the northern parts of the North Sea is

typical in winter (January), whereas the variability is significantly lower in summer (July).

The ratio between the standard deviation of the RCMs and ERA-40 are mapped in Figs. 3.2.8 (annual mean), 3.2.10 (January) and 3.2.12 (July). There are pronounced differences between the three distributions, with more extreme values (positive and negative) found in July.

The annual cycles for the four North Sea subregions demonstrate good agreement of the ENSEMBLES RCMs with ERA-40 and, the ensemble mean reflects the ERA-40 course very well. Only one RCM shows a permanent positive bias (see Figs. 3.2.13 and 3.2.14). This bias is also evident in the frequency distributions (see Fig. 3.2.15).

Despite the differences in sea level pressure between the RCMs and ERA-40, spatially as well as in the sign of difference, overall good agreement is apparent. The regional climate models thus follow to a great extent their driving model ERA-40.

Similar results were shown for Continental Europe investigating the influence of different global models as boundary conditions for RCMs (Kjellström et al. 2011).

3.3 Wind Speed

Wind results from horizontal differences in air pressure. It is primarily affected by the pressure gradient. If the pressure gradient is sharp the wind speed is high. The influences of other factors like the Coriolis force, the centrifugal force and the friction have altogether smaller impact on the wind speed. The friction of the sea surface differs in comparison to land surfaces in two respects: friction is mostly smaller over sea and it is variable in time, depending on the changing state of the sea. For marine areas, it is the most important meteorological parameter as wind generates waves and drives the currents. At the coasts, it causes of one of the most dangerous natural hazard, the storm surge. The World Meteorological Organization (WMO) recommends that wind measurements should commonly be performed at 10 m height above ground to avoid inhomogeneities in the data sets due to the increase of wind speed with height in the lower atmosphere. 10 m-wind speed is one of the output parameters from the RCMs.

In Fig. 3.3.1, the long-term means of the 10 m-wind speed in the North Sea area are displayed for the ERA-40 reanalysis and the ENSEMBLES RCMs for the period 1971-2000. While the ERA-40 wind fields show a significant decrease from north to south this is much less pronounced in some of the RCMs results (5 out of the 12 wind fields).

Only two of the RCMs (MPI-REMO and ETHZ-CLM) show similar west/east wind speed gradients to ERA-40 with lower wind speeds in the east. All RCMs agree with ERA-40 in an increase of wind speed from the coasts towards the open sea. Because

of the higher grid resolutions of the RCMs compared to ERA-40, it should be expected that a lee effect is smoothed out in the ERA-40 fields. Coastal waters have therefore been excluded from the following calculation of differences in wind fields.

Five of the RCMs produce yearly means of wind speed which differ less than ±0.5 m/s from ERA-40 wind speeds in the entire North Sea area (see Fig. 3.3.2). Seven of the RCMs give results that deviate at most ± 1.5 m/s from ERA-40 means. Except from the above mentioned coastal grid points the wind fields of six RCMs show smaller wind speeds in the whole North Sea area compared to those of ERA-40. These RCMs also produce less frequently wind above than 10 m/s, as frequency distributions in Fig. 3.3.15 indicate. Only one model (DMI-HIRLAM) produces higher mean wind speeds than ERA-40 over the whole North Sea area. Its frequency distribution shows wind speeds above10 m/s more often than the distribution of ERA-40. For this single model, spatial and monthly means of wind speed are also higher than those of ERA-40 for all four North Sea regions during the entire year and (see Figs. 3.3.13 and 3.3.14).

The spatial structures of the January wind fields are identical to the annual means for both ERA-40 and RCM data; compare Fig. 3.3.1 and Fig. 3.3.3. Mean winds are approximately 2 m/s higher in January than on annual average. The deviations between individual RCMs and ERA-40 wind field are in the same range for the yearly means and for the monthly means of January, compare Fig. 3.3.2 and Fig. 3.3.4. For the January mean, seven RCMs have smaller wind speeds than ERA-40 over the entire North Sea area. There are two RCMs (ETHZ-CLM and DMI-HIRAM) with higher wind speeds than ERA-40 in most of the North Sea region.

Monthly means of wind speed in July calculated from ERA-40 or the 12 RCMs show increased wind speed in the eastern part of the North Sea compared to the central areas (see Fig. 3.3.5). For July, only one RCM has smaller mean wind speeds over most parts of the North Sea area and again DMI-HIRHAM is the only RCM with higher means than ERA-40 in the entire North Sea area (see Fig. 3.3.6).

As shown in Fig. 3.3.7, the variability of the wind speed both from RCMs and ERA-40 for the period 1970 – 2000 decreases from north to south. Standard deviations of only one RCM (ETHZ-CLM) are larger in the entire North Sea region than those of ERA-40 (see Fig. 3.3.8). As expected for a winter month, standard deviations in January are larger (for both ERA-40 and all RCMs) than on annual average (see Fig. 3.3.9) whereas they are smaller in summer (see Fig. 3.3.11). In July, the variability of the RCM wind fields is for most parts of the North Sea larger than that of ERA-40, see Fig. 3.3.12.

Higher areal and monthly means of wind speeds than ERA-40 during the entire year can be found in the results of DMI-HIRHAM in all four areas, ETHZ-CLM in both eastern areas, MPI-REMO in the northeastern and ICTP-REGCM in the northeastern and southwestern areas (see Fig. 3.3.13).

The differences between the monthly mean wind speed of ERA-40 and the RCMs show no systematic behaviour (see Fig. 3.3.14): There is no seasonal cycle in the differences and there are positive as well as negative deviations.

However, the comparisons with ERA-40 do not provide the conclusion that wind fields of one specific RCM give more realistic results than others. One reason is the reliability of the ERA-40 wind fields over the North Sea. This is due to the fact that validations of wind speed over sea are difficult because of the lack of suitable observational data. One reason for that is the spatially varying friction, therefore it is problematic to compare the point measurements from the observations with the spatial averages provided by models (e.g. ERA-40 grid 1.125° x 1.125°). Wind fields derived from satellite data reflect the spatial pattern of observed wind fields quite well. However, they are not available for a period long enough to calculate reliable climatological averages. Nevertheless, the 10 year mean of wind speeds over the North Sea, calculated from QuikScat data show very similar structures and velocities compared to ERA-40 fields (see Fig. 3 in Badger et al. 2010). Comparisons of wind speeds from satellite observations and in situ data for short periods of one year (Winterfeldt et al. 2010) show that root-mean-square errors of satellite data compared to buoy measurements are roughly in the range of 1.5 m/s - 2.36 m/s, depending on the satellite product. The differences between ERA-40 and RCM wind fields are in the same range, which means that the results are in the same range as the uncertainties the of the observed wind fields.

3.4 Wind Direction

Since wind is a vector, properties of its directions has also to be considered in terms of impact on the ocean state. Wind direction is the direction from which wind is blowing, contrary to ocean currents. It is reported in the normal geographical coordinate system, e.g. south wind reported as 180°. As described in chapter 3.3, wind is caused by pressure differences. The wind blows roughly parallel to the isobars, surrounding high pressure systems clockwise and low pressure systems counter clockwise on the northern hemisphere. However, it is directed away from the high and towards the low pressure region with an angle that depends on the roughness of the underlying surface.

30 year means of the wind direction were evaluated from the means of wind components of the model output (Fig. 3.4.1). Due to the lower mean pressure being centred in the northwestern part of the North Sea area (see Fig. 3.2.1), southwestern winds prevail in this region. This can roughly be found in the wind fields of all models (Fig. 3.4.1). However, some of the ENSEMBLES regional models deviate distinctly from the mean wind direction of ERA-40, as the prevailing wind direction in these models is west instead of southwest.

Frequency distributions of daily mean wind directions were calculated with ERA-40 and RCM data for the four areas of the North Sea and the period 1971-2000. For all grid points in each of the four North Sea subregions, the data of wind speed and direction were separated into five classes for wind speed and eight for wind direction. Wind speed classes have a width of 4 m/s, the last class includes all wind speeds above 16 m/s. Wind direction classes cover an angle of 45°. They are centred at the values 0°, 45°, 90°, … 315°.

A comparison of wind roses from ERA-40 data (orange) and the 12 RCMs (blue) for the four subregions of the North Sea area is shown in Figs. 3.4.2 – 3.4.5. The lengths of the spokes of the wind roses are proportional to the frequencies of the wind direction and their widths broaden with increasing wind speed class.

For all subregions, the frequencies of wind directions of RCMs in all wind speed and wind direction classes differ from those of ERA-40. Largest deviations of the wind direction frequencies of all RCMs from those of ERA-40 are smaller than 7.6 %.

In the northwestern subregion for the ERA-40 and eight of the RCM wind fields, southwest is the most frequent wind direction (Fig. 3.4.2). This is in agreement with the mean wind direction in Fig. 3.4.1 and the mean pressure field in Fig. 3.2.1. In the wind fields of the other four models, west is the most frequent direction. East is the least frequent wind direction in most models.

In the northeastern subregion, ERA-40 winds preferably show southwesterly directions (Fig. 3.4.3). In five of the RCM, southwest is also the prevailing wind direction, in five RCM fields, it is west and in two fields south. Northeasterly winds are least likely in this area for 8 RCMs and ERA-40. For the resulting four RCMs wind directions, northeast and east are less frequent directions (about equally shared).

In the southwestern and the southeastern subregion, the most frequent wind direction in eight models and ERA-40 is southwest (Figs. 3.4.4 and 3.4.5), but west for the other four models. In this, there is special interest in winds with high speeds (storms) from westerly directions because they potentially can cause storm surges at the German coast (Müller-Navarra and Giese 1999, Befort et al. 2012). For northwesterly winds and high wind speeds (above 16 m/s) the frequencies of 10 RCMs are higher than those of ERA-40. The largest frequency among the results of all RCMs (0.52 %) is four times the value of ERA-40 (0.14 %). Storm surges occurring on both the Lower Saxony and the Schleswig-Holstein coasts can be induced by northwesterly storms, whereas storms from west and southwest only can lead to surges along the coast of Schleswig-Holstein. ERA-40 wind speeds above 16 m/s from west have a frequency of 0.35 %. In five of the RCMs these wind conditions are more frequent than in the ERA-40 results with a maximum frequency of 0.77 %. For storms from southwest, there are six RCMs with higher frequencies of occurrence. In this case, the maximum RCM frequency is 0.45 %, compared to 0.21 % for ERA-40. The evaluation of the RCM data suggests a higher risk of storm surges compared to ERA-40 data.

A comparison of wind direction measurements at the station FINO1, about 40 km north of the German island of Borkum, and satellite data for the time period 2005 – 2008 in Badger et al. (2010) shows a similar distribution of directions of both in-situ and satellite data compared to ERA-40 data in subregion southwest shown in Fig. 3.4.5. Larsén et al. (2009) compared wind directions from two offshore stations (FINO 1, Horns Rev) in the southeastern part of the North Sea with results from two REMO runs with two different grid resolutions (10 km and 50 km). For frequency distributions of wind directions both resolutions were in good agreement with the measured data.

3.5 Air Temperature

Off the coasts, the air temperature of the lower atmosphere is mainly determined by the temperature of the sea surface. For the North Sea, there is a significant influence of the two branches of the North Atlantic current entering the sea area through the English Channel and through the Fair Isle Channel between Scotland and the Shetland Islands. Additionally, the air temperatures are influenced by the adjacent European land masses and the geographical latitude. The air temperature at sea is of particular interest because it allows estimates of the stability of the temperature stratification in lower air levels, which can provide information about e.g. cloud formation and mixing processes. Air temperature has a pronounced vertical gradient, especially close to the ground.

In the analyses carried out here air temperatures refer to 2 m above the sea surface. The map of mean air temperatures of the ERA-40 reanalysis for the period of 1971-2000 over the North Sea shows a distinct zonal gradient with values of about 11 °C in the south and 7-8 °C in the north (Fig. 3.5.1). The maxima (about 12-13 °C) are located within the southwest region, connected with the inflow of warm North Atlantic Current water through the English Channel eastward into the North Sea.

Temperatures in the ENSEMBLES regional models show a similar pattern, with higher values in the south western parts, and lower values north of the British Islands (Fig. 3.5.2). Differences between all RCM and ERA-40 temperatures over the North Sea are relatively small (about 1 K), with an increasing tendency near the coast in the winter months (up to 4 K; Fig. 3.5.4, January). This feature can be seen in all RCMs and is probably due to better spatial resolution of the ENSEMBLE regional models. The spatial resolution of the RCMs is five times higher than that of the ERA-40 reanalysis and thus, RCMs resolve the coastline much better, whereas the coarser ERA-40 grid fields extends the land/sea gradient further towards the sea in mixed land/sea grid boxes. There is a significant difference in the RCM behaviour compared to ERA-40 between winter and summer: The RCMs are in winter consistently warmer than ERA-40 (Fig. 3.5.4), but colder in July (Fig. 3.5.6).

All regional models show for the annual means a smaller variability than ERA-40 (Fig. 3.5.7 and 3.5.8). This is also the case for 9 models in January and for 10 models in July (Figs. 3.5.9 and 3.5.11).

The annual cycles of all models for the subregions are presented in Fig. 3.5.13. The differences between the mean monthly temperatures of the RCMs and of ERA-40 are presented in Fig. 3.5.14. Nearly all RCMs are warmer than ERA-40 in winter and colder in summer. An influence from the land in the coastal ERA-40 grid points is apparent, too. Since comparisons of in-situ observations with ERA-40 (SCHADE et al. 2013) show similar results near the coasts, it can be assumed, that the regional models are closer to the reality, mainly because of the increased spatial resolution.

These findings are supported by the frequency distributions, displayed in Fig. 3.5.15. Here, clearly can be seen, that ERA-40 shows for temperatures lower than 5 °C a higher frequency than the RCM. Between 5 °C and 12 °C in the RCM more often higher temperatures occur than in ERA-40. Above 12 °C the ERA-40 distribution represents the average of the RCM with a warmer tendency towards the warm tail. As a consequence, the ERA-40 distribution is wider than those of the RCM.

3.6 Global Radiation

The downward short wave radiation at the sea surface has an important effect on the thermal structure and the dynamics of the ocean and thus, on the climate system of the Earth. This is because more than 90 % of the solar radiation irradiance that arrives at the sea surface is absorbed by the ocean. The knowledge of the radiation budget and its components at the sea surface is important for the evaluation of the sea surface temperature and, subsequently the temperature driven ocean currents influencing the heat exchange between ocean and atmosphere. On the other hand the radiation budget at sea steers the growth of phytoplankton and other organisms in the water column. The total of direct solar radiation and diffuse sky radiation received by a unit horizontal surface is called global radiation.

According to the varying annual sunshine duration and the solar altitude, all models show for the North Sea area an increase of global radiation from north to south (Fig. 3.6.1). However, there are big differences in the gradients and the absolute amounts. Nevertheless, the maps of global radiation exhibit the expected pronounced seasonal cycle in all RCMs as does the ERA-40 reanalysis data set, which is illustrated with the fields for January and July in Figs. 3.6.3 to 3.6.6. Temporal variability at each grid point is much larger in the RCMs than in ERA-40 (Figs. 3.6.10 und 3.6.12). Variations of the mean monthly values are mostly due to temporal variations in the 30 year averaging period and to a lesser extend from spatial variations in the subregions. ERA-40 data show similar annual cycles in all four North Sea boxes with average minimum values of 20 W/m^2 in December/January and maximum values of

220 W/m^2 in June (Fig. 3.6.13). The RCM can basically be divided into two groups (Fig. 3.6.14), those which overestimate the annual cycle of global radiation and those that underestimate it. All models share the tendency for growing differences to ERA-40 during the summer maximum, i.e. those who over estimate simulate a stronger seasonal cycle and those who under estimate a weaker seasonal cycle (Fig. 3.6.14). Maximum differences in summer time range from -60 W/m^2 to +40 W/m^2.

Table 2: List of RCMs that underestimate global radiation and, respectively, overestimate global radiation. Asterisks mark models which do not display the behaviour throughout the entire annual cycle

RCM-name	
Underestimator	Overestimator
CAIRCA3*	CNRM-RM
DMI-HIRHAM	HADRM3Q0
EHTZ-CLM	HADRM3Q3
ICTP-RegCM3	HADRM3Q16
METNO-HIRHAM	KNMI-RACMO3
MPIOM	
SMHIRCA*	

All RCMs show a much higher temporal variability (Fig. 3.6.7 and 3.6.8) over land than the ERA-40 data because of the lower spatial resolution of the latter. The models that underestimate global radiation additionally have the tendency to show less variability in the northern North Sea. All three Hadley Centre models show pronounced variability over the continent; of these the most extreme is HadRM3Q3 which has standard deviations nearly twice the size of those in ERA-40 (Fig. 3.6.8).

In January, according to the small values, the absolute differences between ERA-40 and the RCM simulations are also small (Figs. 3.6.3 and 3.6.4). However, temporal variability in the RCMs (Figs. 3.6.9 and 3.6.10) is much higher compared to ERA-40. In the time of strong irradiation (July) differences between ERA-40 and the RCMs are considerably larger (Figs. 3.6.5 and 3.6.6). All RCMs from the underestimator group are exaggerating meridional gradients in global radiation. Again, none of the RCMs captures the localized radiation maximum of ERA-40 in the central North Sea.

The frequency distributions of global radiation in the four North Sea subregions (Fig. 3.6.15), show two maxima, a strong maximum at low radiation and a second weaker maximum, most pronounced in the ERA-40 data, associated with summer time radiation at 220-240 W/m^2. No values in ERA-40 exceed 320 W/m^2, while all of the RCMs do. The frequency distribution at the low end of global radiation differs in the northern and southern North Sea boxes in the ERA-40 data, but not in the RCMs.

3.7 Cloud Cover

Clouds are the visible aggregates of water droplets and/or ice crystals in the atmosphere. The cloud cover is the portion of the sky that is attributed to clouds. It is traditionally measured in octa of sky covered or tenth (WMO 2012). According to the amount, height, thickness, layering and types, clouds have an important influence on the heat and radiation budget of the atmosphere. There are, however, still large gaps in understanding the interactions. The knowledge of the cloud cover alone is not sufficient to describe the processes.

The annual cycle of the cloud cover shows a flat minimum in the ERA-40 data from May to August (see Fig. 3.7.13). All four North Sea boxes show the same annual cycle. Within the large uncertainty there is no difference between the southern and the northern North Sea. RCMs even exceed the large temporal variations of cloud cover in the ERA-40 data. Less variability compared to ERA-40 occurs in all analysed seasons (annual average, January, July) only in METNO-HIRHAM (Figs. 3.7.8, 3.7.10 and 3.7.12). The largest variability compared to ERA-40 is found in DMI-HIRHAM (Figs. 3.7.8, 3.7.12).

The annual cycles in the RCMs varies in time and amplitude compared to ERA-40 (see Fig. 3.7.13). A completely different annual cycle with a maximum in April and a minimum in October is simulated by HADRM3Q3. Both of the HIRHAM variants (DMI and KNMI) display weak summer maxima in cloud cover over the northern areas. Other models show more or less constant differences with both signs compared to ERA-40 the entire year (see Fig. 3.7.14).

Basically the same separation of the RCMs in the simulations as for global radiation exists for cloud cover (see Tab. 2 and 3) Models in which overestimation of global radiation was detected underestimated cloud cover. However, this relationship does not hold for all models, SMHIRCA for example underestimates global radiation but also underestimates cloud cover in most months of the year.

Table 3: List of RCMs that underestimate cloud cover respectively overestimate cloud cover

RCM-name	
Overestimator	Underestimator
CAIRCA3	CNRM-RM
DMI-HIRHAM	HADRM3Q0
EHTZ-CLM	HADRM3Q3
ICTP-RegCM3	HADRM3Q16
METNO-HIRHAM	KNMI-RACMO3
MPIOM	SMHIRCA

All RCMs simulate similar spatial patterns over the North Sea with an NW/SE oriented decrease in cloud cover, but the differences to the ERA-40 cloud cover vary

strongly between the models (Figs. 3.7.1 and 3.7.2). The entire group of Hadley Centre models shows large-scale underestimations of the mean cloud cover. Even more extreme differences to ERA-40 than in the annual means exist in July (Fig. 3.7.6). HadRM3Q3 has a completely different seasonal cycle (Figs. 3.7.13 and 3.7.14) and thus shows huge differences in January (Fig. 3.7.4) and July (Fig. 3.7.6).

The long-term standard deviations of the majority of the RCMs (Fig. 3.7.7) are larger than that of ERA-40. Here, extreme cases are the Hadley Centre models and DMI-HIRHAM which nearly have twice the variability of ERA-40 in the long-term mean (Fig. 3.7.8). DMI-HIRHAM shows large variability in cloud cover as well in winter as in summer (Figs. 3.7.10 and 3.7.12) and especially the summer variability is far outside of those of the other RCMs.

3.8 Precipitation

Precipitation at sea plays an important role within the hydrological cycle. However, in-situ precipitation sampling is sparse and the satellite observations are supported only by a few validation sites on islands and coastal locations, and by a few rain-gauge equipped surface moorings. Measurements aboard ships are very problematic and data can have large errors, mainly because of wind flow distortion around the ship. The amount of precipitation is usually expressed as millimetres or inches of liquid water deposited on a horizontal surface at a given point over a specified time interval.

The annual mean precipitation in the ERA-40 reanalysis shows for the period of 1971-2000 a region of high values at the Scandinavian coast (Fig. 3.8.1), with a maximum of nearly 1400 mm/year as a consequence of the orographic effect. By contrast, due to the “lee-effect” there is a minimum east of Great Britain with only 300-400 mm/year.

In the ENSEMBLES regional models precipitation shows a similar pattern like ERA-40, with lower values in the south western parts, and higher values in the north of the North Sea, with a maximum near the Norwegian coast. Since the spatial resolution of the RCMs is about five times higher than that of ERA-40, it provides an improved representation of the land-sea distribution and the mountain ranges. Overall, the RCMs simulate much more precipitation than ERA-40 during the entire year, as well in winter as in summer. Summing up annually, the totals are more than 400 mm (i.e. 50 %) higher than those of ERA-40, (Fig. 3.8.2). For most of the RCMs the differences are smaller in winter (Fig. 3.8.4) than in summer (Fig. 3.8.6).

The yearly standard deviations of the RCMs show a higher variability than ERA-40 for the whole area (Fig. 3.8.7 and 3.8.8). While in summer the variability is higher than that of ERA-40, during winter it is lower. (Figs. 3.8.10 and 3.8.12).

The annual precipitation cycles of all investigated models are shown in Fig. 3.8.13. Apparently, the annual cycle is more pronounced in ERA-40 than in the RCMs (more precipitation in winter time and less precipitation during summer (Kjellström et al. 2011).

4 Acknowledgement

We particularly thank Ole Bossing Christensen, Erik van Mijngaard, Erika Coppola and Daniela Jacob and their co-workers who made hourly wind data of the DMI, KNMI, ICTP and MPI model results available to us. We also thank our colleagues at DWD Offenbach, especially Sabrina Plagemann, for the download of the ENSEMBLES data.

The ENSEMBLES work reproduced here is from the EU-funded FP6 Integrated Project ENSEMBLES (Contract number 505539).

Literature

Arguez, A. and R.S. Vose 2011: The Definition of the Standard WMO Climate Normal: The Key to Deriving Alternative Climate Normals. Bull. Amer. Meteor. Soc., 92, 699-704

Befort, D. J., G.C. Leckebusch, U. Ulbrich, G. Rosenhagen, H. Heinrich und A. Ganske 2012: Potentielle Auswirkungen des anthropogenen Klimawandels auf das Sturmflutrisiko an der deutschen Nordseeküste. Abschlussbericht Projekt PAK, FU Berlin

Bengtsson, L., K.I. Hodges and S. Hagemann 2004: Sensitivity of large-scale atmospheric analyses to humidity observations and its impact on the global water cycle and tropical and extratropical weather systems in ERA40. Tellus A56, 202-217. http://dx.doi.org/10.1111/j.1600-0870.2004.00053.x

Bingöl, A., X. Pena Diaz, G. Larsén, J. Badger, A.N. Hahmann, T. Mikkelsen and S.-E. Gryning 2010: Offshore wind resource estimation for wind energy. Annual Report, Techno-Ocean Network

Déqué, M., S. Somot, E. Sanchez-Gomez, C.M. Goodess, D. Jacob, G. Lenderink, and O.B. Christensen 2011: The spread amongst ENSEMBLES regional scenarios: regional climate models, driving general circulation models and interannual variability. Clim. Dyn. 38, 951–964, DOI 10.1007/s00382-011-1053-x

Badger, M., A., J. Badger, M. Nielsen, C. Bay Hasager and A. Pena 2010: Wind class sampling of Satellite SAR Imagery for Offshore Wind Resource Mapping. J. Applied Meteorology and Climatology 49, 2474–2491

Jacob, D., L. Bärring, O.B. Christensen, J.H. Christensen, M. de Castro, M. Déqué, F. Giorgi, S. Hagemann, M. Hirschi, R. Jones, E. Kjellström, G. Lenderink, B. Rockel, E. Sánchez, C. Schär, S.I. Seneviratne, S. Somot, A. van Ulden and B. van den Hurk, 2007: An inter-comparison of regional climate models for Europe: model performance in present-day climate, Climate Change, 81, 31-52, doi:10.1007/s10584-006-9213-4

Keller, J.D, C. Ohlwein, P. Friederichs, A. Hense, S. Crewell, C. Wosnitza, I. Pscheidt, S. Kneifel, S. Redl, and S. Steinke 2012: High resolution regional reanalysis for Europe and Germany, 4th WCRP – International Conference on Reanalysis, 7-11 May 2012, Silver Spring, Maryland, USA

Kjellström, E., G. Nikulin, U. Hansson, G. Strandberg and A. Ullerstieg 2011: 21st century changes in the European climate: uncertainties derived from an ensemble of regional climate model simulations. Tellus, 63A, 24-40, DOI: 10.1111/j.1600-0870.2010.00475.x

Larsén, X.G., J. Mann, J. Berg, H. Göttel and D. Jacob 2009: Wind climate from the regional climate model REMO. Wind Energy 13, 279-296

Lindenberg, J., H.-T. Mengelkamp and G. Rosenhagen 2012: Representativity of near surface wind measurements from coastal stations at the German Bight. Meteorologische Zeitschrift, 99–106

Müller-Navarra, S.H. and H. Giese 1999: Improvements of an empirical model to forecast wind surge in the German Bight. Ocean Dynamics 51, 385-405

Nikulin, G., E. Kjellström, U. Hansson, G. Strandberg and A. Ullerstig 2011: Evaluation and future projections of temperature, precipitation and wind extremes over Europe in an ensemble of regional climate simulations. Tellus, 63 A, 41-55

Räisänen, J. and J. Eklund 2012: 21st Century changes in snow climate in Northern Europe: a high-resolution view from ENSEMBLES regional climate models, Clim. Dyn. 38, 2575-2591

Schade, N.H., G. Rosenhagen and H. Heinrich 2013: Regional Evaluation of ERA-40 Reanalysis Data with Marine Atmopsheric Observations in the North Sea Area, Meteorologische Zeitschrift (in review)

Solomon, S., D. Qin, M. Manning, Z. Chen, M. Marquis, K.B. Averyt, M. Tignor and H.L. Miller (eds.) 2007: Climate Change 2007: The Physical Science Basis. Cambridge University Press, Cambridge, United Kingdom and New York, NY, USA

Uppala, S.M., P.W. Kållberg, A.J. Simmons, U. Andrae, V. da Costa Bechtold, M. Fiorino, J.K. Gibson, J. Haseler, A. Hernandez, G.A. Kelly, X. Li, K. Onogi, S. Saarinen, N. Sokka, R.P. Allan, E. Andersson, K. Arpe, M.A. Balmaseda, A.C.M. Beljaars, L. van de Berg, J. Bidlot, N. Bormann, S. Caires, F. Chevallier, A. Dethof, M. Dragosavac, M. Fisher, M. Fuentes, S. Hagemann, E. Hólm, B.J. Hoskins, L. Isaksen, P.A.E.M. Janssen, R. Jenne, A.P. McNally, J.-F. Mahfouf, J.-J. Morcrette, N.A. Rayner, R.W. Saunders, P. Simon, A. Sterl, K.E. Trenberth, A. Untch, D. Vasiljevic, P. Viterbo and J. Woollen 2005: The ERA-40 re-analysis. Quart. J. R. Meteorol. Soc., 131, 2961-3012.doi:10.1256/qj.04.176

Van den Linden, P. and J.F.B. Mitchell (Eds.) 2009: ENSEMBLES: Climate Change and its Impacts: Summary of research and results from the ENSEMBLES project. MET Office Hadley Centre, FritzRoy Road, Exeter EX1 3PB, UK. 160 pp.

Winterfeldt, J., A. Andersson, C. Klepp, S. Bakan and R. Weisse 2010: Comparison of HOAPS, QuikSCAT, and Buoy Wind Speed in the Eastern North Atlantic and the North Sea. IEEE Transactions on Geoscience and Remote Sensing 48, 338-348

WMO 2012 Recommended Methods for Evaluating Cloud and Related Parameters. WWRP/WGNE Joint Working Group on Forecast Verification Research (JWGFVR), Word Meteorological Organisation, Geneva, 34 pp.

Page Figure

Appendix

Appendix

Page Figure

Appendix

Page Figure

Appendix

Page Figure

Appendix

Page Figure

Appendix

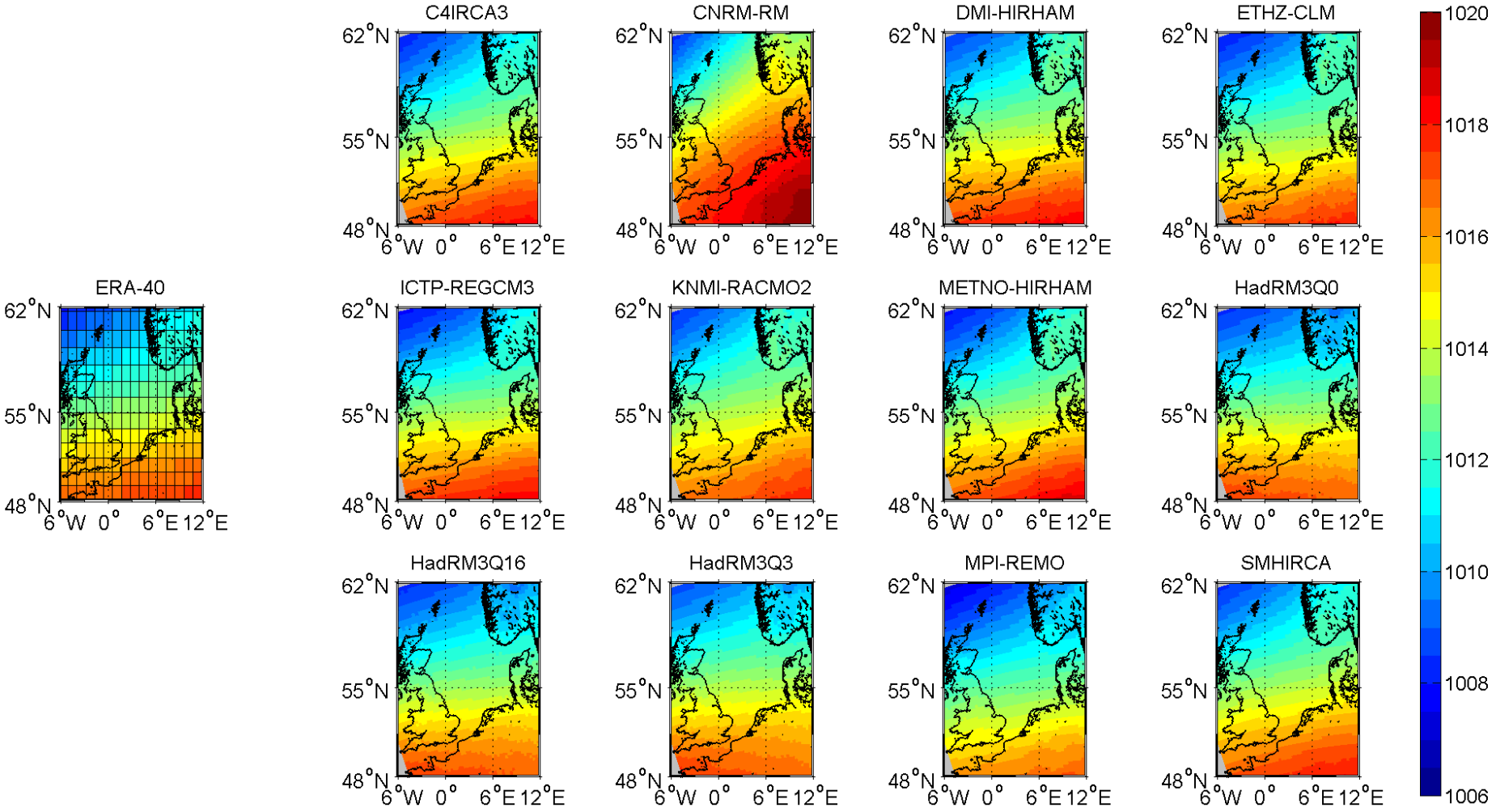

Figure 3.2.1: Mean sea level pressure [hPa] in the North Sea area for the period 1971-2000: ERA-40 (left) and the ENSEMBLES regional models (right)

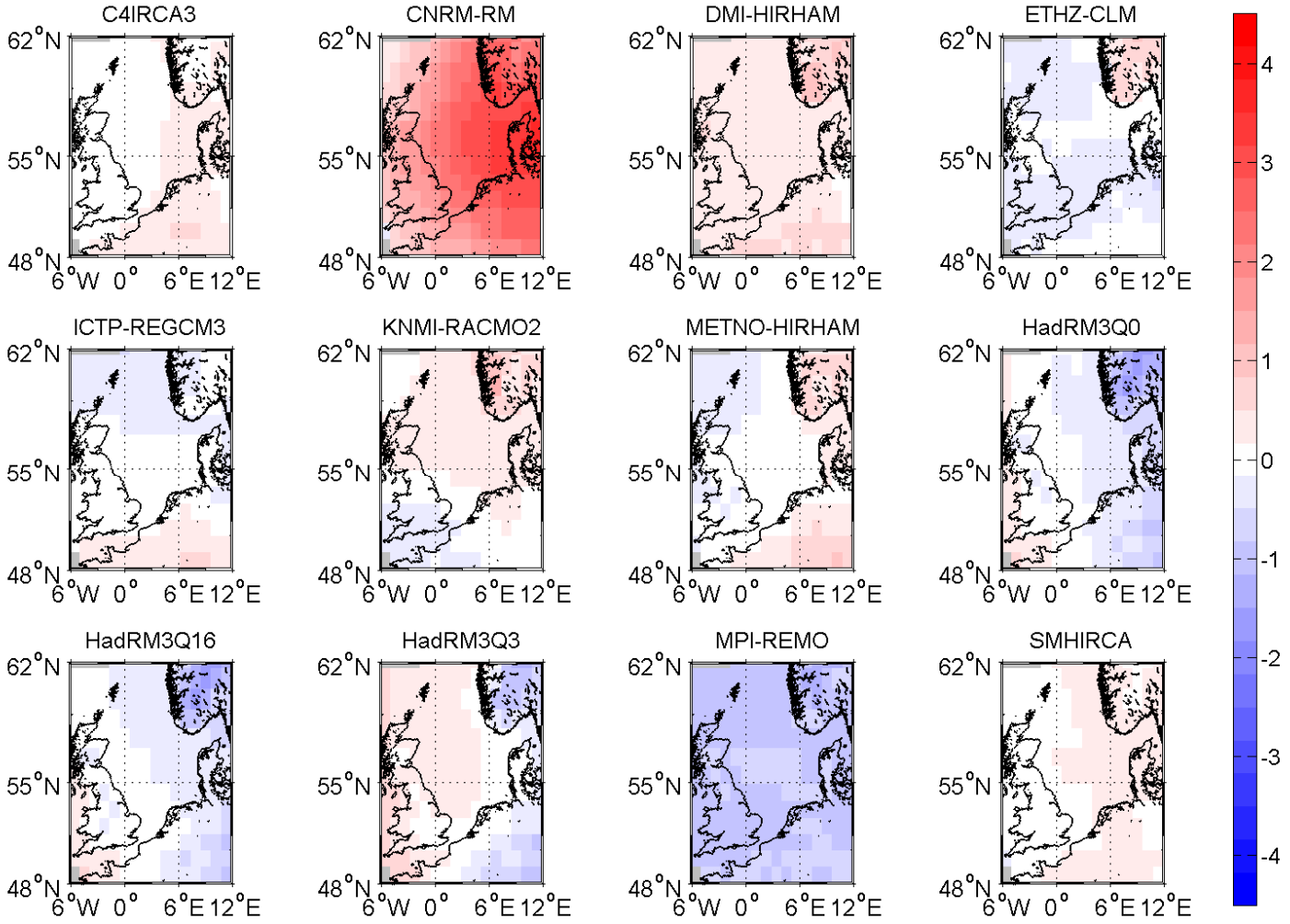

Figure 3.2.2: Differences of sea level pressures [hPa]: RCMs minus ERA-40 from Fig. 3.2.1

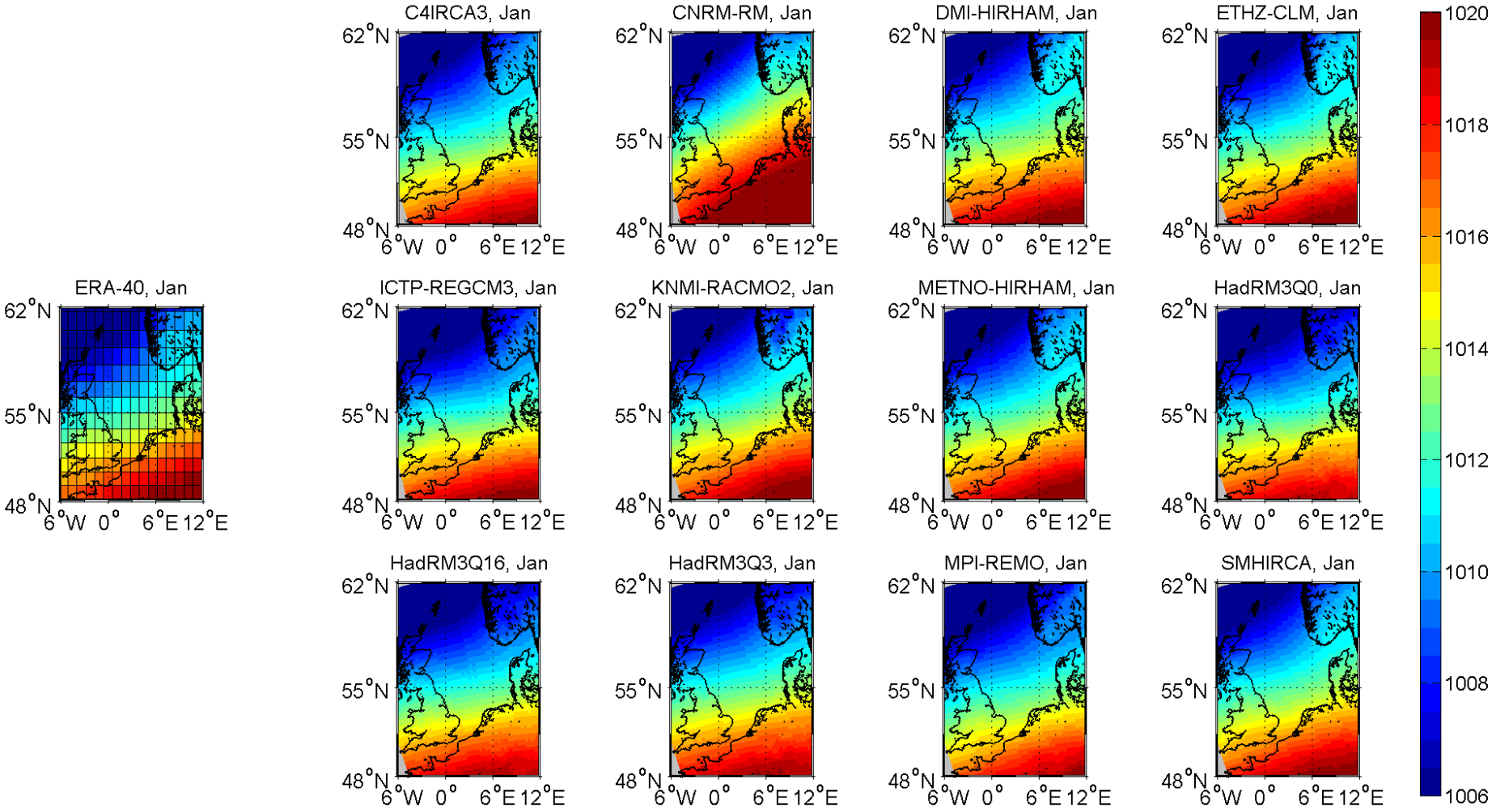

Figure 3.2.3: January mean sea level pressures [hPa] in the North Sea area for the period 1971-2000: ERA-40 (left) and the ENSEMBLES regional models (right)

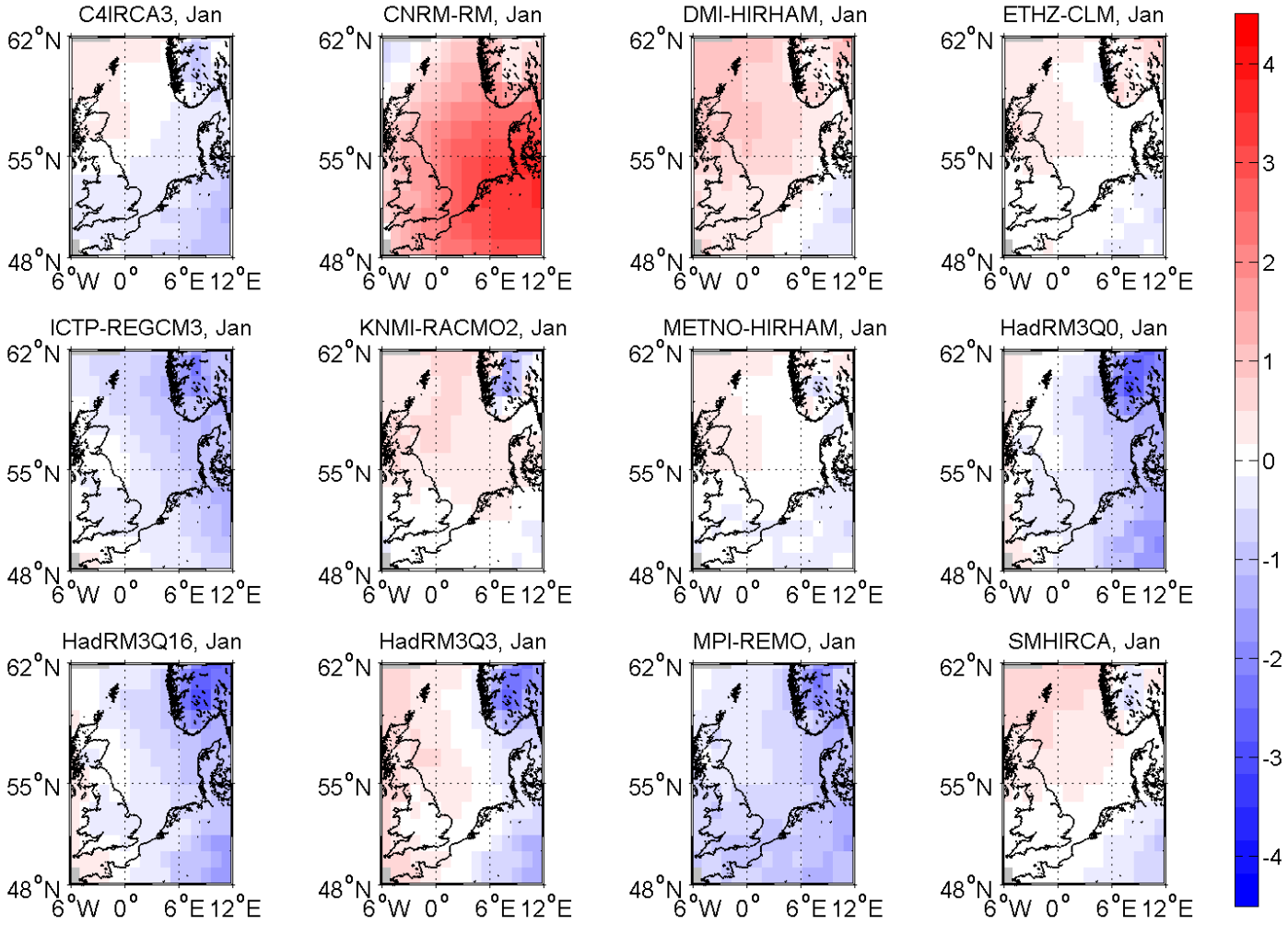

Figure 3.2.4: January differences of mean sea level pressures [hPa]: RCMs minus ERA-40 from Fig. 3.2.3

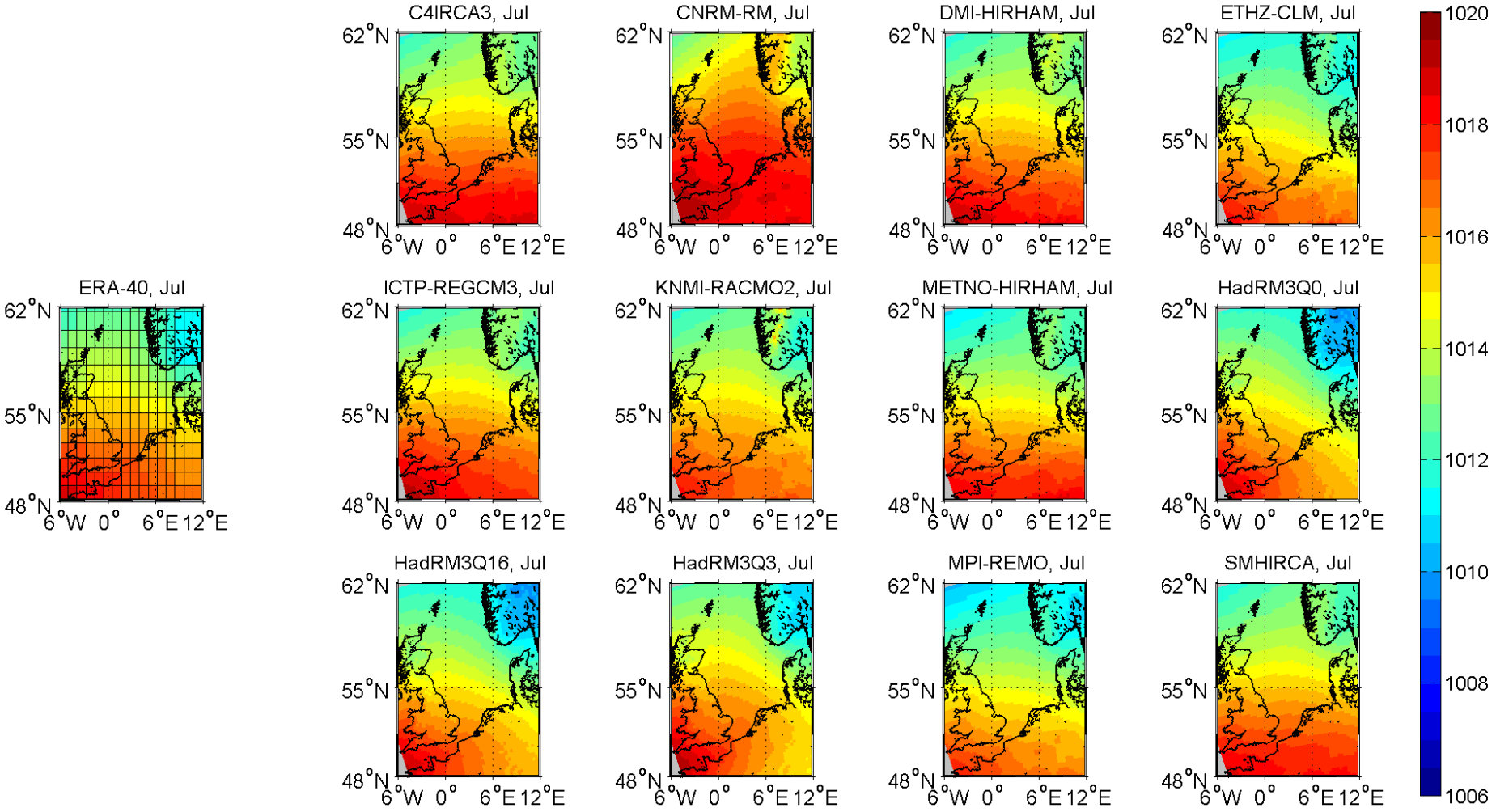

Figure 3.2.5: July mean sea level pressures [hPa] in the North Sea area for the period 1971-2000: ERA-40 (left) and the ENSEMBLES regional models (right)

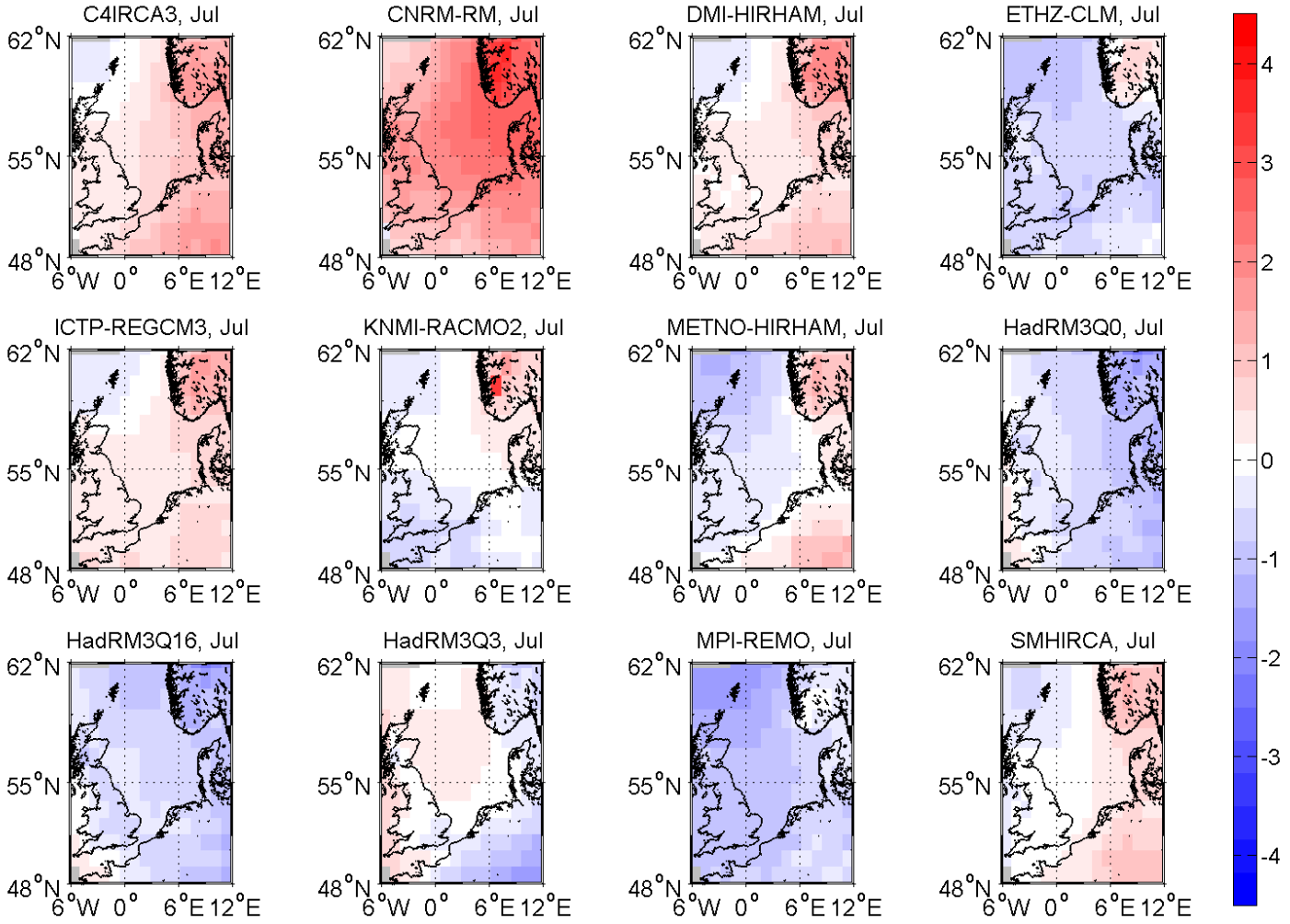

Figure 3.2.6: July differences of sea level pressures [hPa]: RCMs minus ERA-40 from Fig. 3.2.5

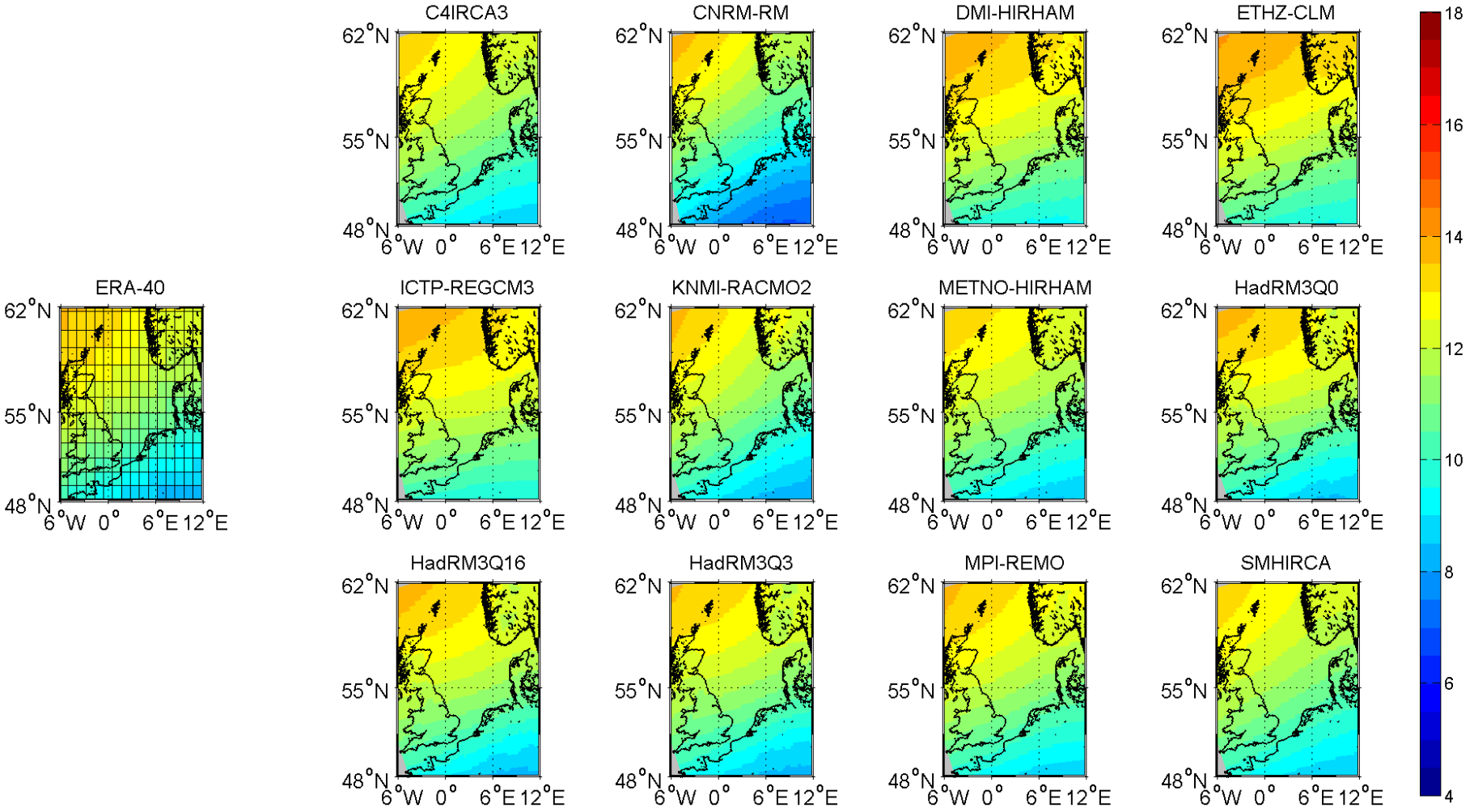

Figure 3.2.7: Standard deviations of sea level pressures [hPa] in the North Sea area for the period 1971-2000: ERA-40 (left) and the ENSEMBLES regional models (right)

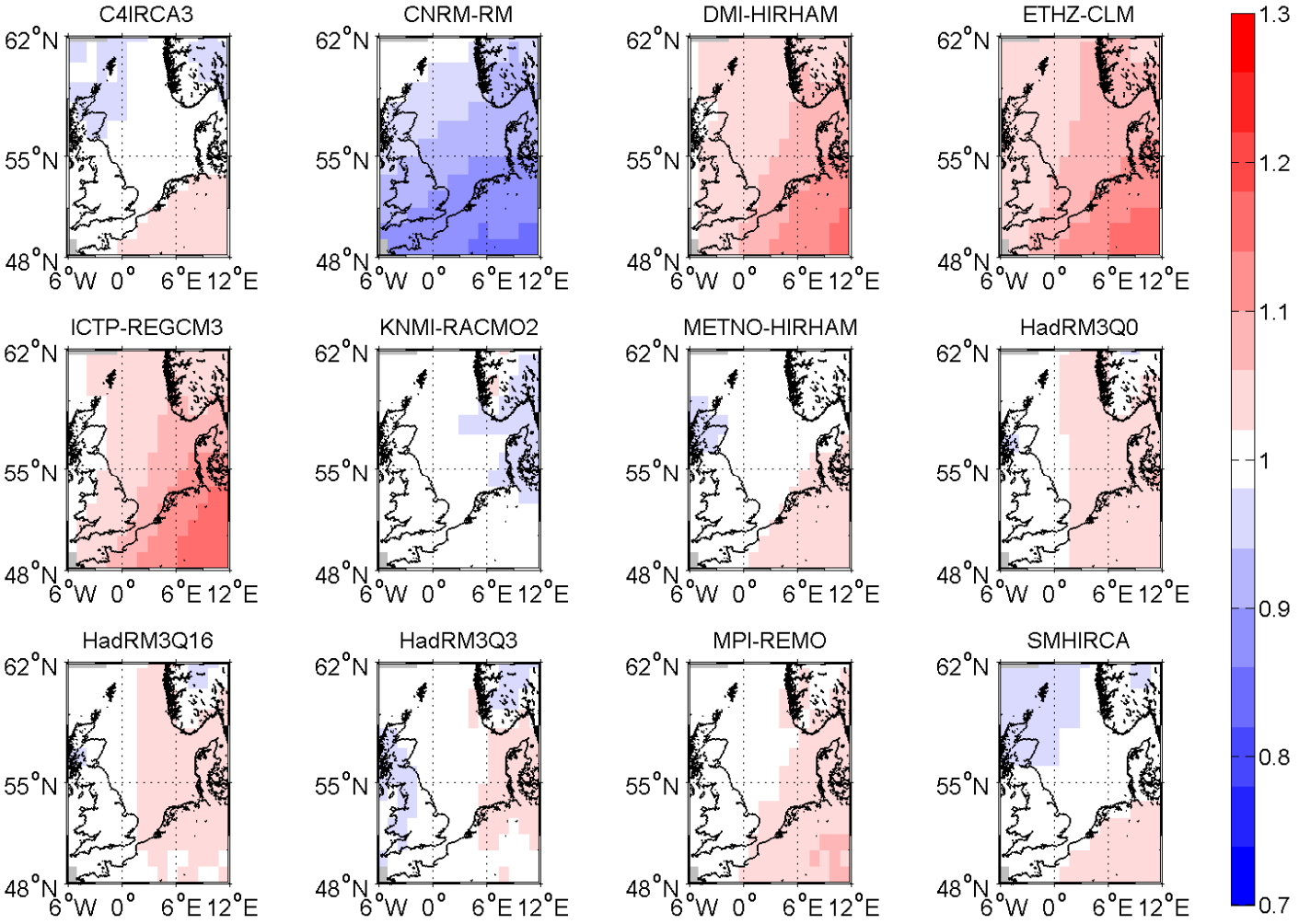

Figure 3.2.8: Ratio of standard deviations of sea level pressures: RCMs / ERA-40 from Fig. 3.2.7

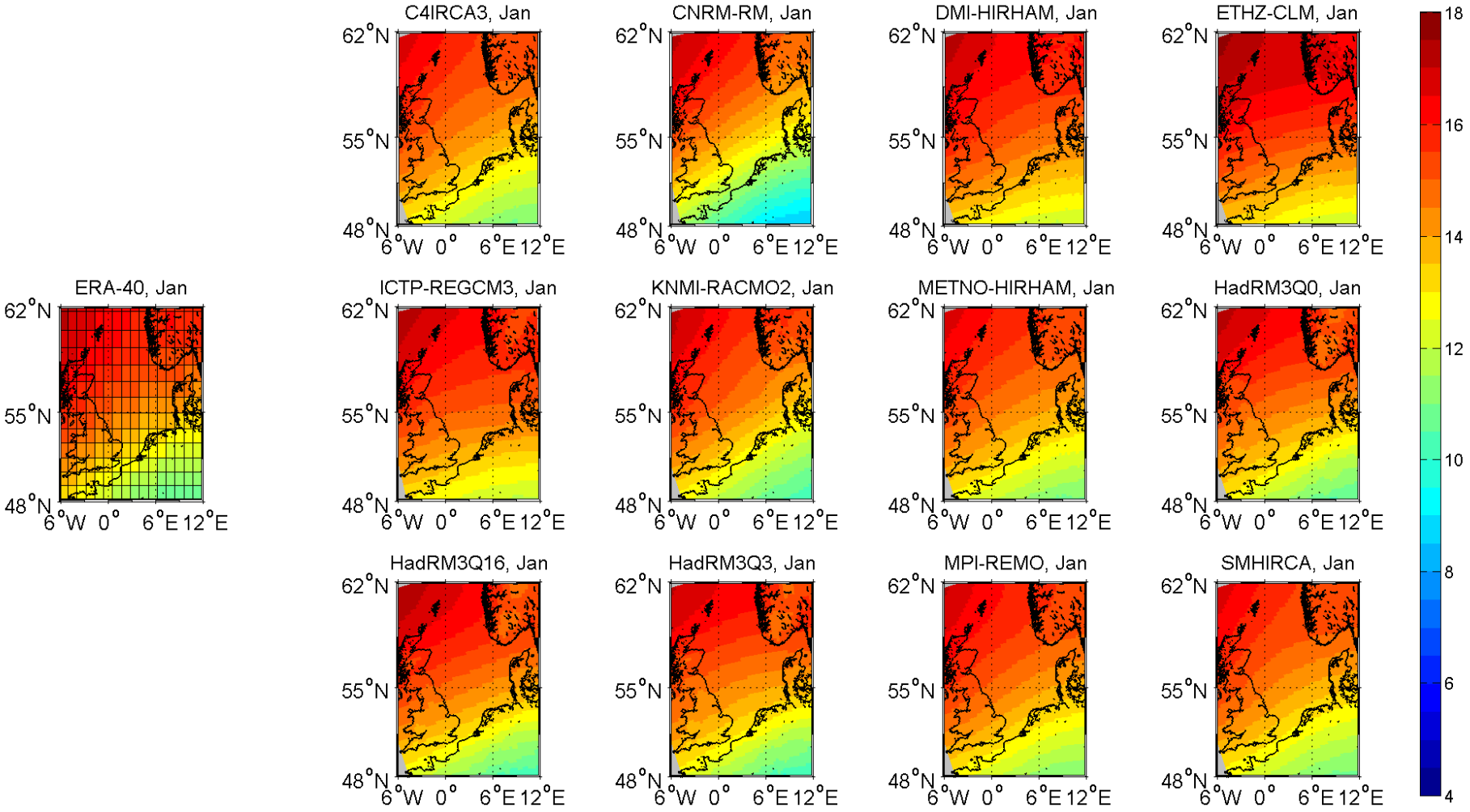

Figure 3.2.9: January standard deviations of sea level pressures [hPa] in the North Sea area for the period 1971-2000: ERA-40 (left) and the ENSEMBLES regional models (right)

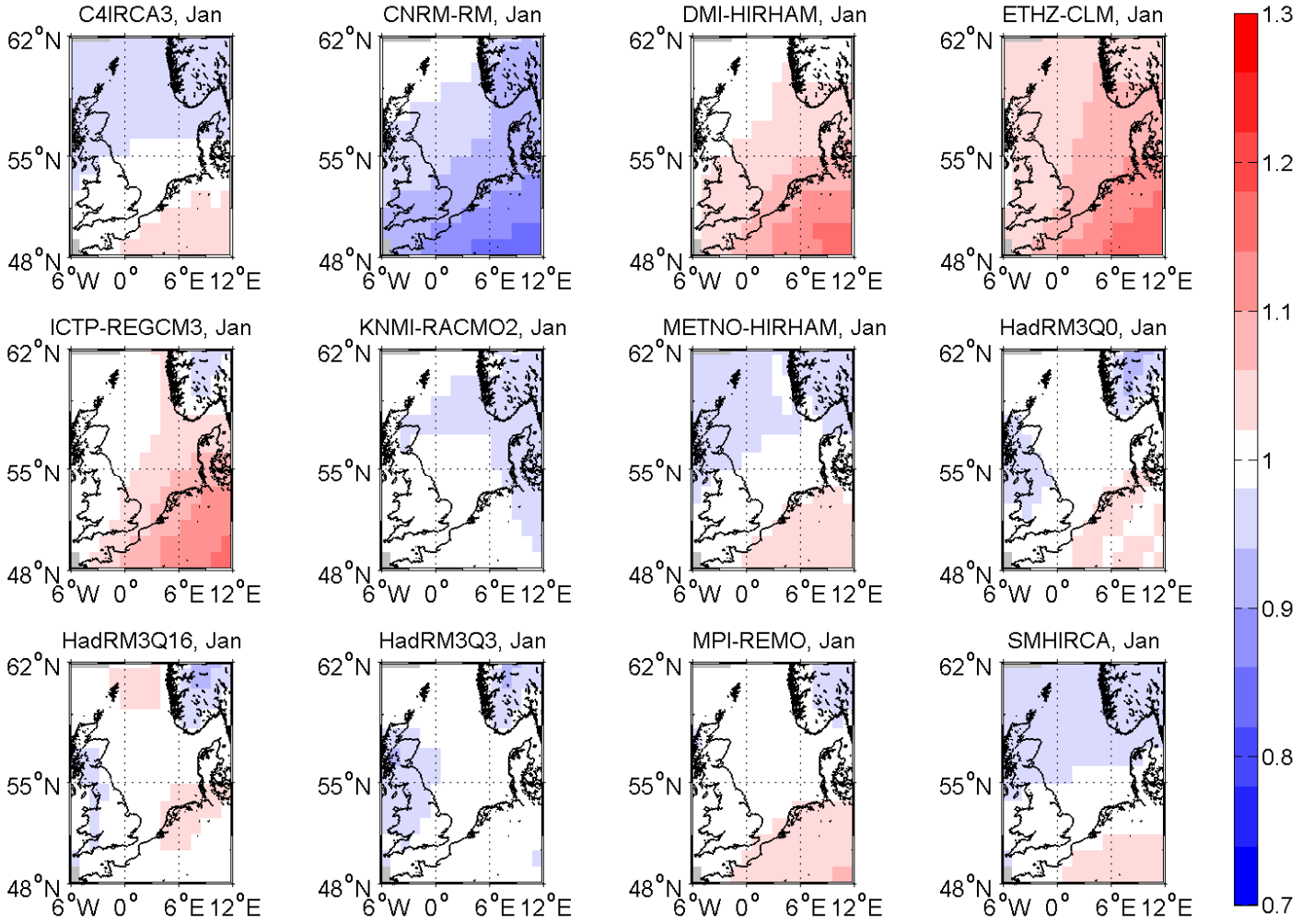

Figure 3.2.10: January ratio of standard deviations of sea level pressures: RCMs / ERA-40 from Fig. 3.2.9

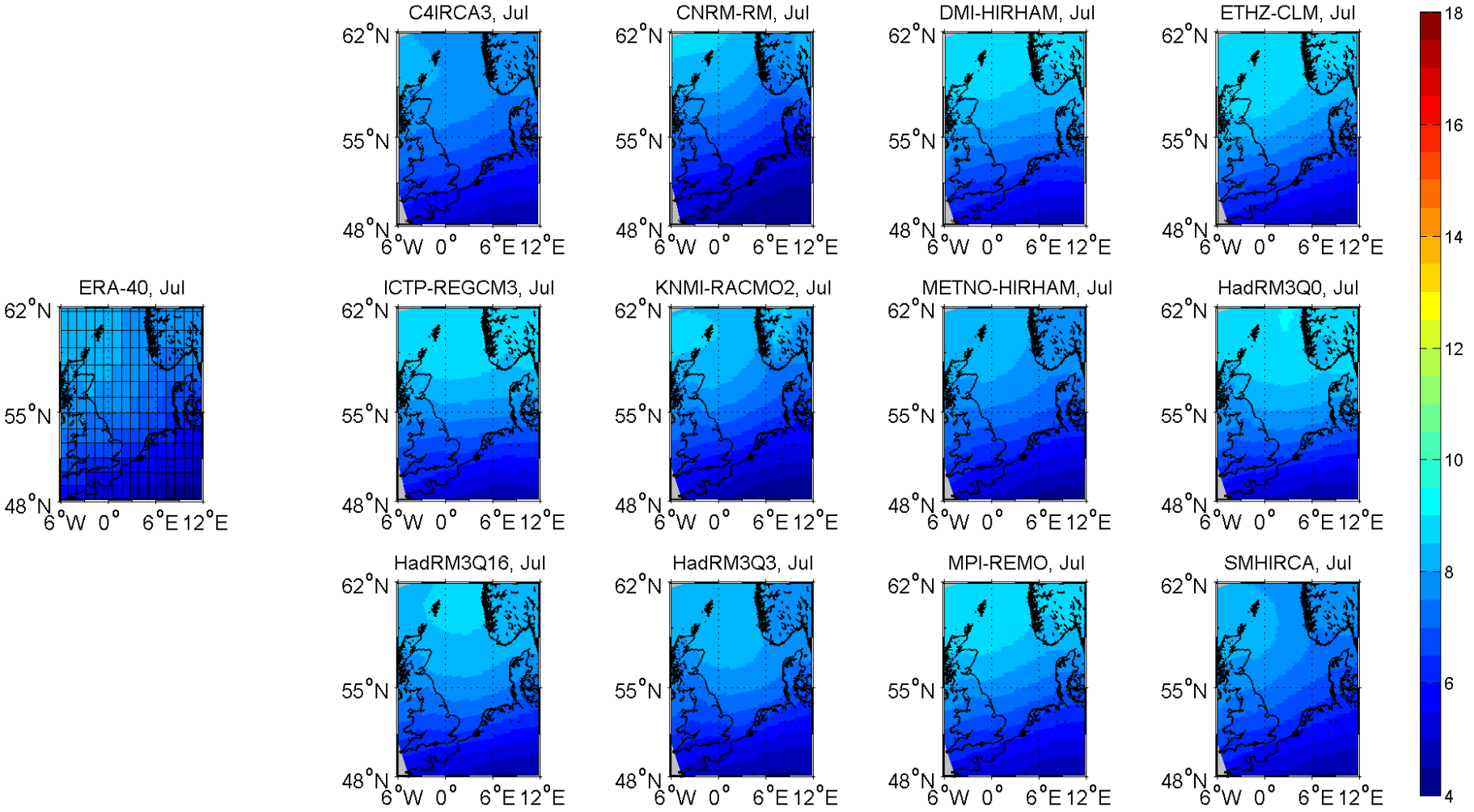

Figure 3.2.11: July standard deviations of sea level pressures [hPa] in the North Sea area for the period 1971-2000: ERA-40 (left) and the ENSEMBLES regional models (right)

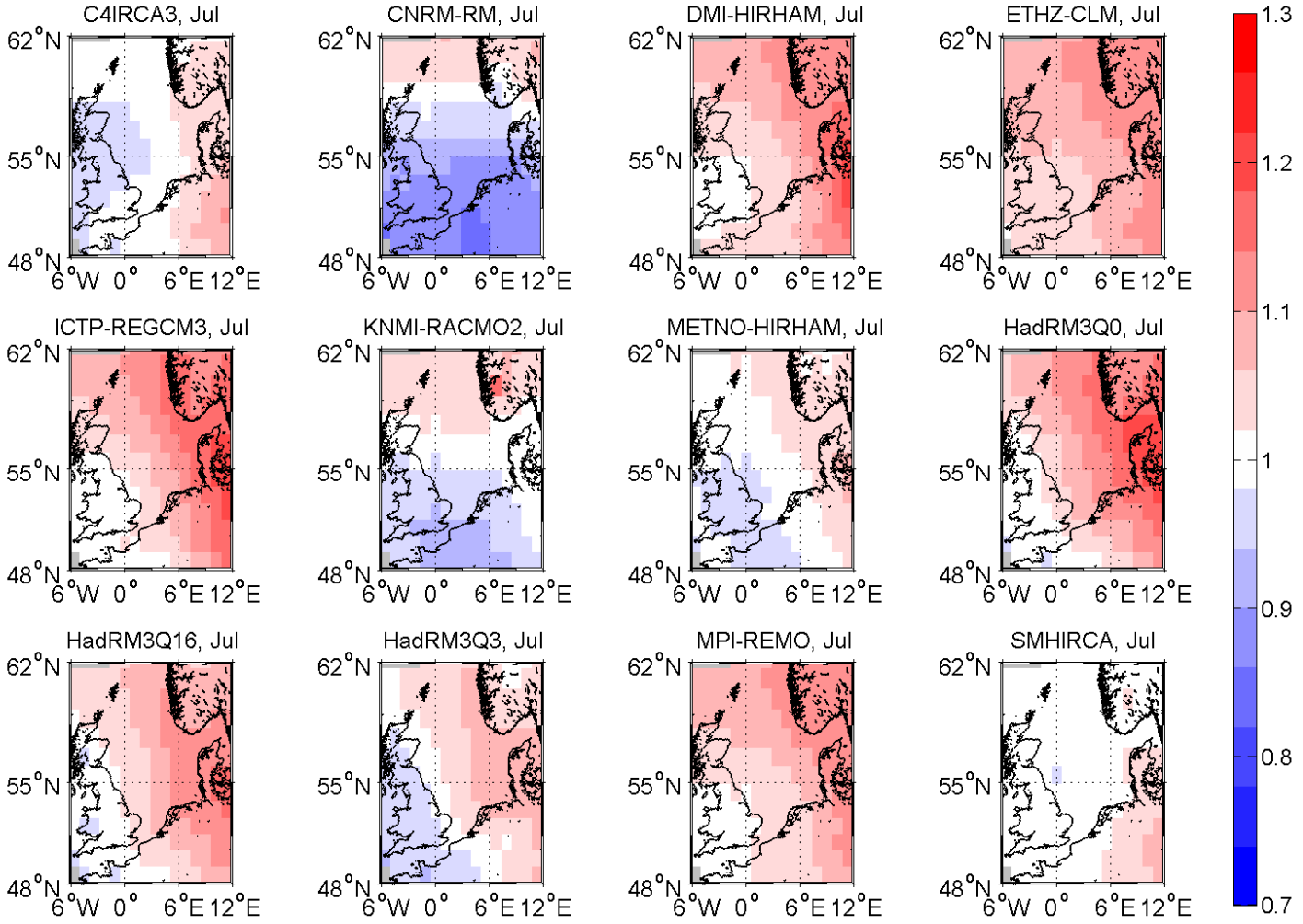

Figure 3.2.12: July ratio of standard deviations of sea level pressures: RCMs / ERA-40 from Fig. 3.2.11

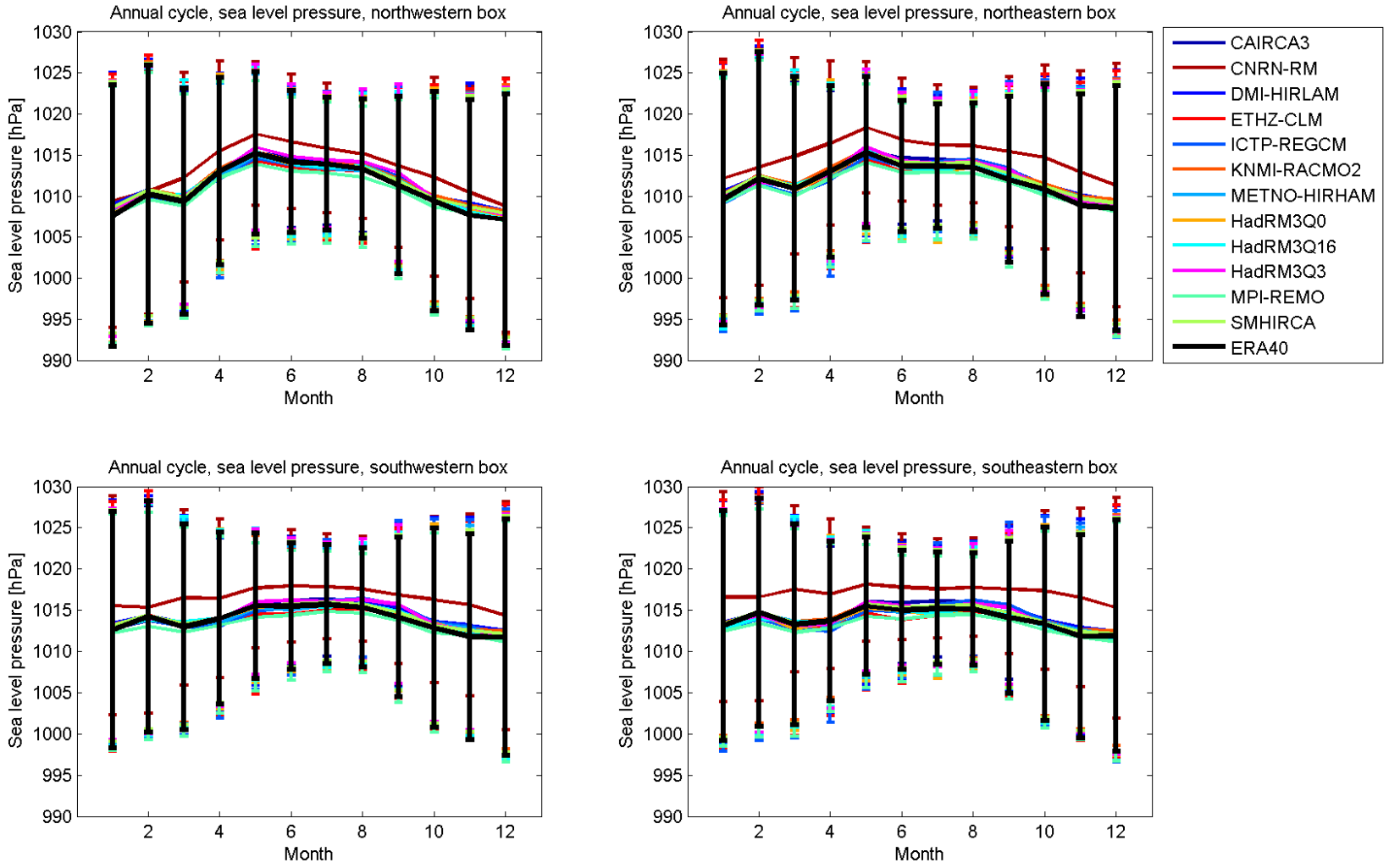

Figure 3.2.13: Annual cycles of sea level pressures [hPa] of the ENSEMBLES RCMs and ERA-40 in the four North Sea boxes for the period of 1971-2000

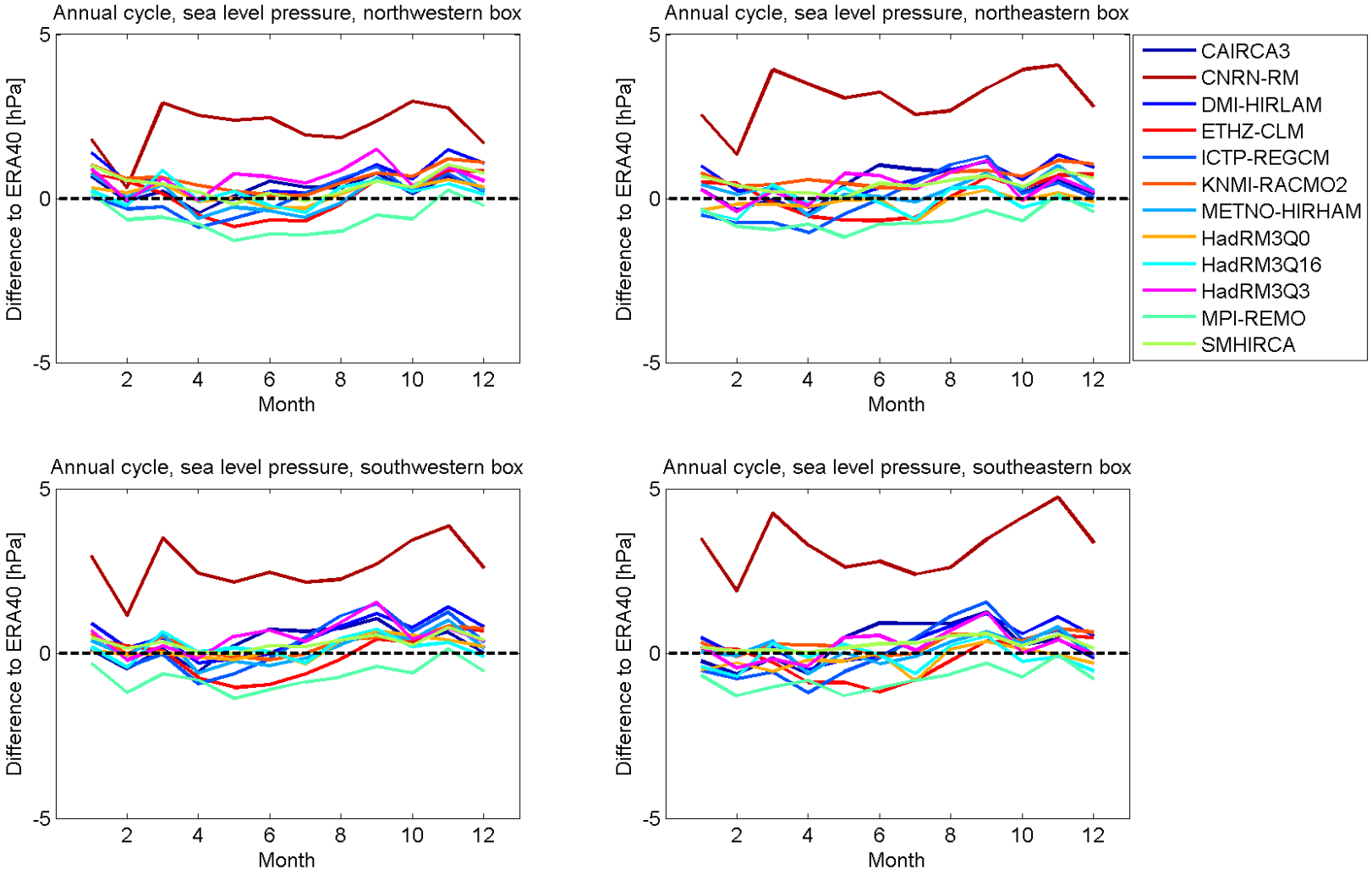

Figure 3.2.14: Differences of annual cycles of sea level pressures [hPa] of the ENSEMBLES RCMs minus ERA-40 in the four North Sea boxes for the period of 1971-2000

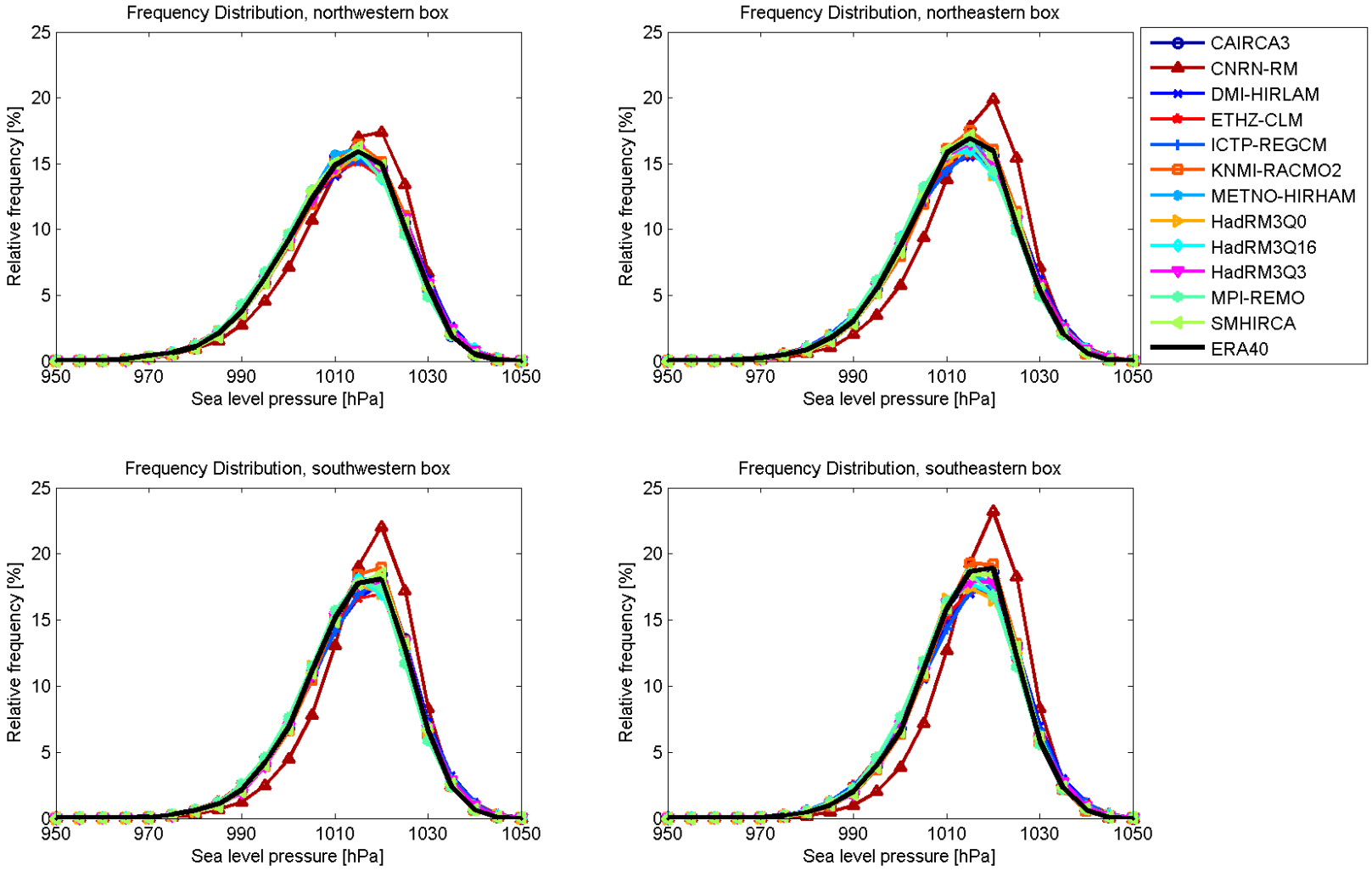

Figure 3.2.15: Frequency distributions of sea level pressures [%] of the ENSEMBLES RCMs and ERA-40 in the four North Sea boxes for the period of 1971-2000

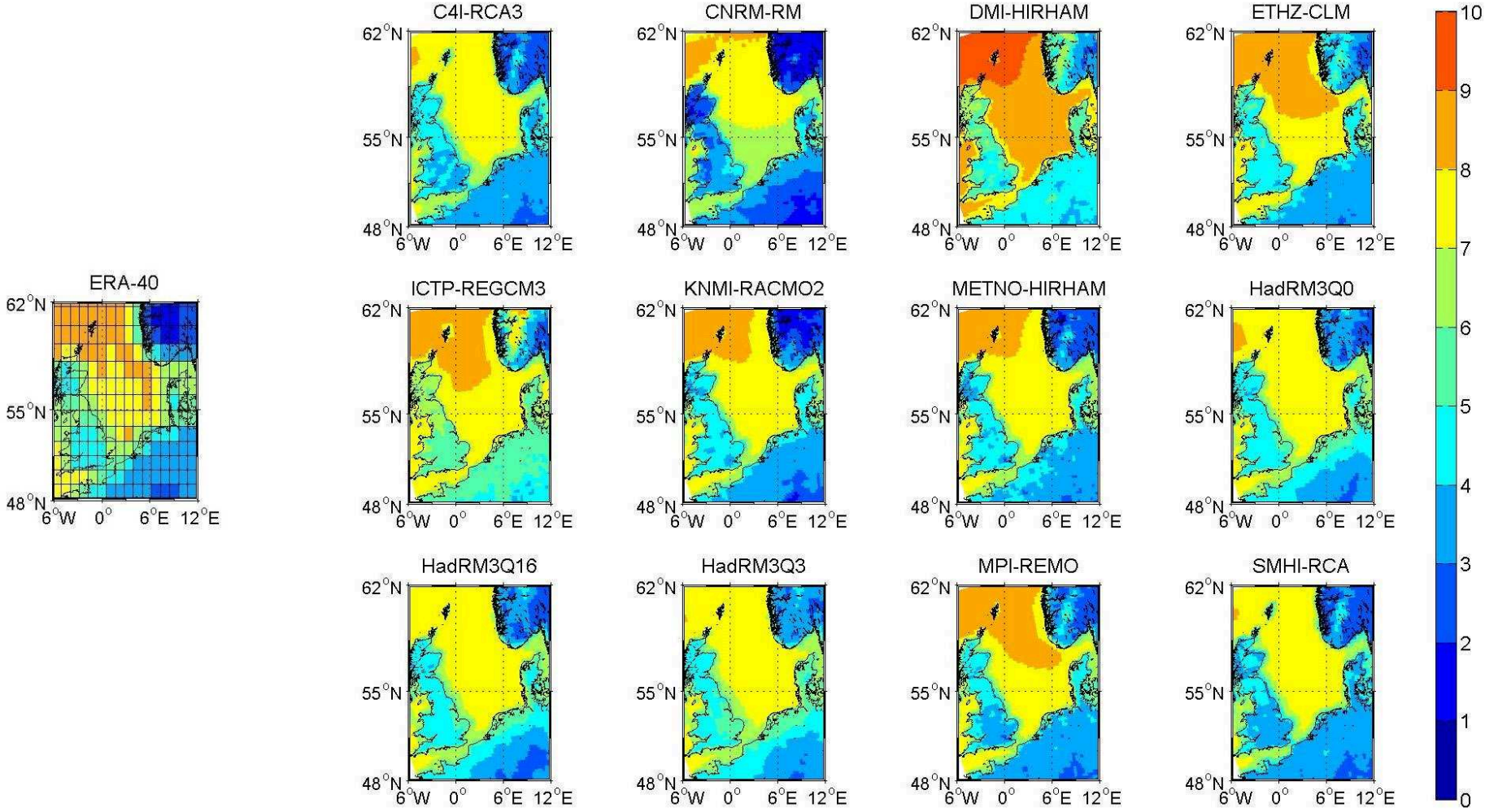

Figure 3.3.1: Mean wind speed [m/s] in the North Sea area for the period 1971-2000: ERA-40 (left) and the ENSEMBLES regional models (right)

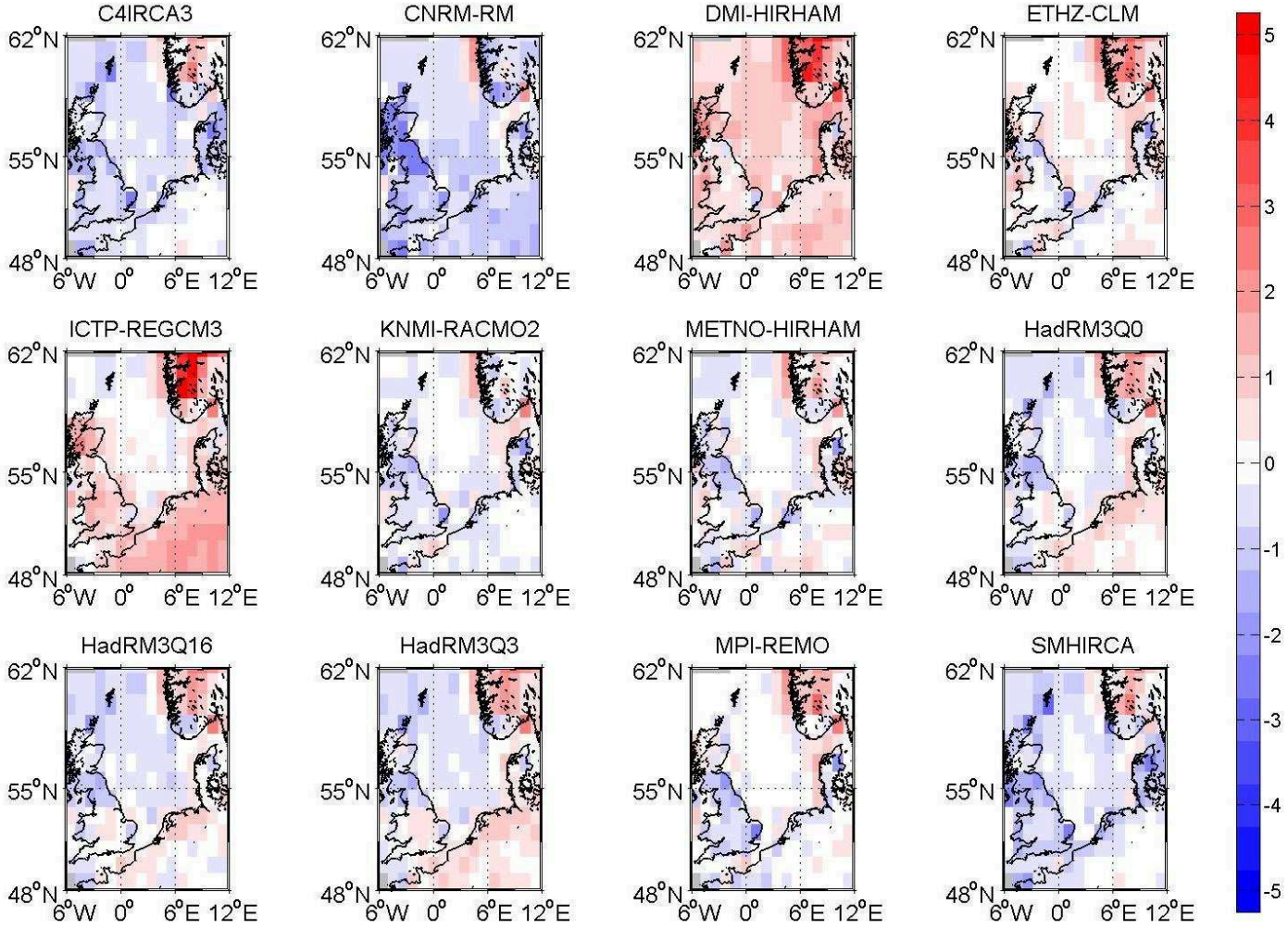

Figure 3.3.2: Differences of wind speed [m/s]: RCMs minus ERA-40 from Fig. 3.3.1

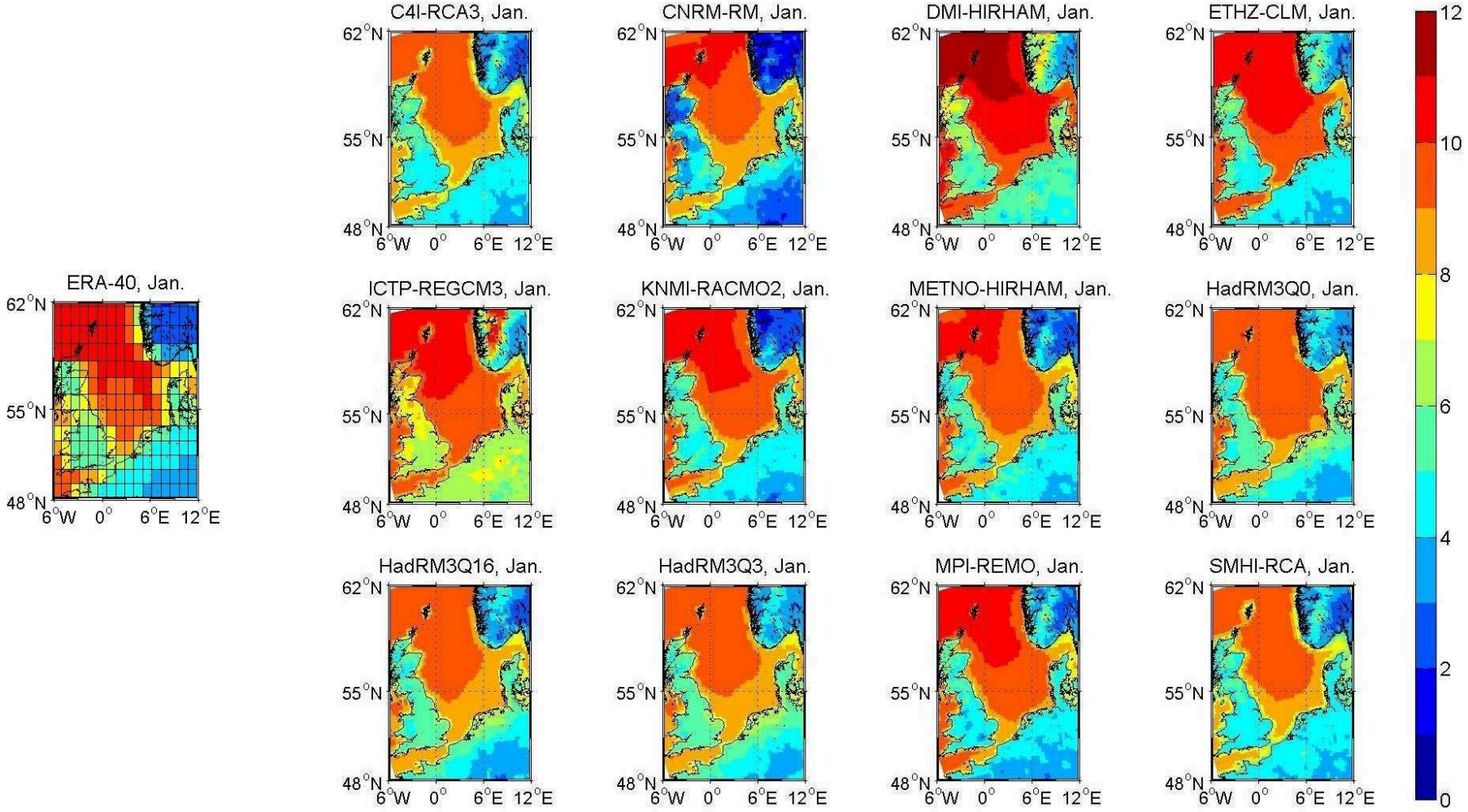

Figure 3.3.3: January mean wind speed [m/s] in the North Sea area for the period 1971-2000: ERA-40 (left) and the ENSEMBLES regional models (right)

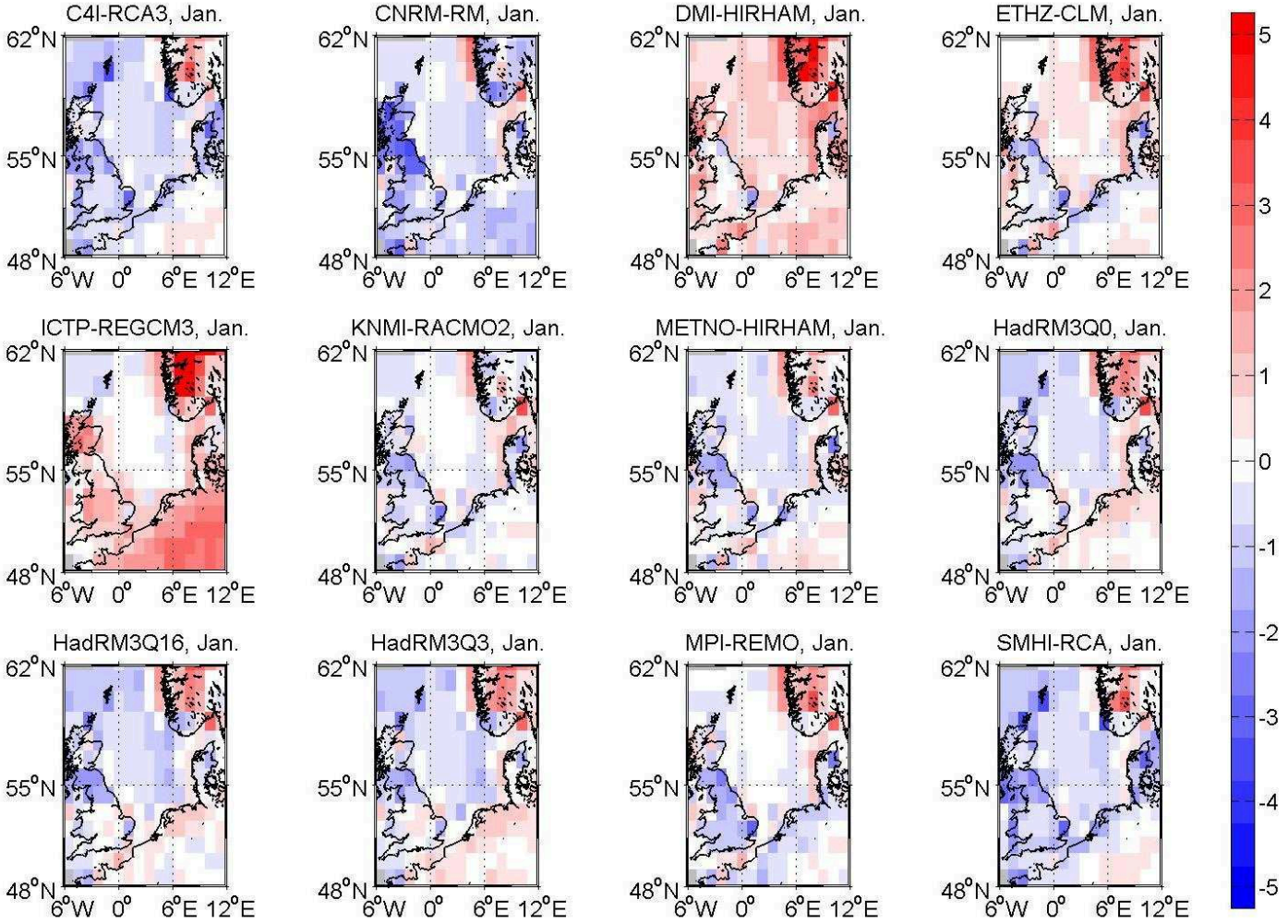

Figure 3.3.4: January differences of wind speed [m/s]: RCMs minus ERA-40 from Fig. 3.3.3

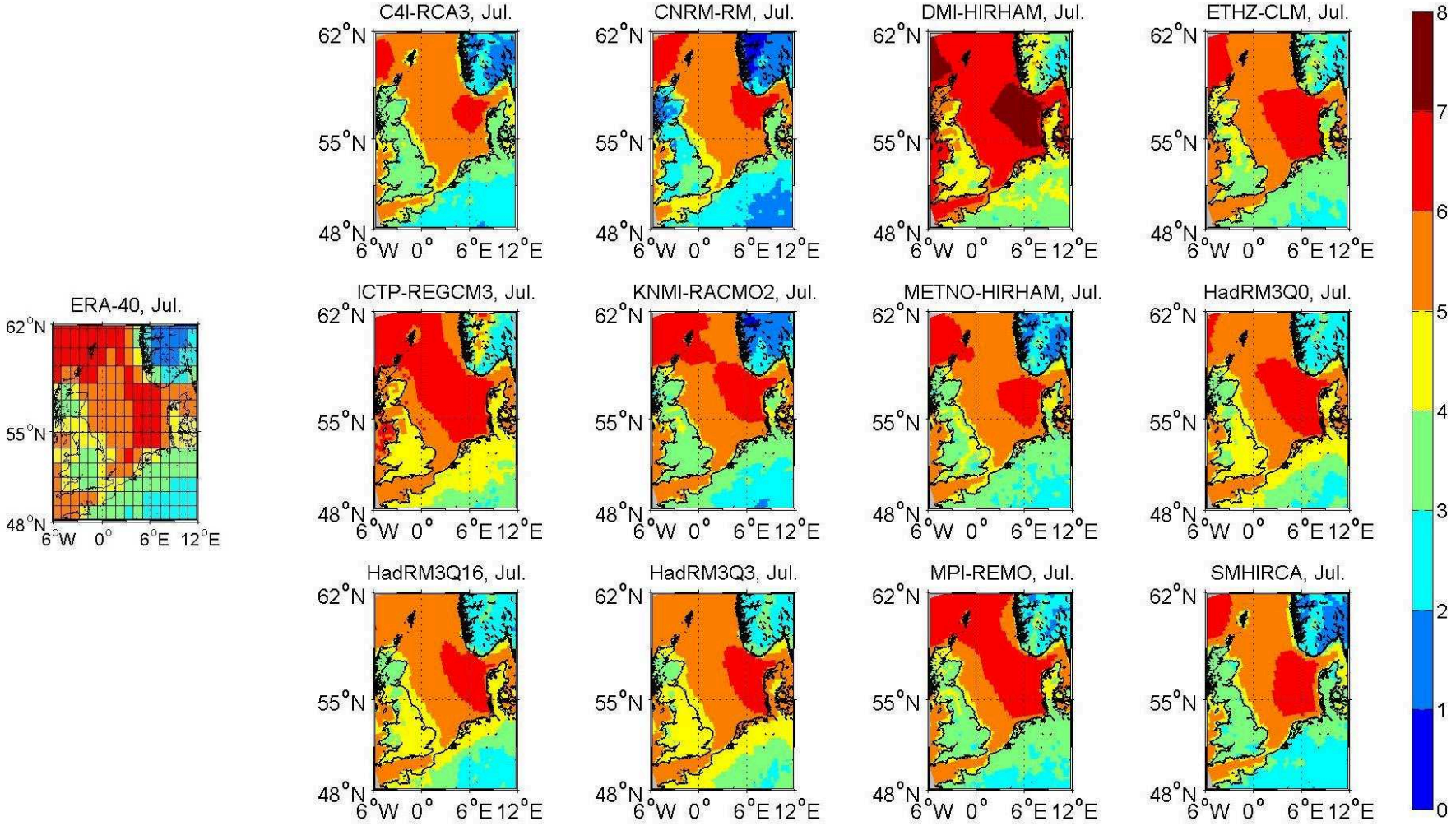

Figure 3.3.5: July mean wind speed [m/s] in the North Sea area for the period 1971-2000: ERA-40 (left) and the ENSEMBLES regional models (right)

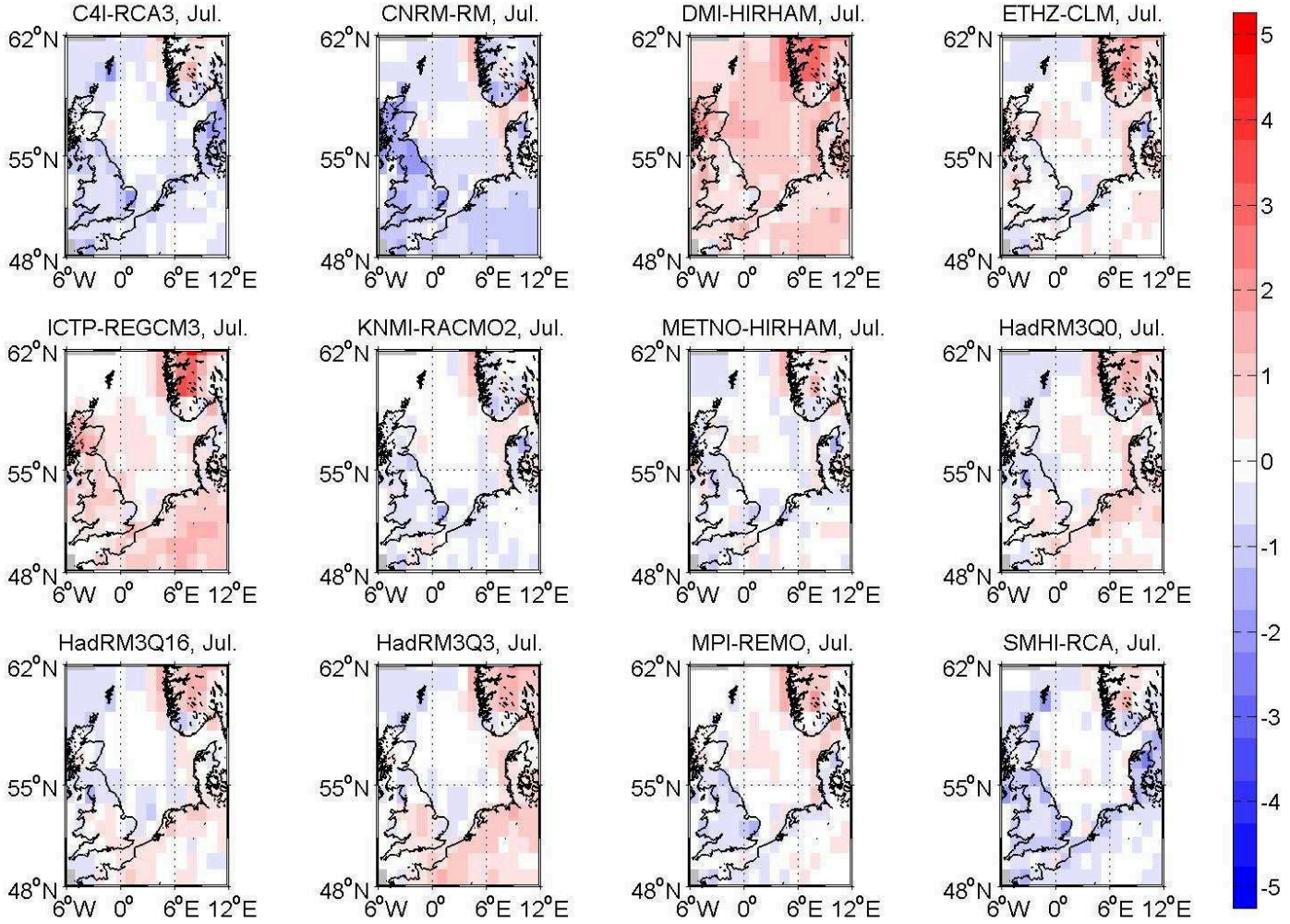

Figure 3.3.6: July differences of wind speed [m/s]: RCMs minus ERA-40 from Figure 3.3.5

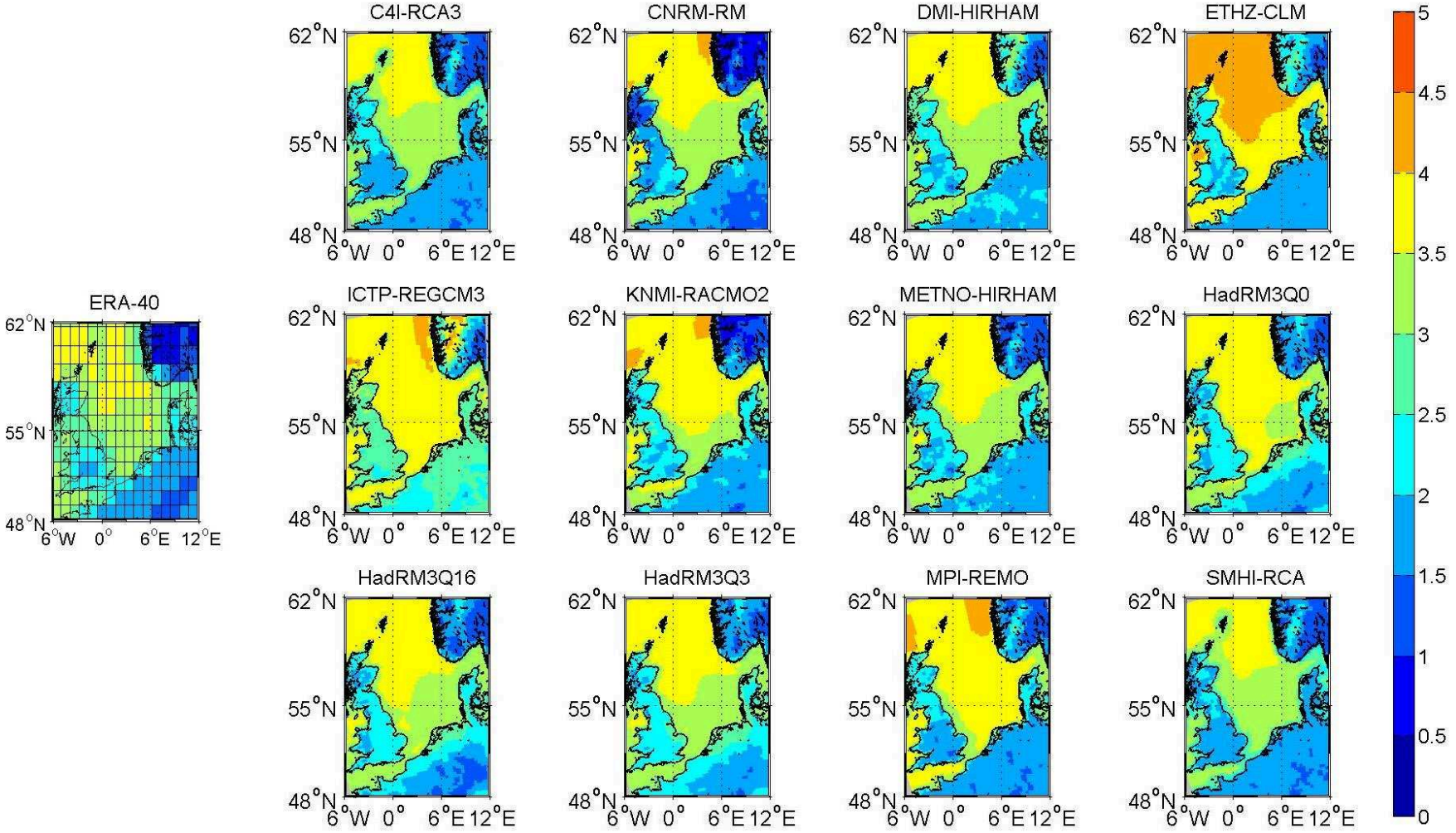

Figure 3.3.7: Standard deviation of wind speed [m/s] in the North Sea area for the period 1971-2000: ERA-40 (left) and the ENSEMBLES regional models (right)

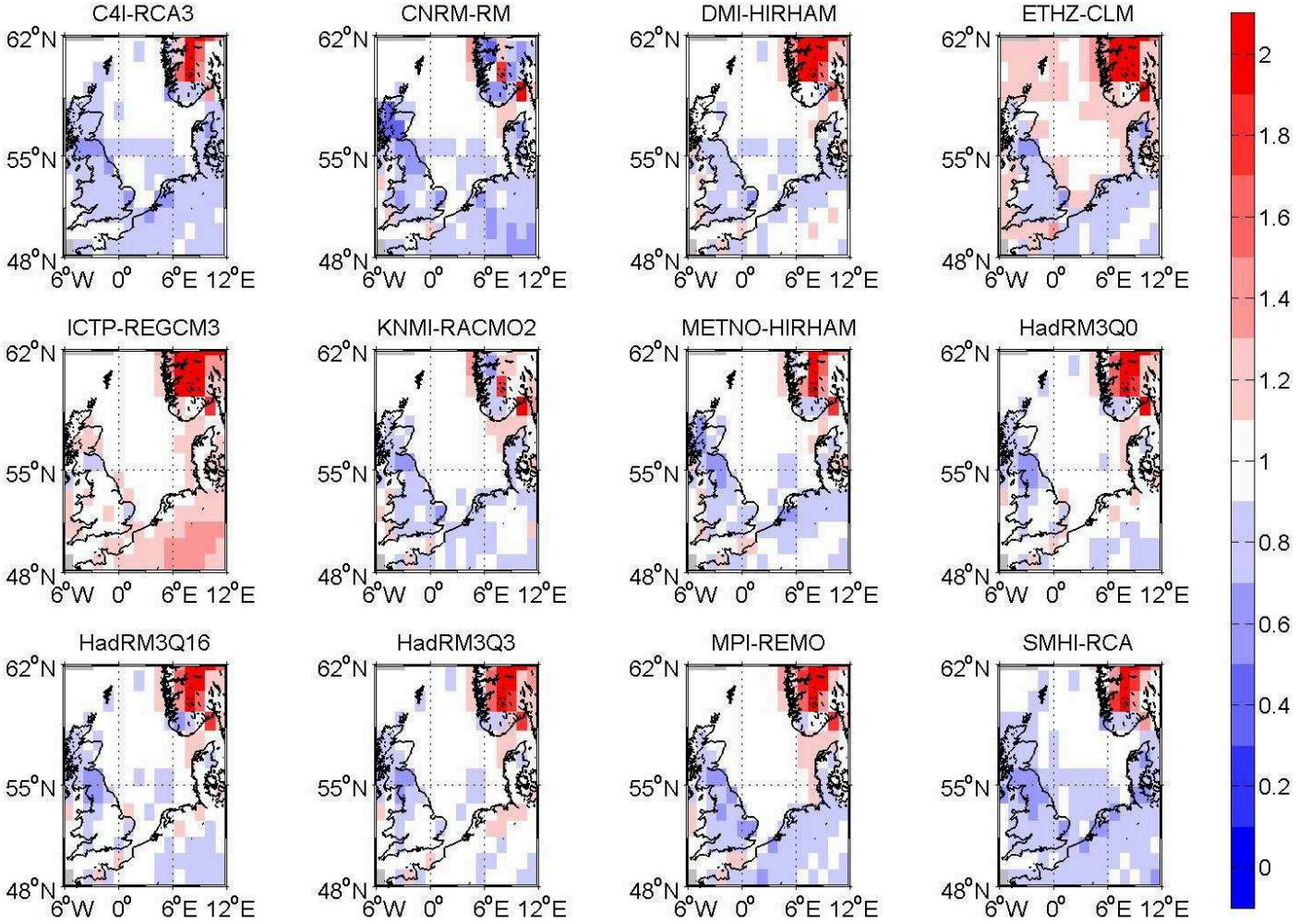

Figure 3.3.8: Ratio of standard deviations of wind speed: RCMs / ERA-40 from Fig. 3.3.7

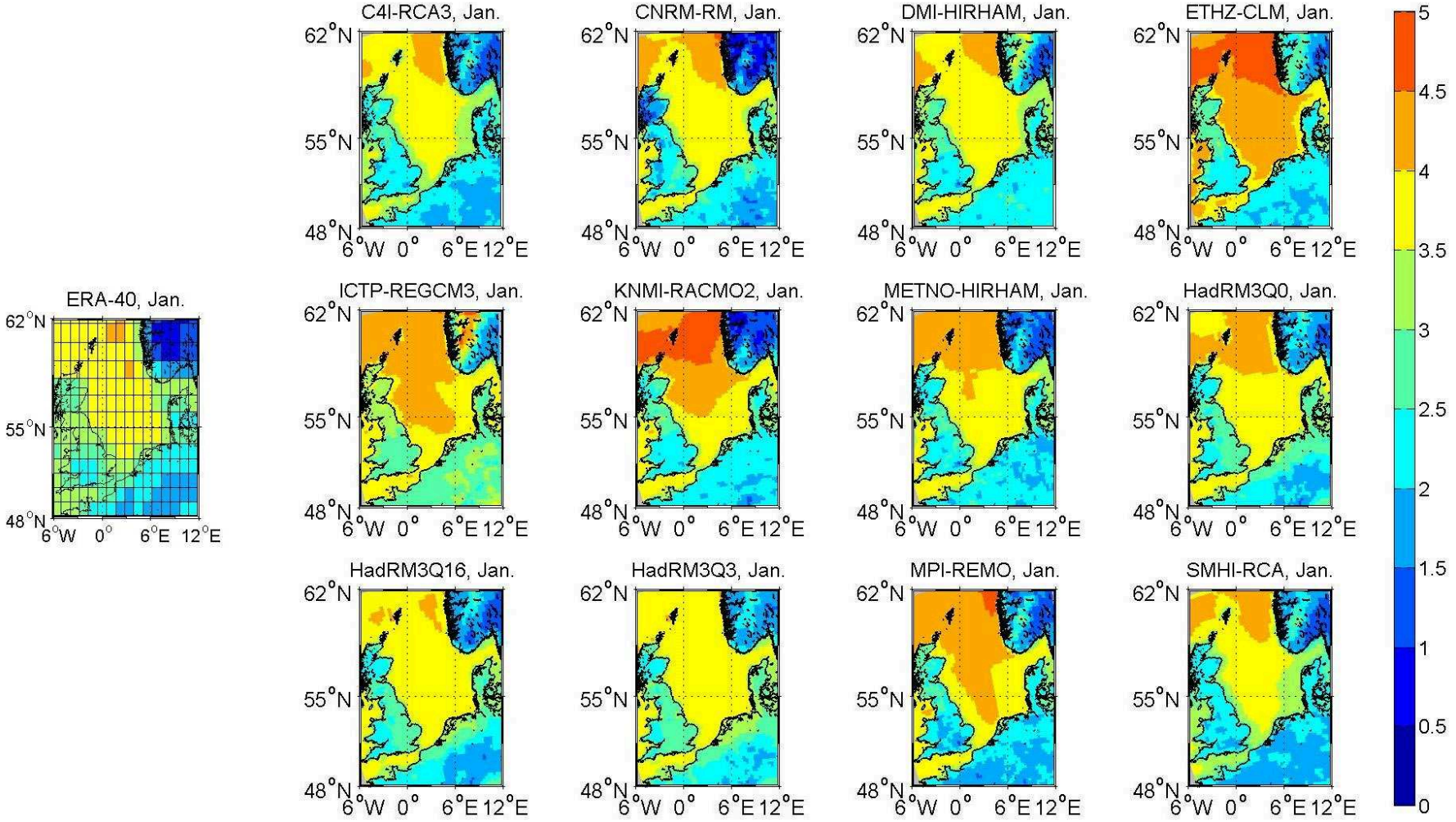

Figure 3.3.9: January standard deviation of wind speed [m/s] in the North Sea area for the period 1971-2000: ERA-40 (left) and the ENSEMBLES regional models (right)

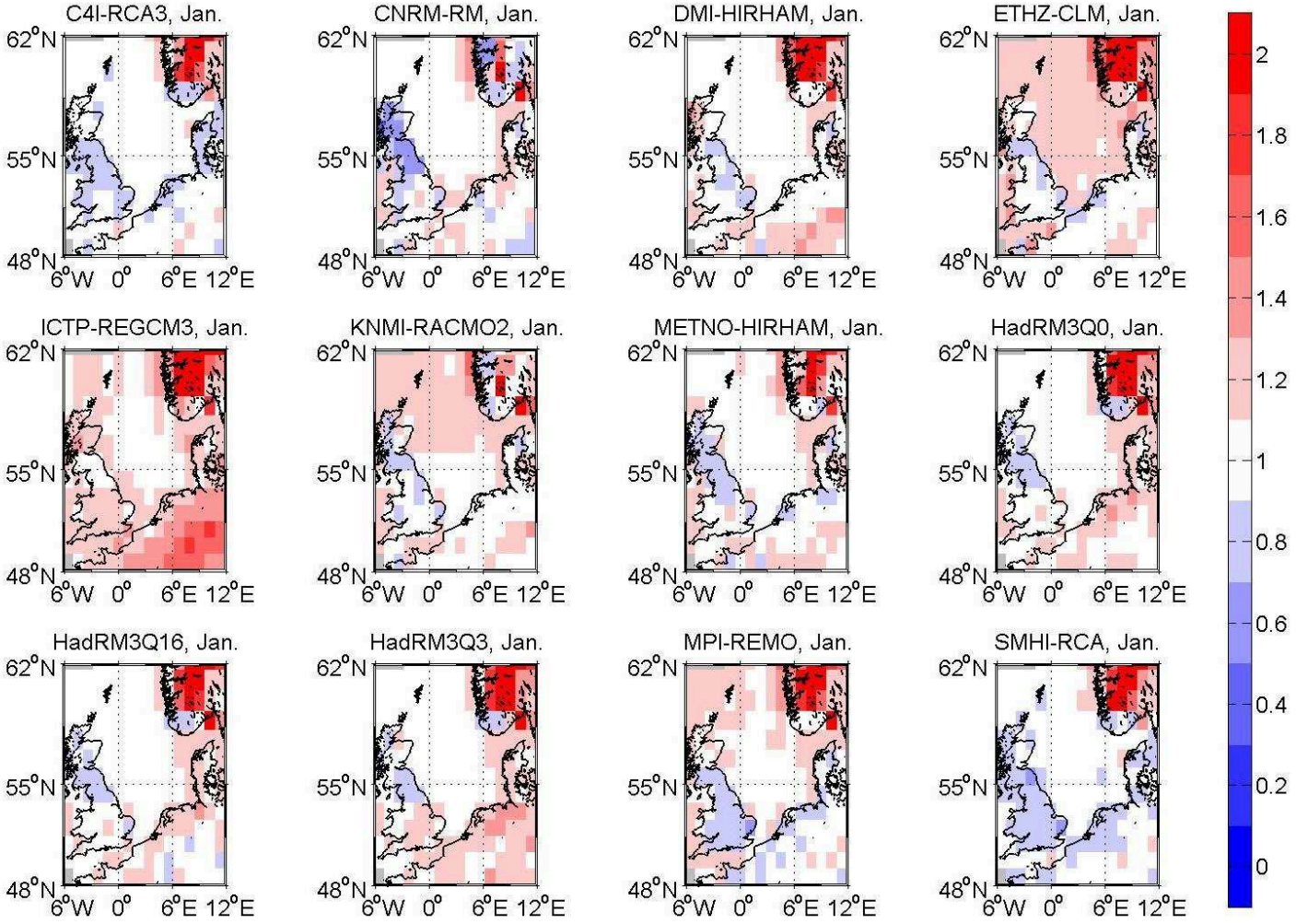

Figure 3.3.10: January ratio of standard deviations of wind speed: RCMs / ERA-40 from Fig. 3.3.9. Values are higher than 2.0 in red coloured areas in Norway

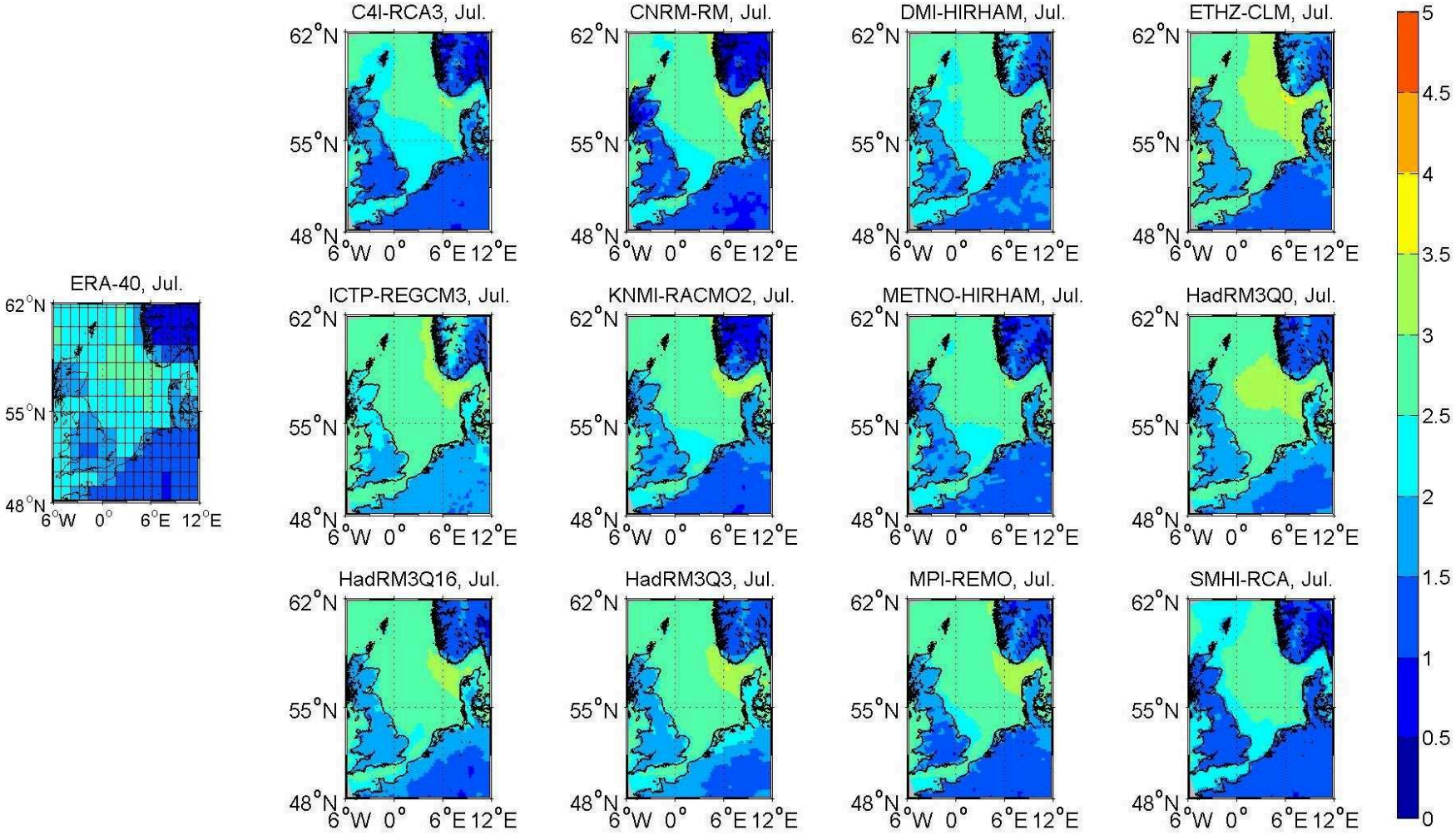

Figure 3.3.11: July standard deviation of wind speed [m/s] in the North Sea area for the period 1971-2000: ERA-40 (left) and the ENSEMBLES regional models (right)

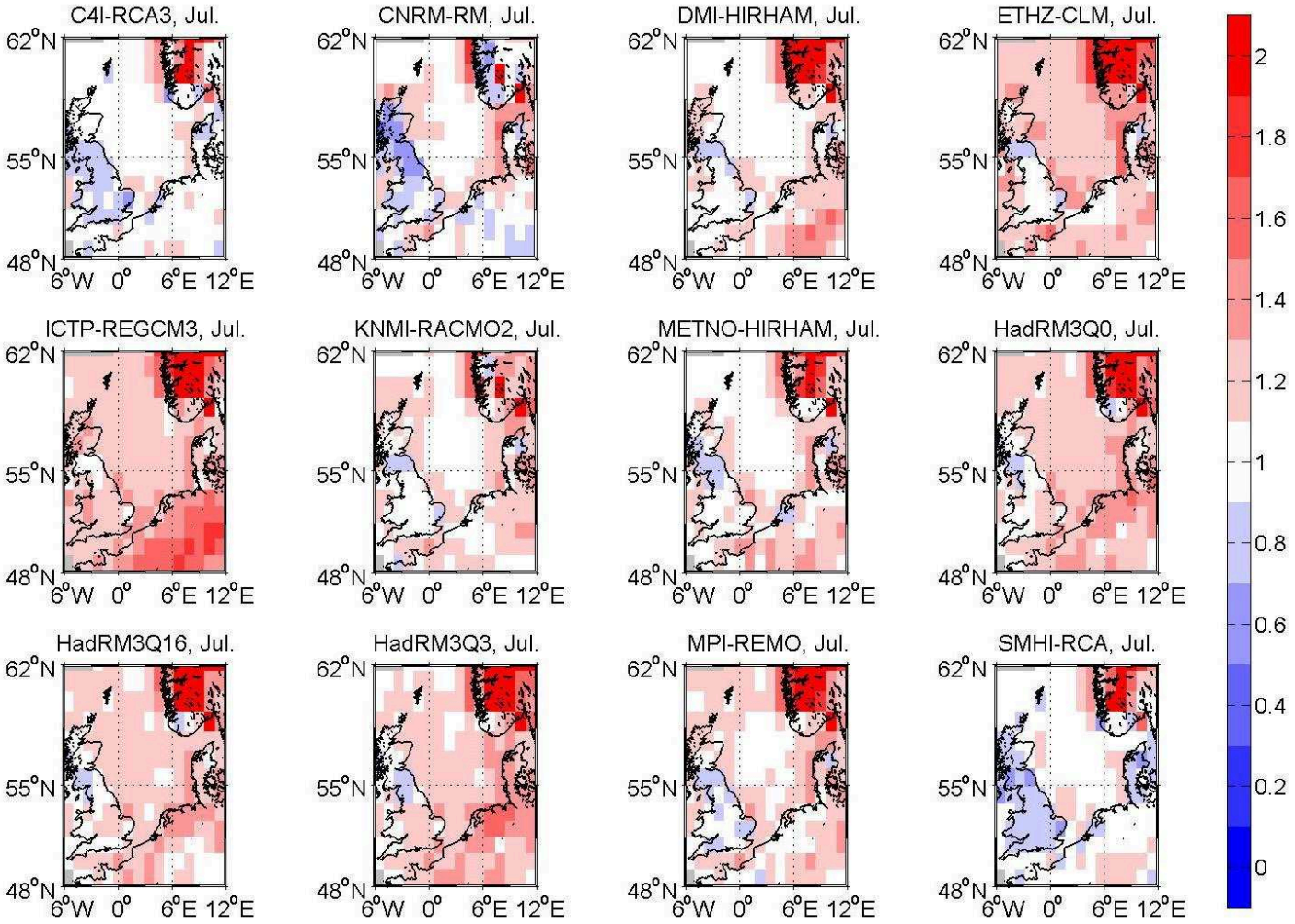

Figure 3.3.12: July ratio of standard deviations of wind speed: RCMs / ERA-40 from Fig. 3.3.11. Values are higher than 2.0 in red coloured areas in Norway

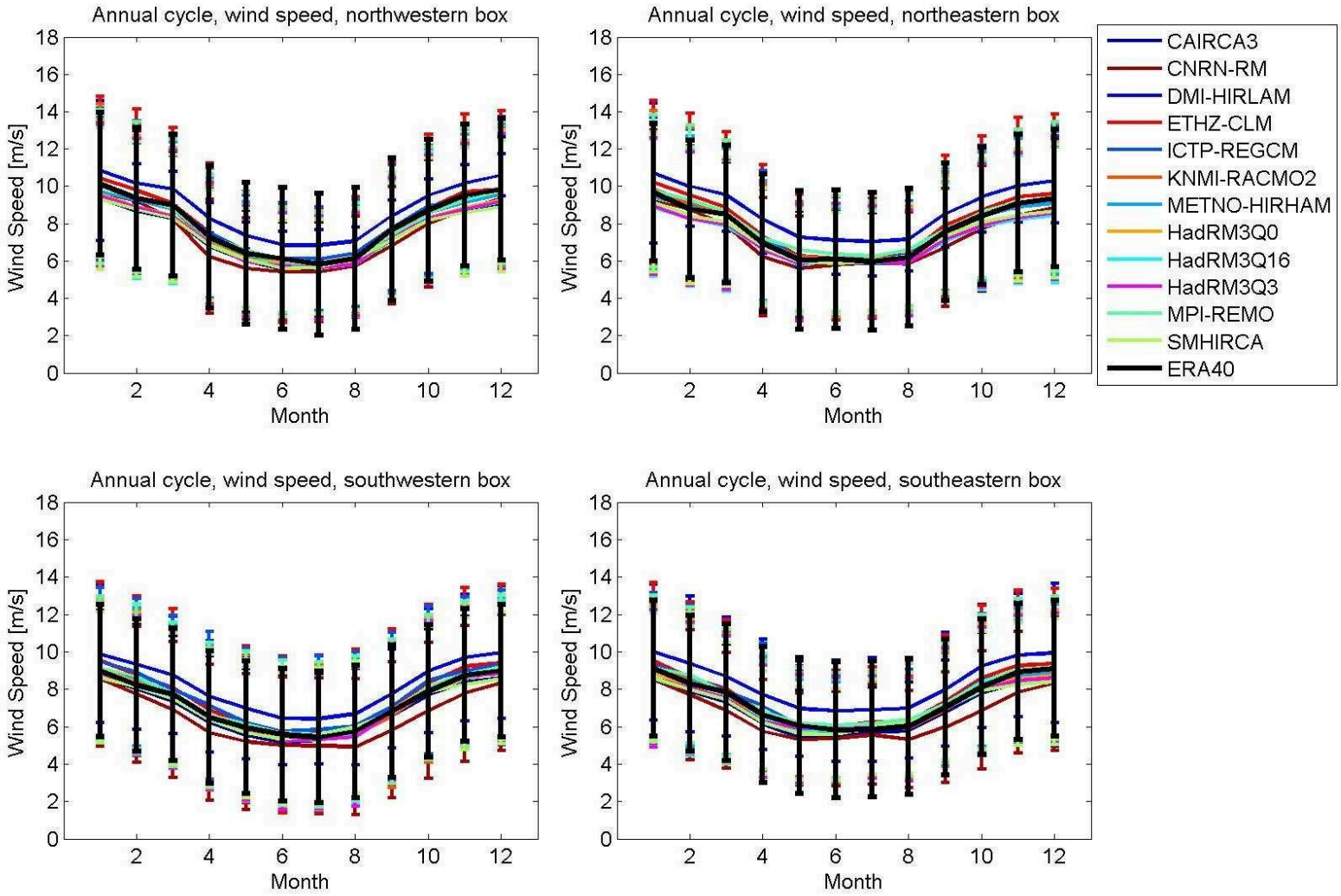

Figure 3.3.13: Annual cycles of wind speed [m/s] of the ENSEMBLES RCMs and ERA-40 in the four North Sea boxes for the period of 1971-2000

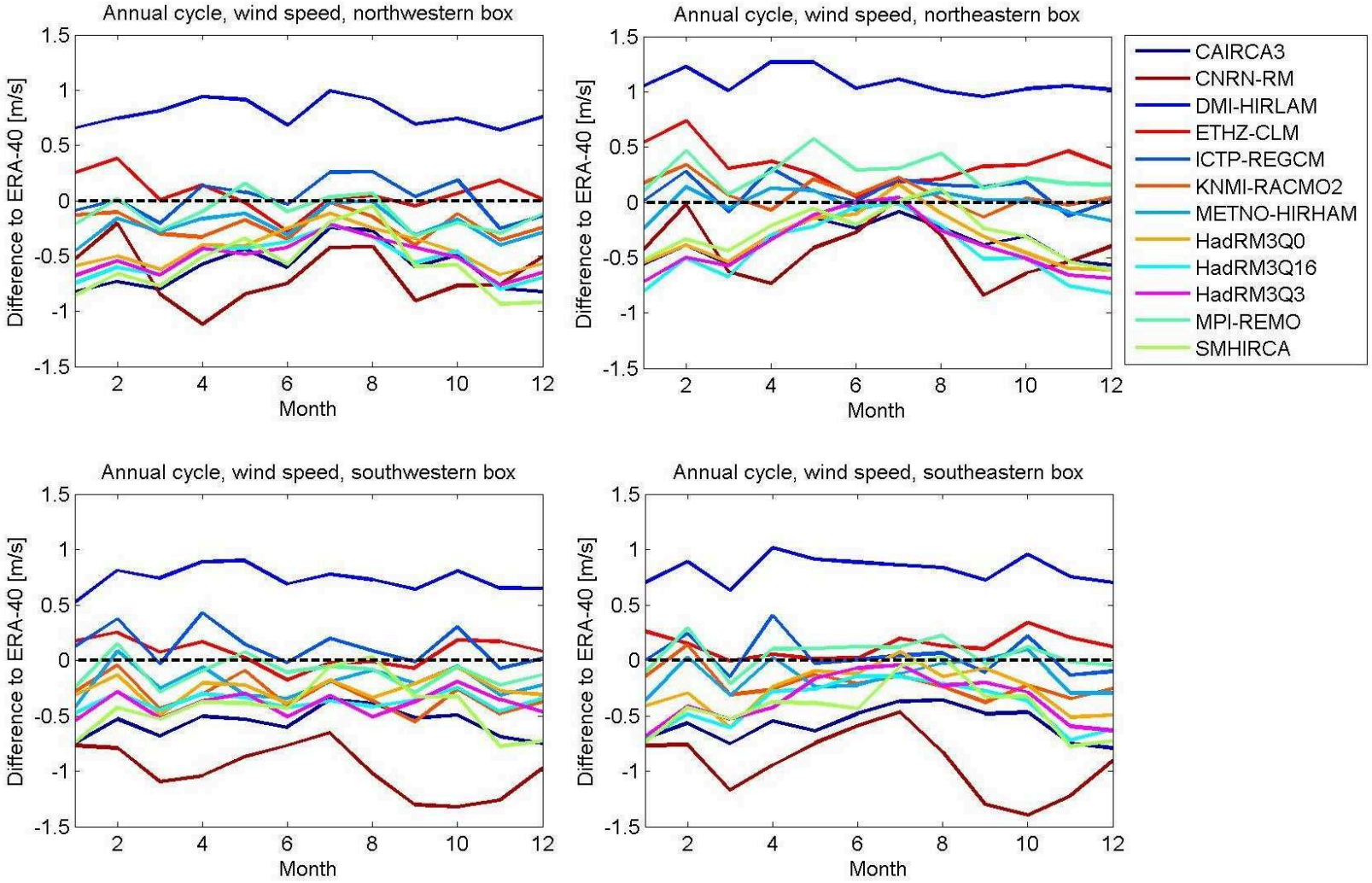

Figure 3.3.14: Difference of annual cycles of wind speed [m/s] of the ENSEMBLES RCMs minus ERA-40 in the four North Sea boxes for the period of 1971-2000

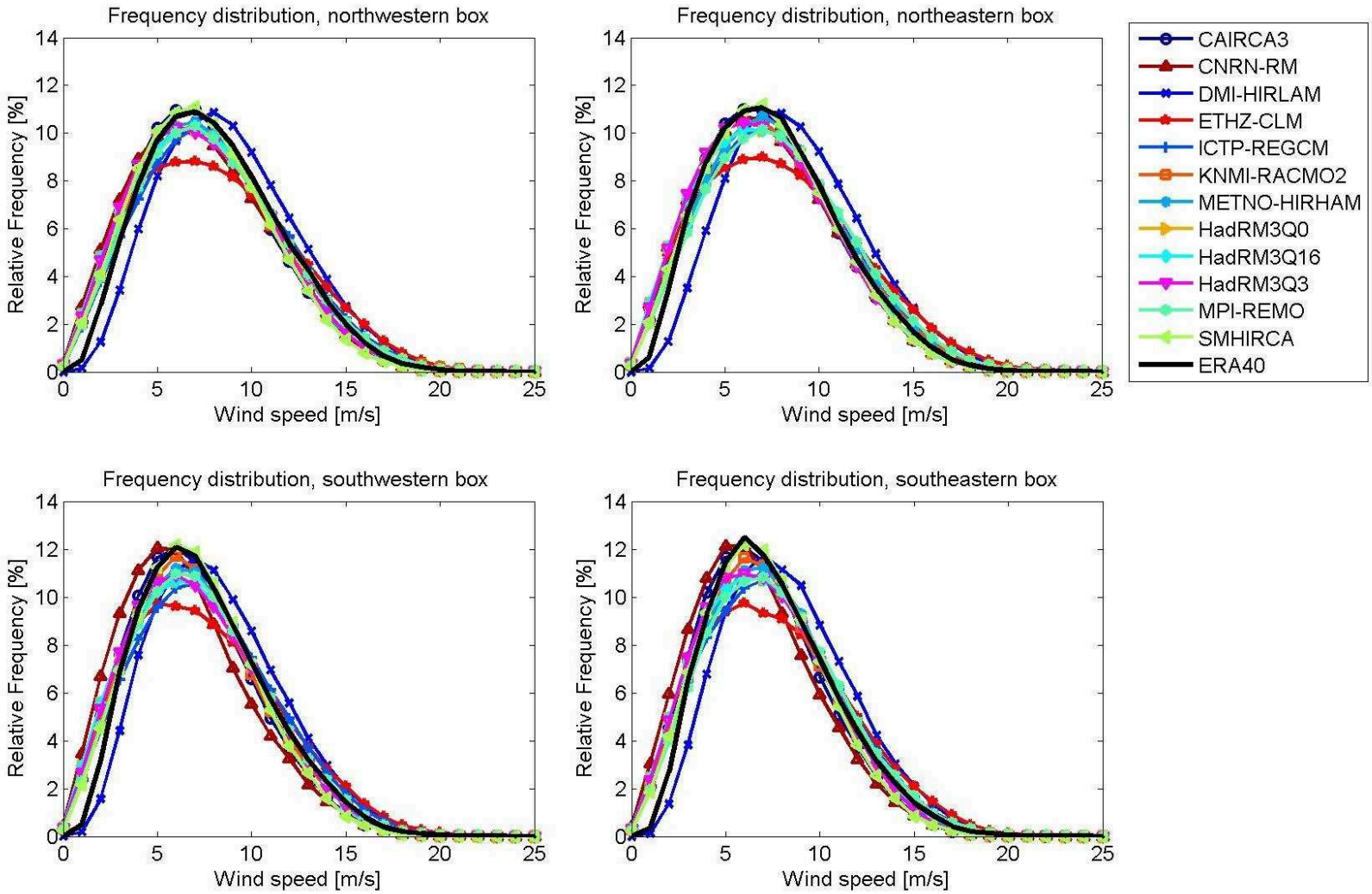

Figure 3.3.15: Relative frequency distribution of wind speed [%] of the ENSEMBLES RCMs and ERA-40 in the four North Sea boxes for the period of 1971-2000. X-axis does not show whole range of possible wind speeds, to enhance details for smaller wind speeds. Maximum wind speed of all models, days and grid points in the four areas is 29.12 m/s

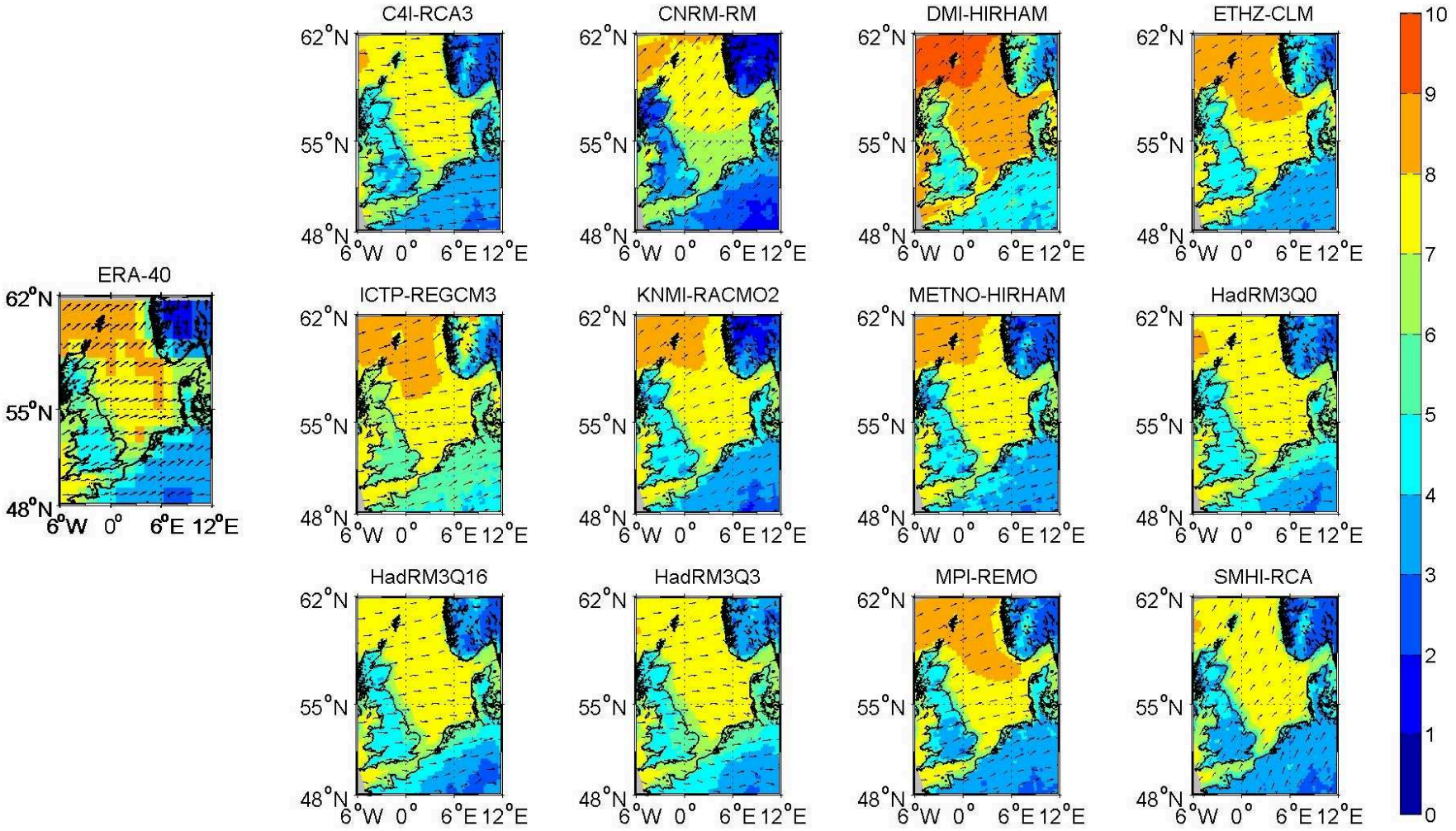

Figure 3.4.1: Mean wind speed [m/s] and mean wind directions (arrows) in the North Sea area for the period 1971-2000: ERA-40 (left) and the ENSEMBLES regional models (right). Length of arrows is standardised

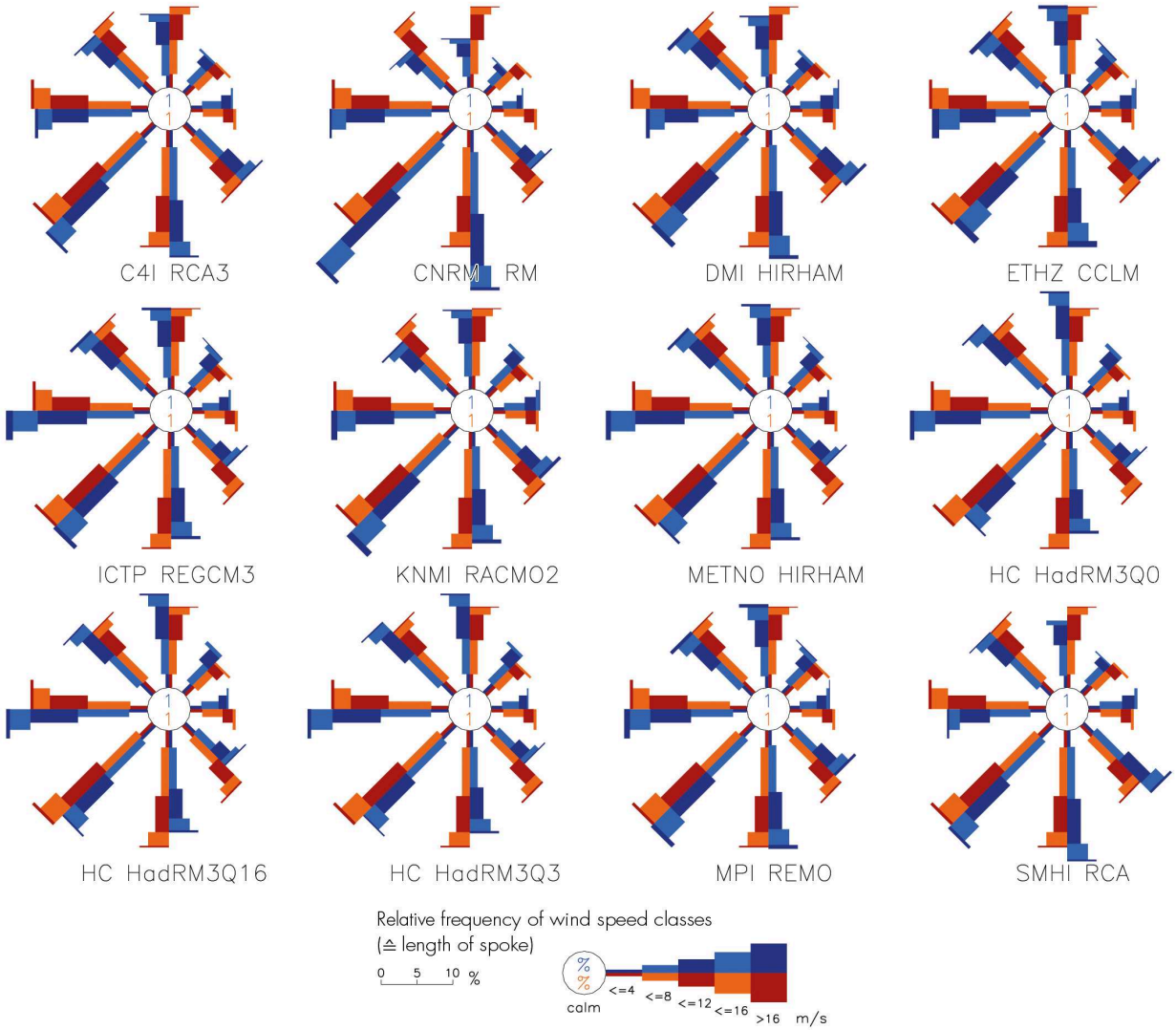

Figure 3.4.2: Wind roses from ERA-40 data (orange) compared to RCM-data (blue) in the northwestern area of the North Sea area for the period 1971-2000. Length of each branch is related to the frequency of occurrence of the respective wind direction, see legend for relation between frequencies and lengths. Width of each branch broadens with increasing speed range. Numbers in circles denote frequencies of calm winds

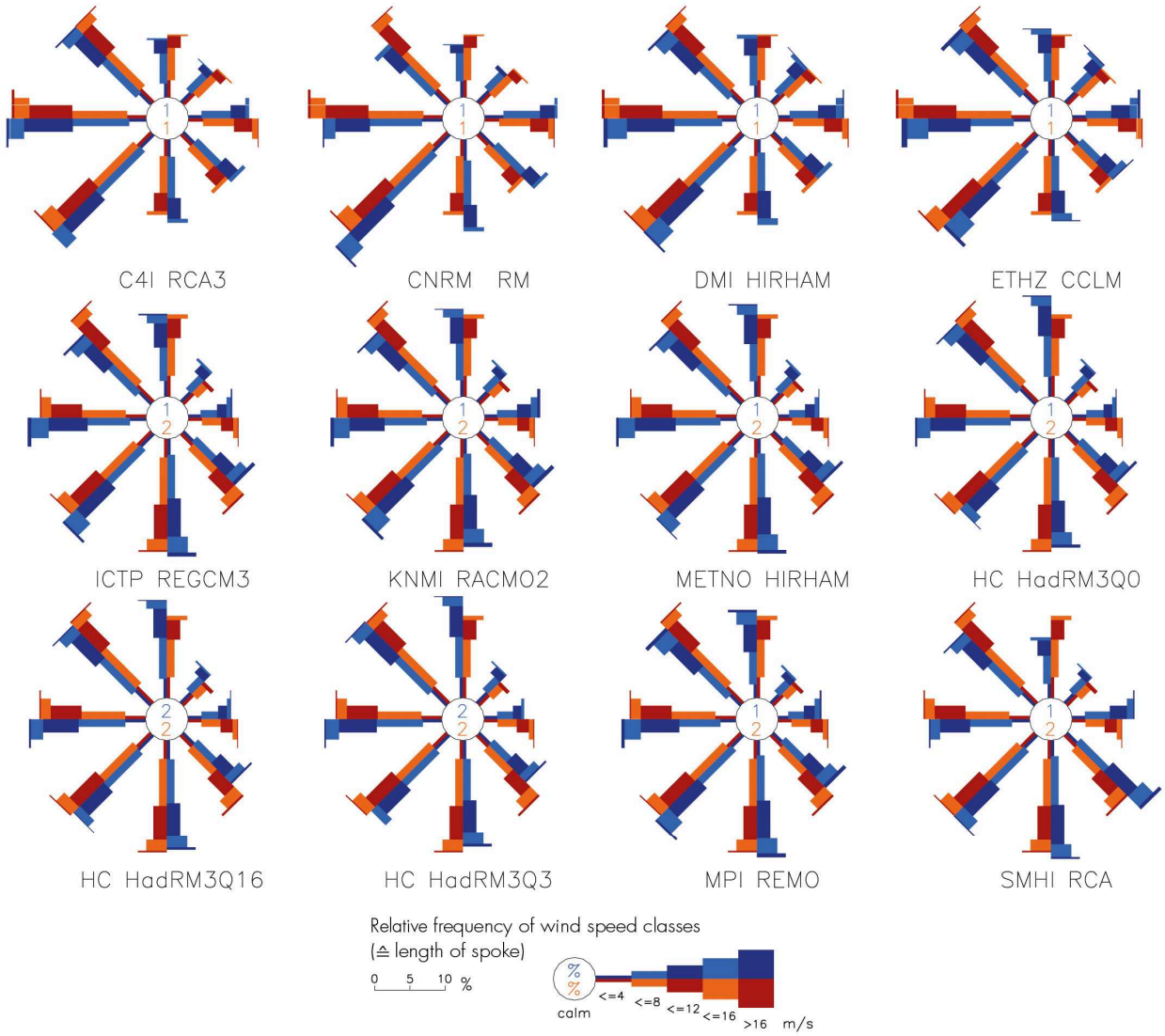

Figure 3.4.3: Wind roses from ERA-40 data (orange) compared to RCM-data (blue). Same as Fig. 3.4.2, but for the northeastern area of the North Sea area

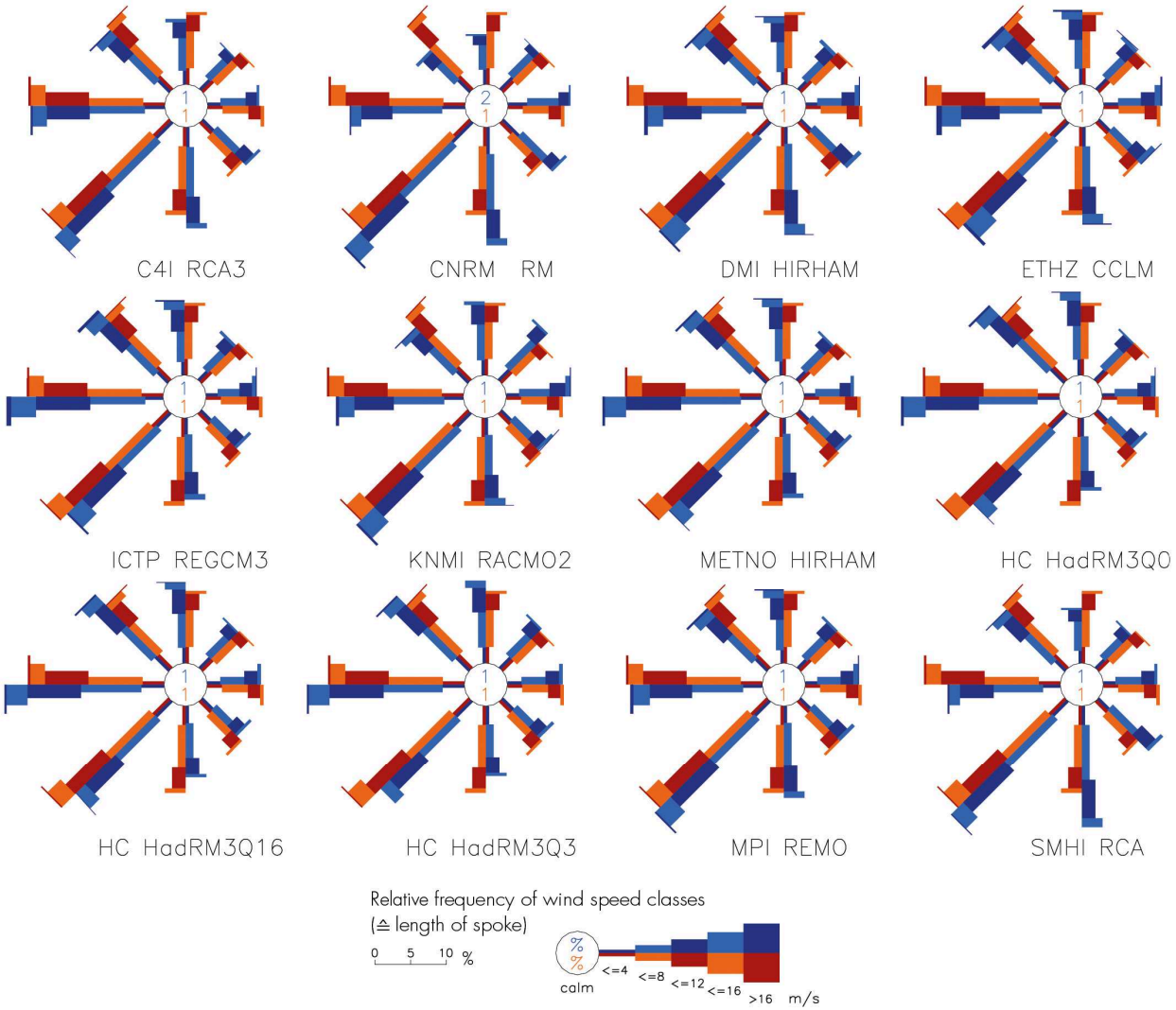

Figure 3.4.4: Wind roses from ERA-40 data (orange) compared to RCM-data (blue). Same as Fig. 3.4.2, but for the southwestern area of the North Sea

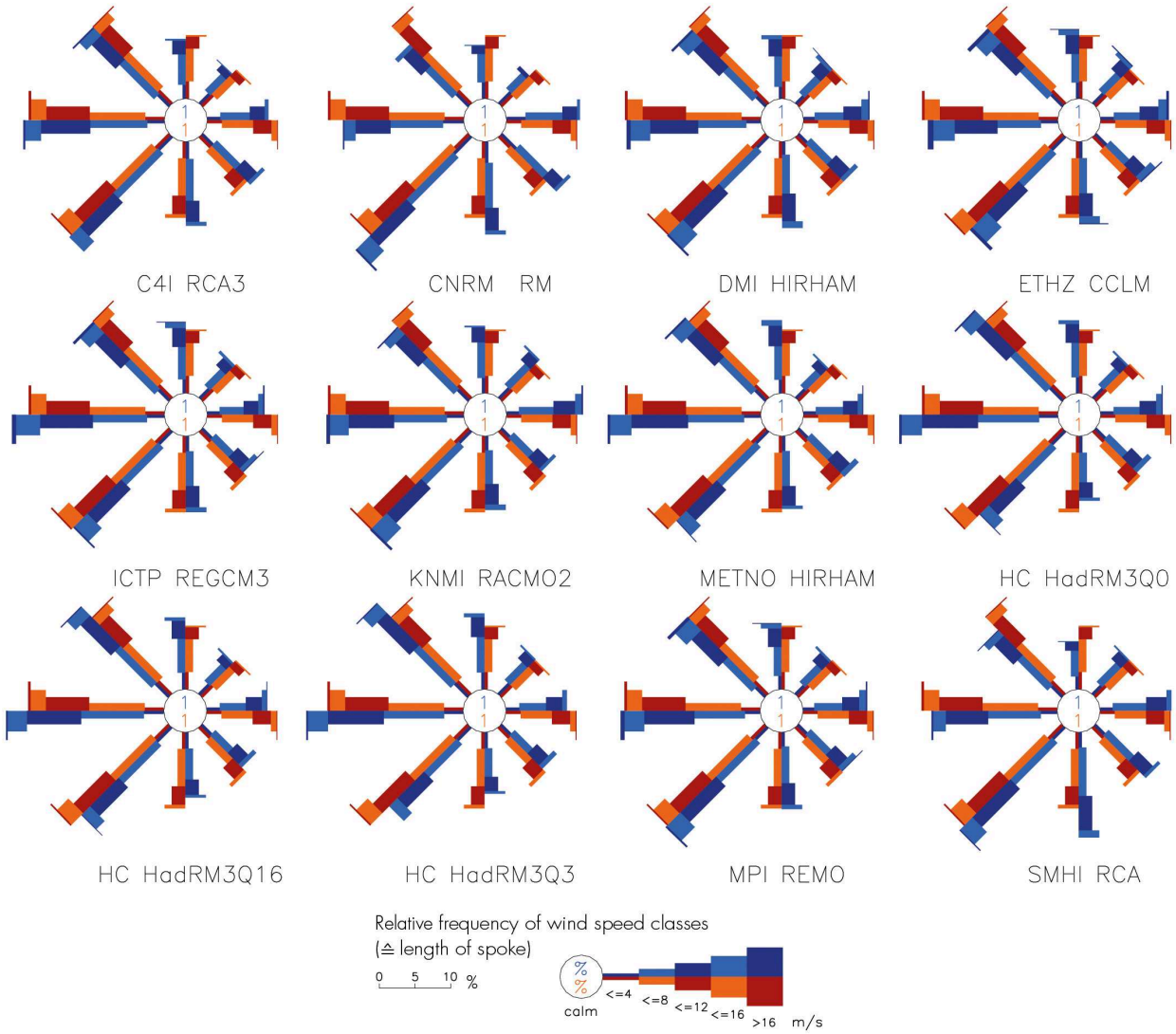

Figure 3.4.5: Wind roses from ERA-40 data (orange) compared to RCM-data (blue). Same as Fig. 3.4.2, but for the southeastern area of the North Sea

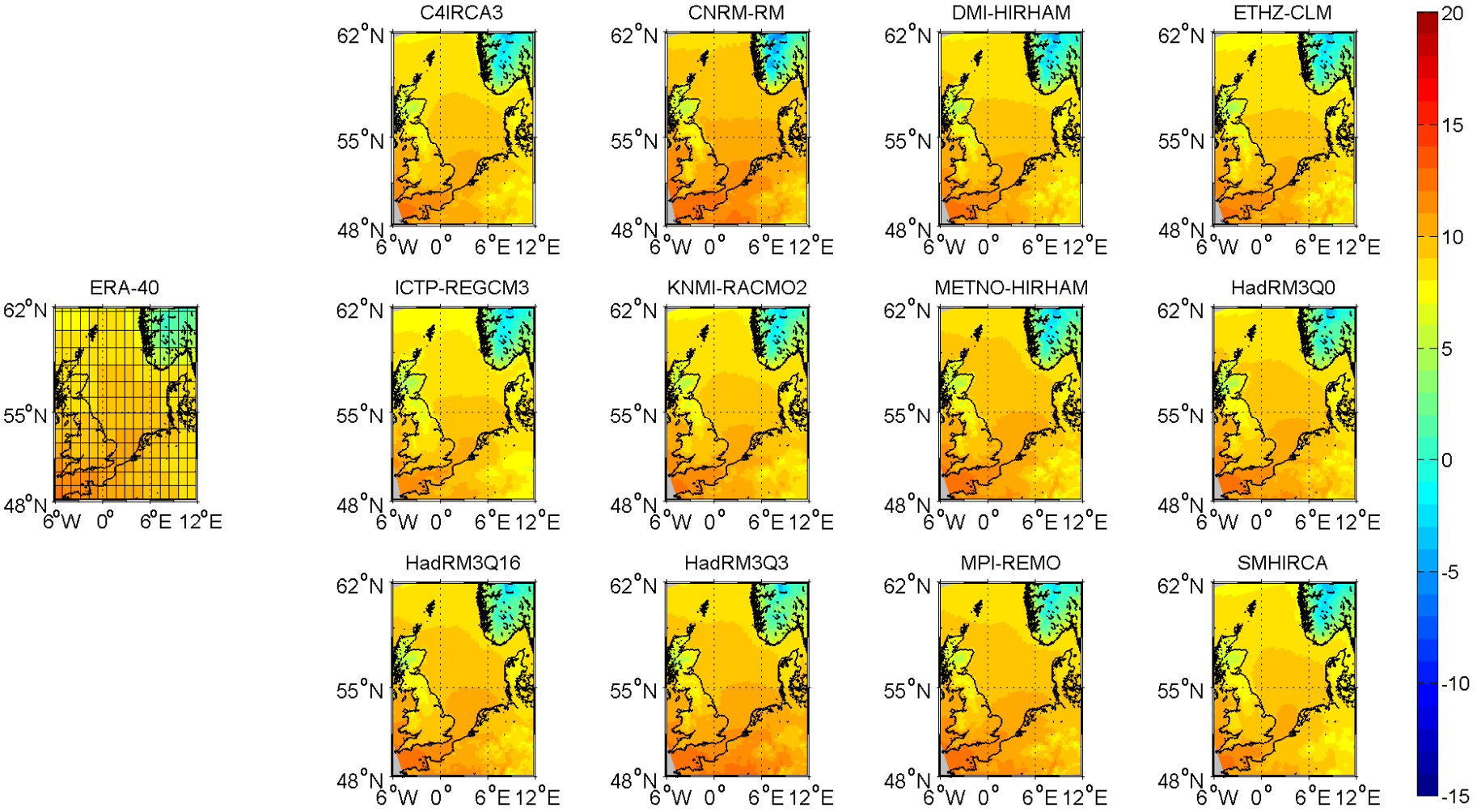

Figure 3.5.1: Mean 2 m air temperatures [°C] in the North Sea area for the period 1971-2000: ERA-40 (left) and the ENSEMBLES regional models (right)

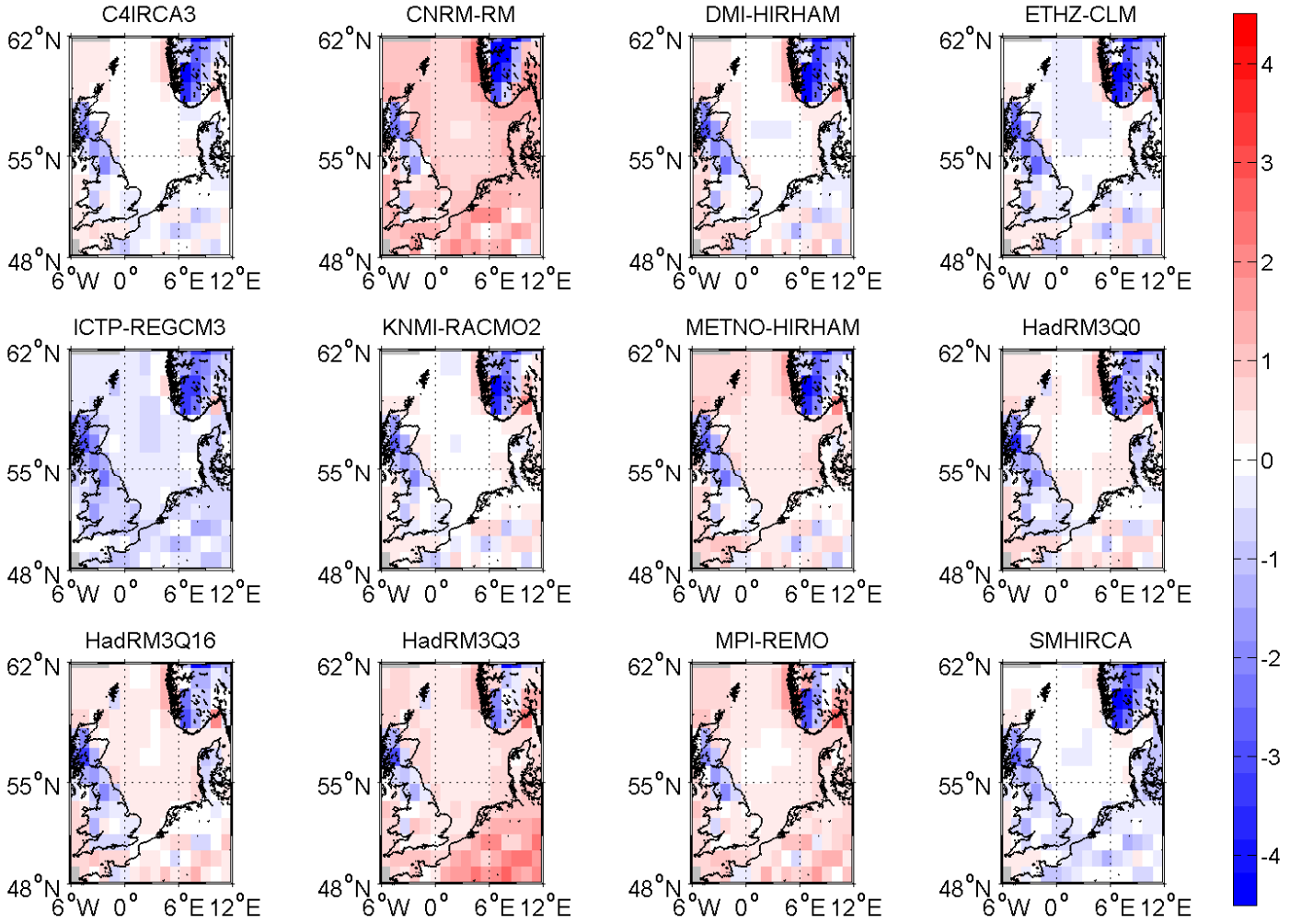

Figure 3.5.2: Differences of 2 m air temperatures [K]: RCMs minus ERA-40 from Fig. 3.5.1

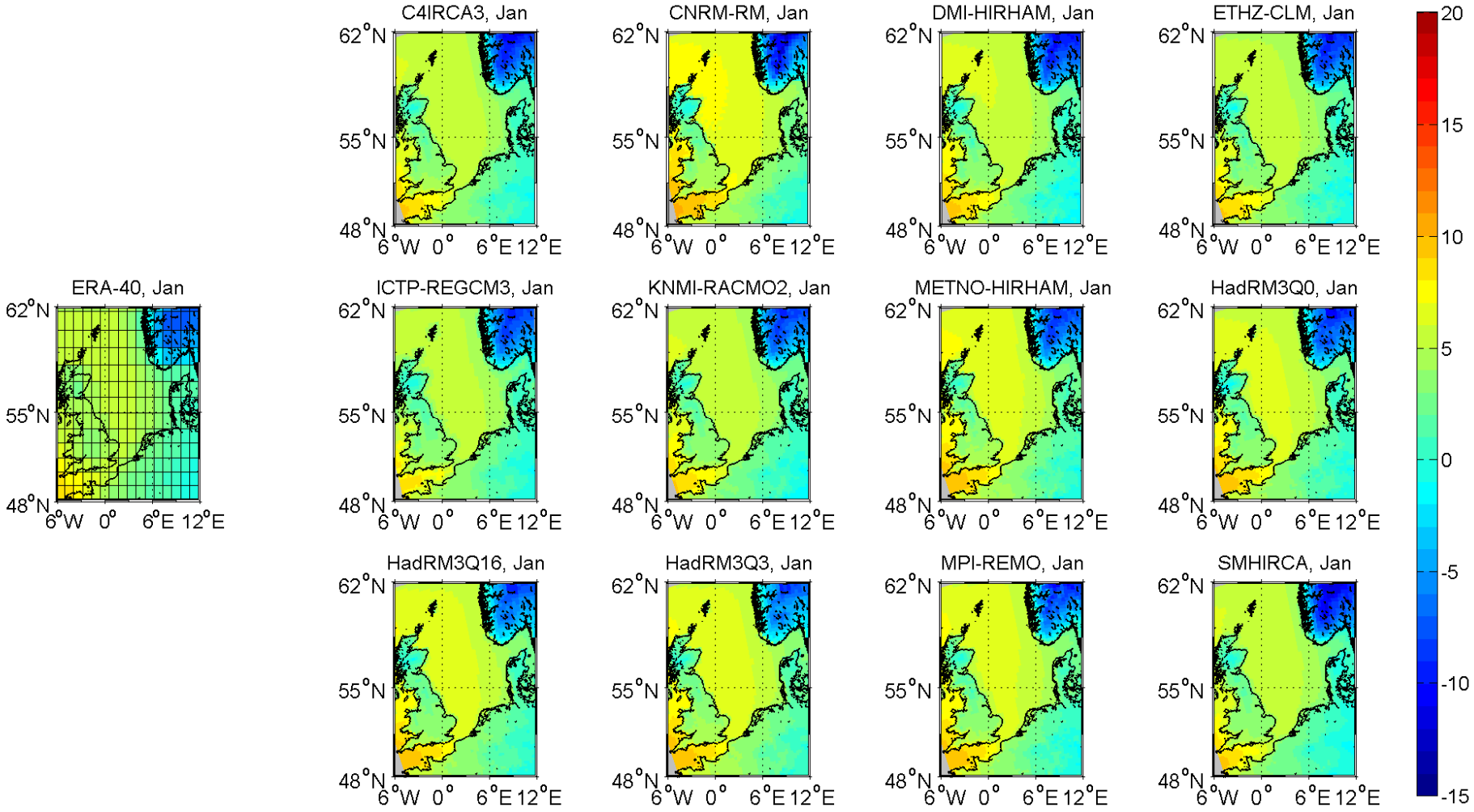

Figure 3.5.3: January mean 2m air temperatures [°C] in the North Sea area for the period 1971-2000: ERA-40 (left) and the ENSEMBLES regional models (right)

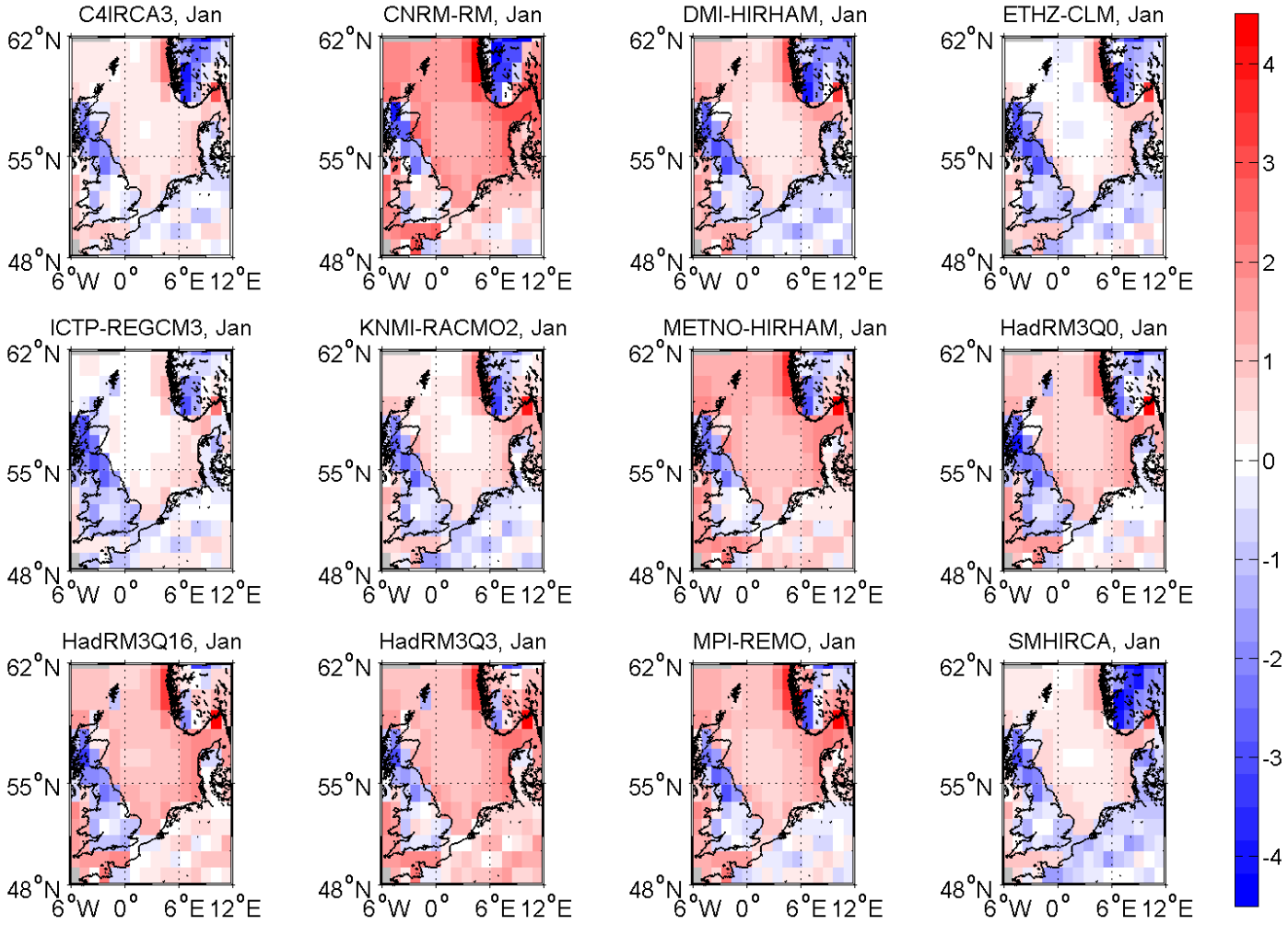

Figure 3.5.4: January differences of 2 m air temperatures [K]: RCMs minus ERA-40 from Fig. 3.5.3

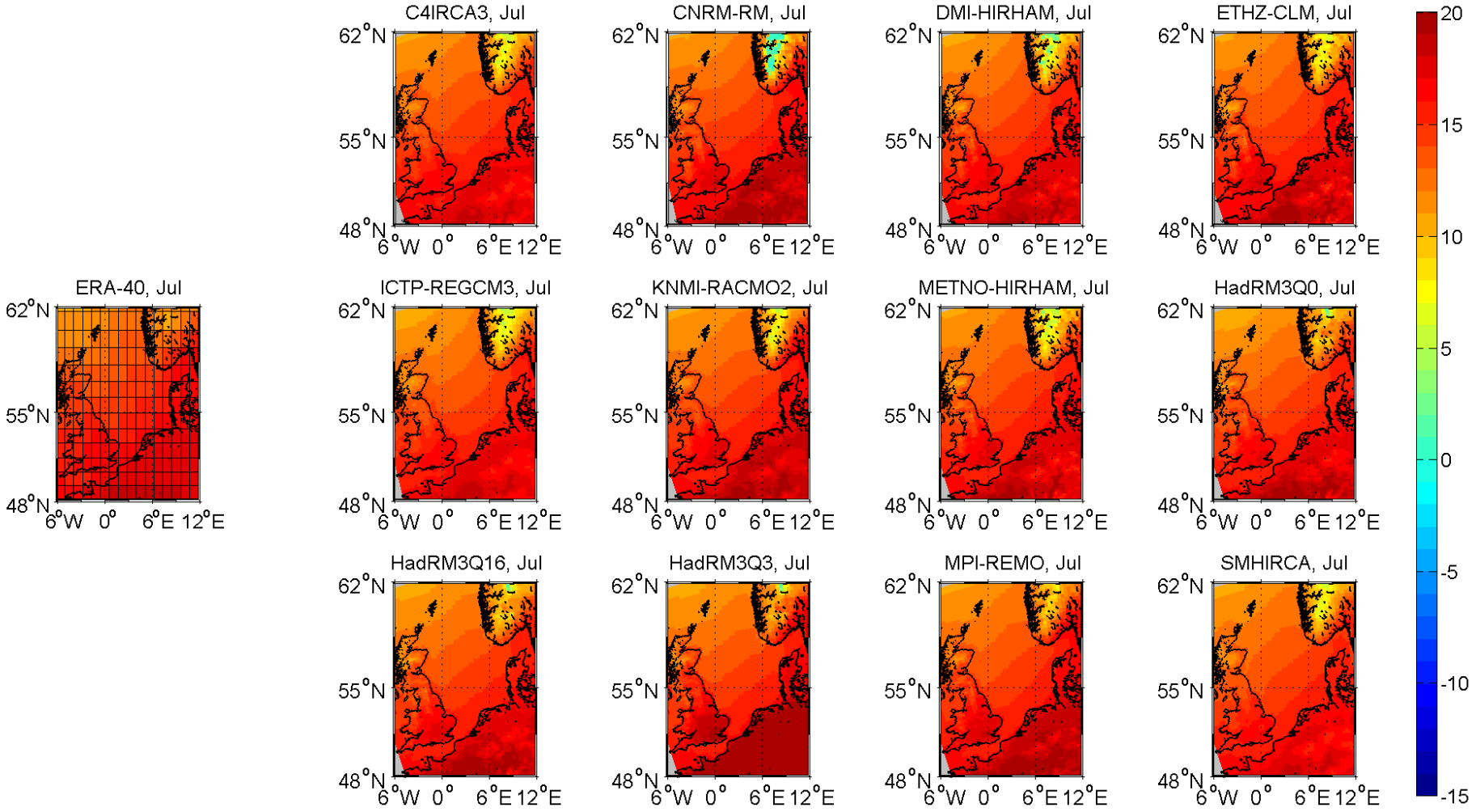

Figure 3.5.5: July mean 2 m air temperatures [°C] in the North Sea area for the period 1971-2000: ERA-40 (left) and the ENSEMBLES regional models (right)

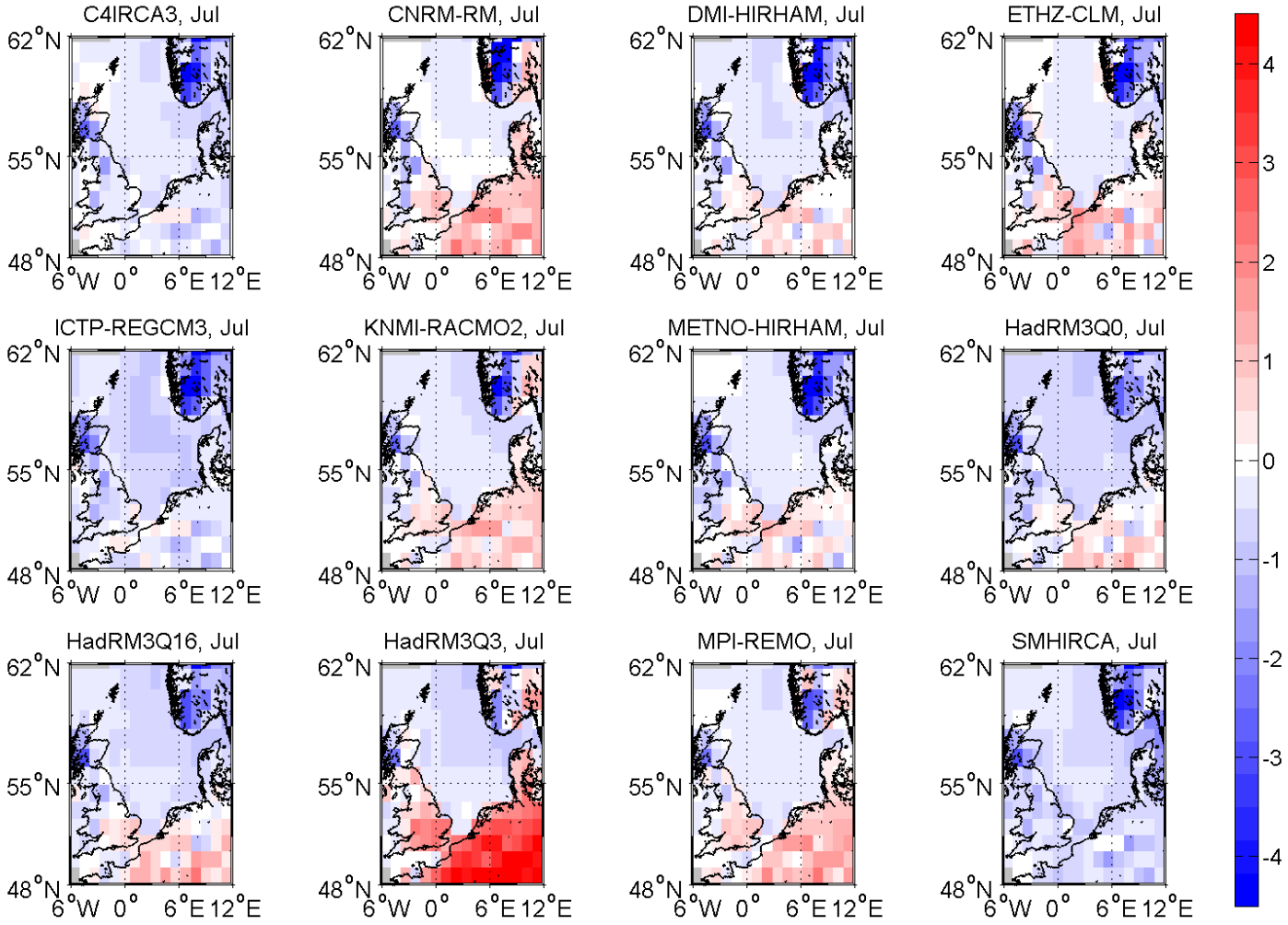

Figure 3.5.6: July differences of 2 m air temperatures [K]: RCMs minus ERA-40 from Fig. 3.5.5

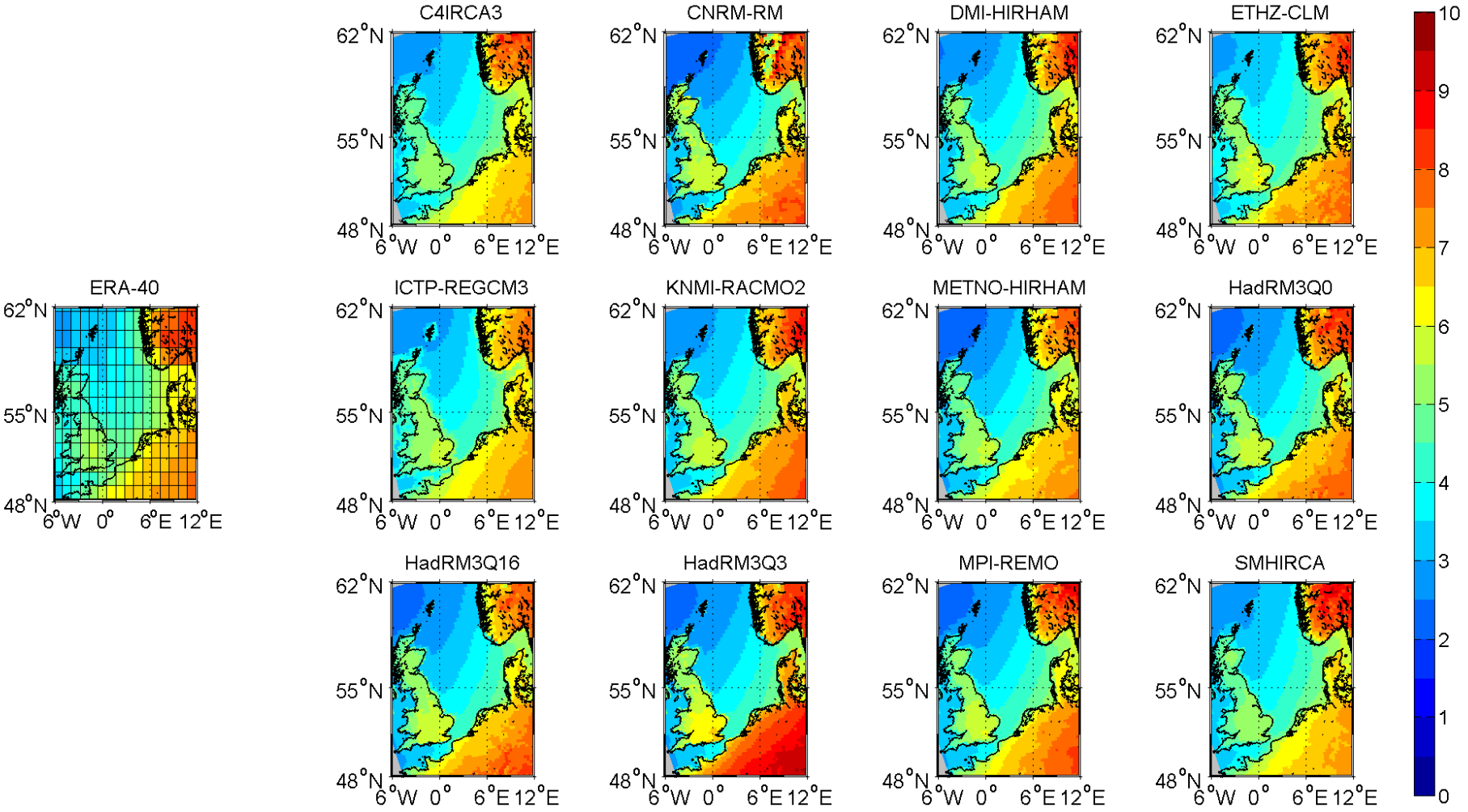

Figure 3.5.7: Standard deviation of 2 m air temperatures [K] in the North Sea area for the period 1971-2000: ERA-40 (left) and the ENSEMBLES regional models (right)

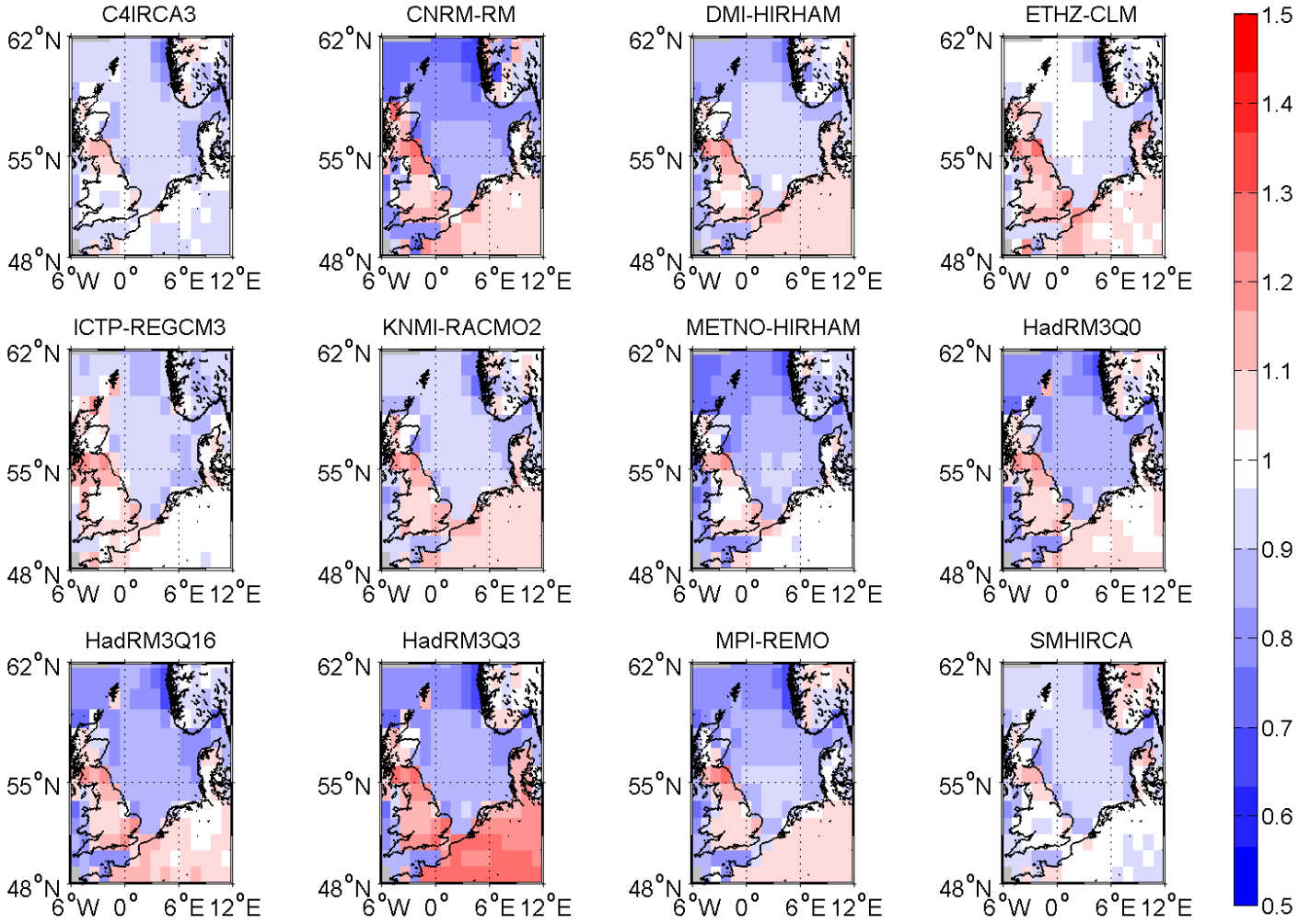

Figure 3.5.8: Ratio of standard deviations of 2 m air temperatures: RCMs / ERA-40 from Fig. 3.5.7

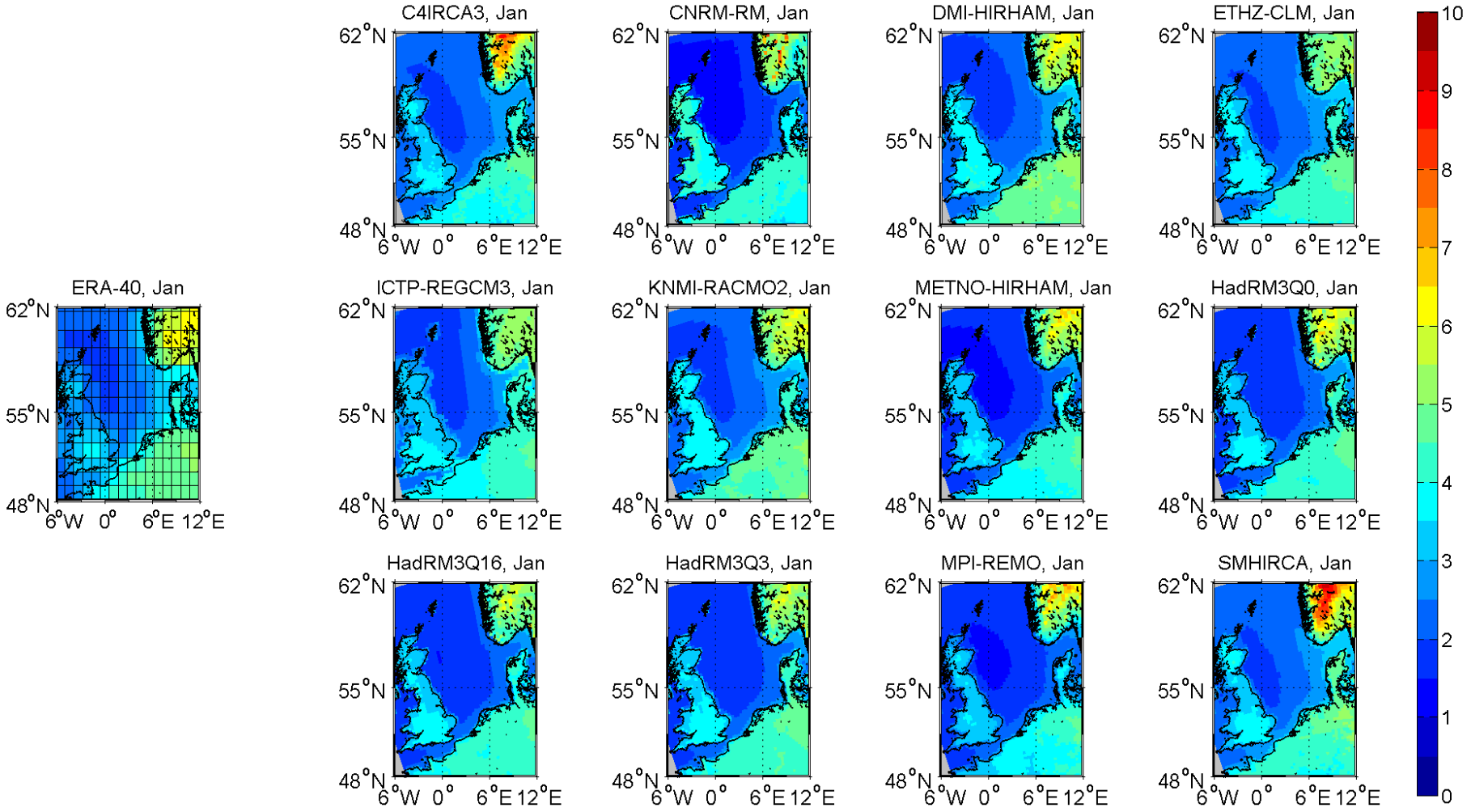

Figure 3.5.9: January standard deviations of 2 m air temperatures [K] in the North Sea area for the period 1971-2000: ERA-40 (left) and the ENSEMBLES regional models (right)

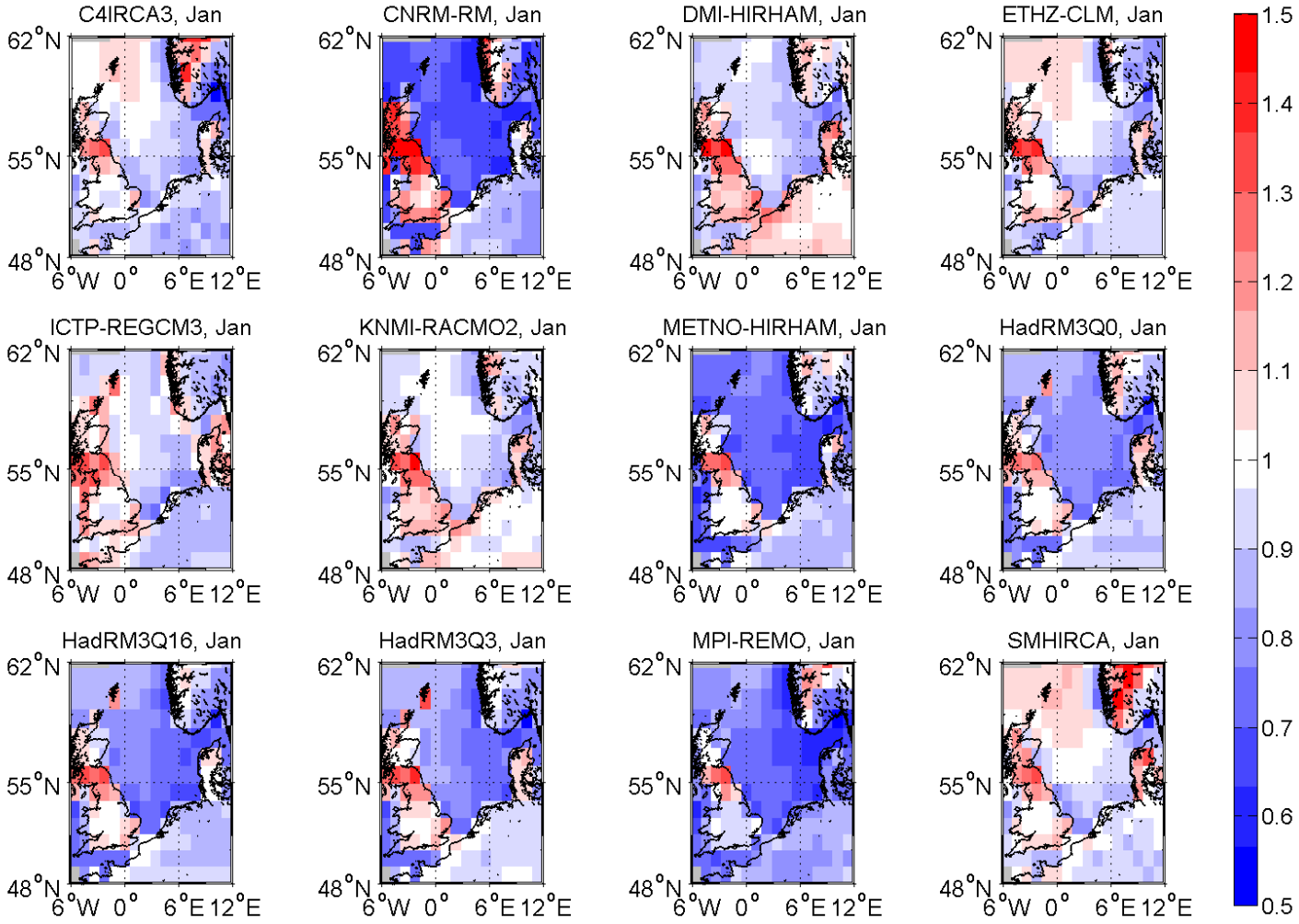

Figure 3.5.10: January ratio of standard deviations of 2 m air temperatures: RCMs / ERA-40 from Fig. 3.5.9

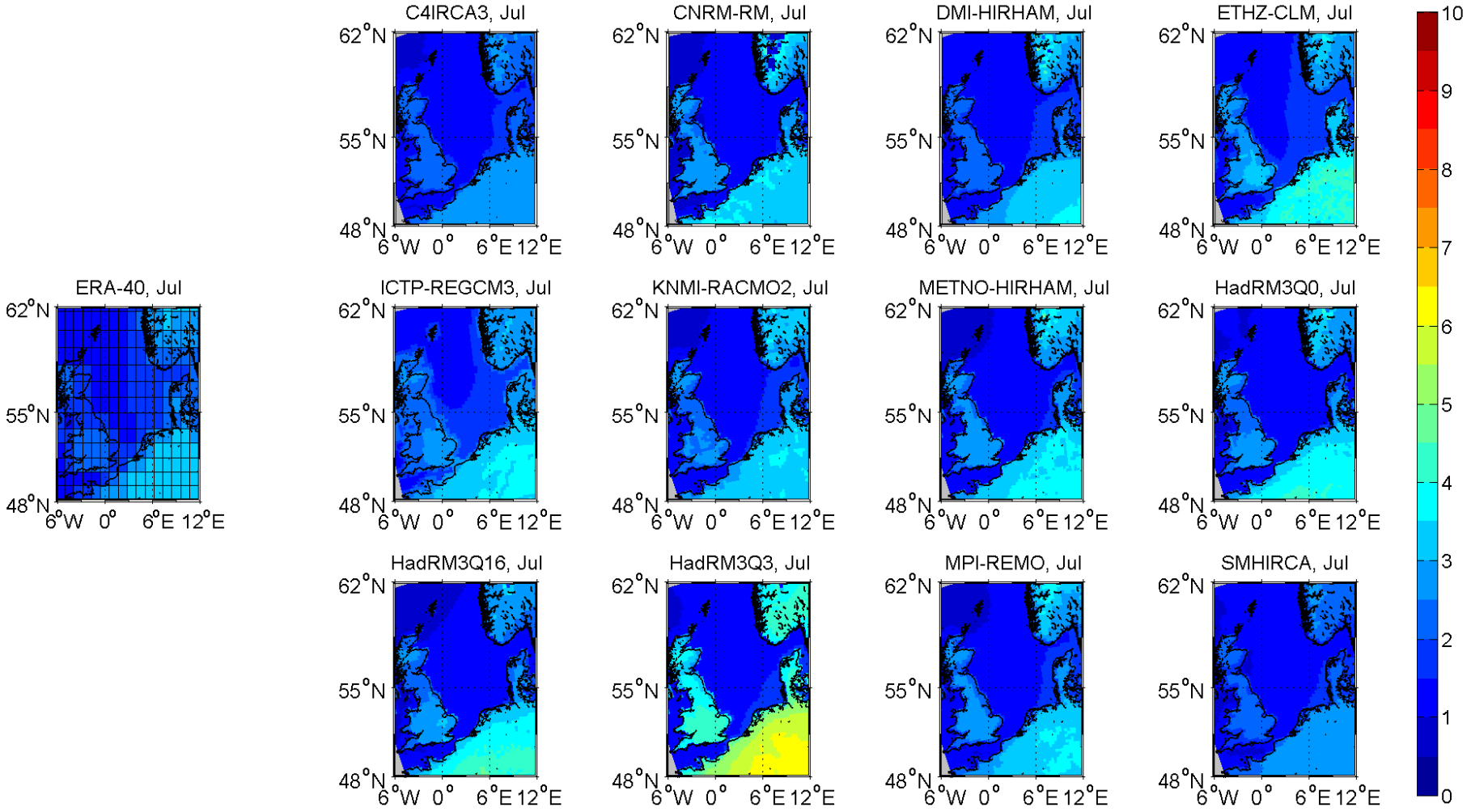

Figure 3.5.11: July standard deviation of 2 m air temperature [K] in the North Sea area for the period 1971-2000: ERA-40 (left) and the ENSEMBLES regional models (right)

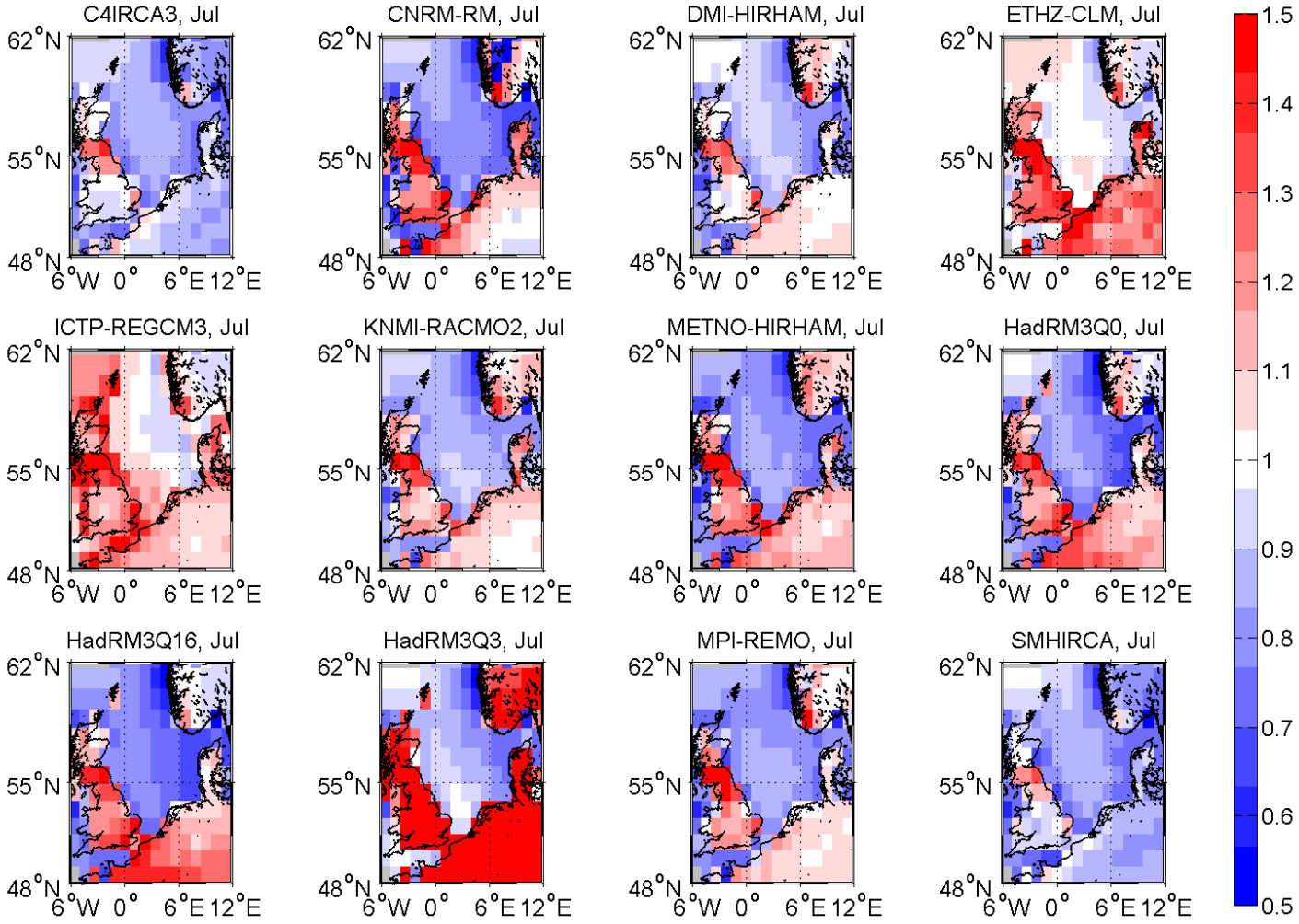

Figure 3.5.12: July ratio of standard deviations of 2 m air temperatures: RCMs / ERA-40 from Fig. 3.5.11

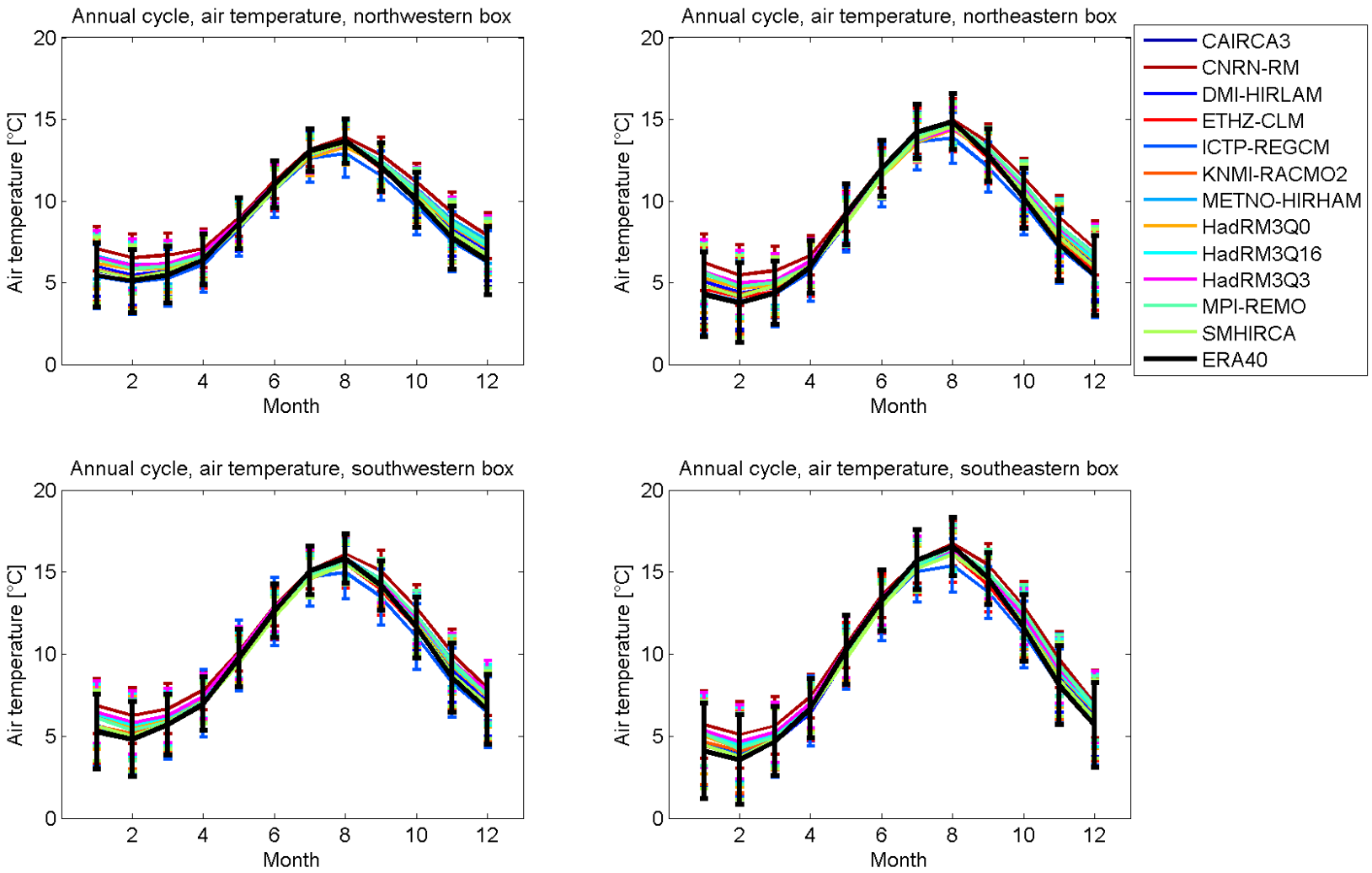

Figure 3.5.13: Annual cycles of 2 m air temperatures [°C] of the ENSEMBLES RCMs and ERA-40 in the four North Sea boxes for the period of 1971-2000

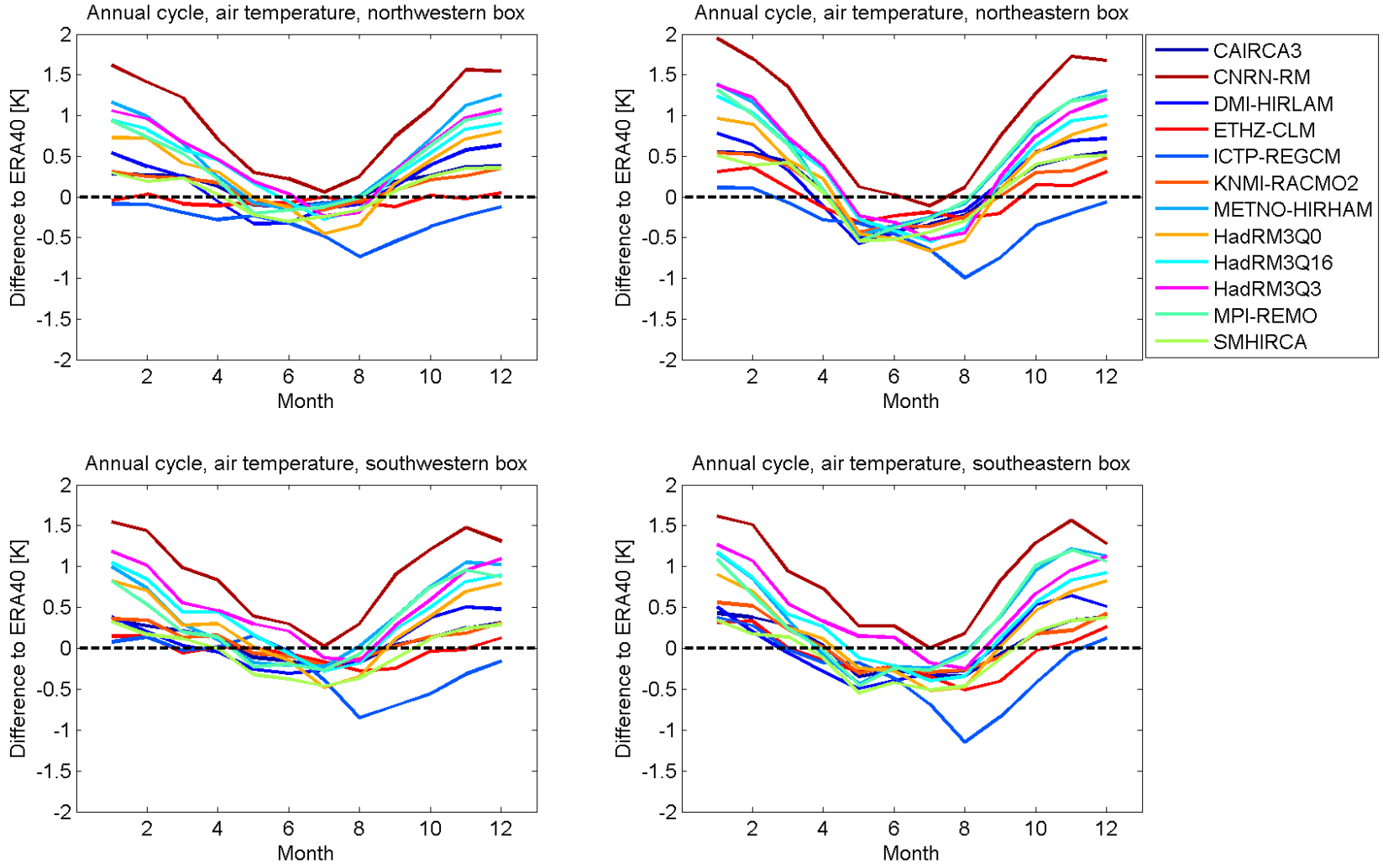

Figure 3.5.14: Differences of annual cycles of 2 m air temperatures [K] of the ENSEMBLES RCMs to ERA-40 in the four North Sea boxes for the period of 1971-2000

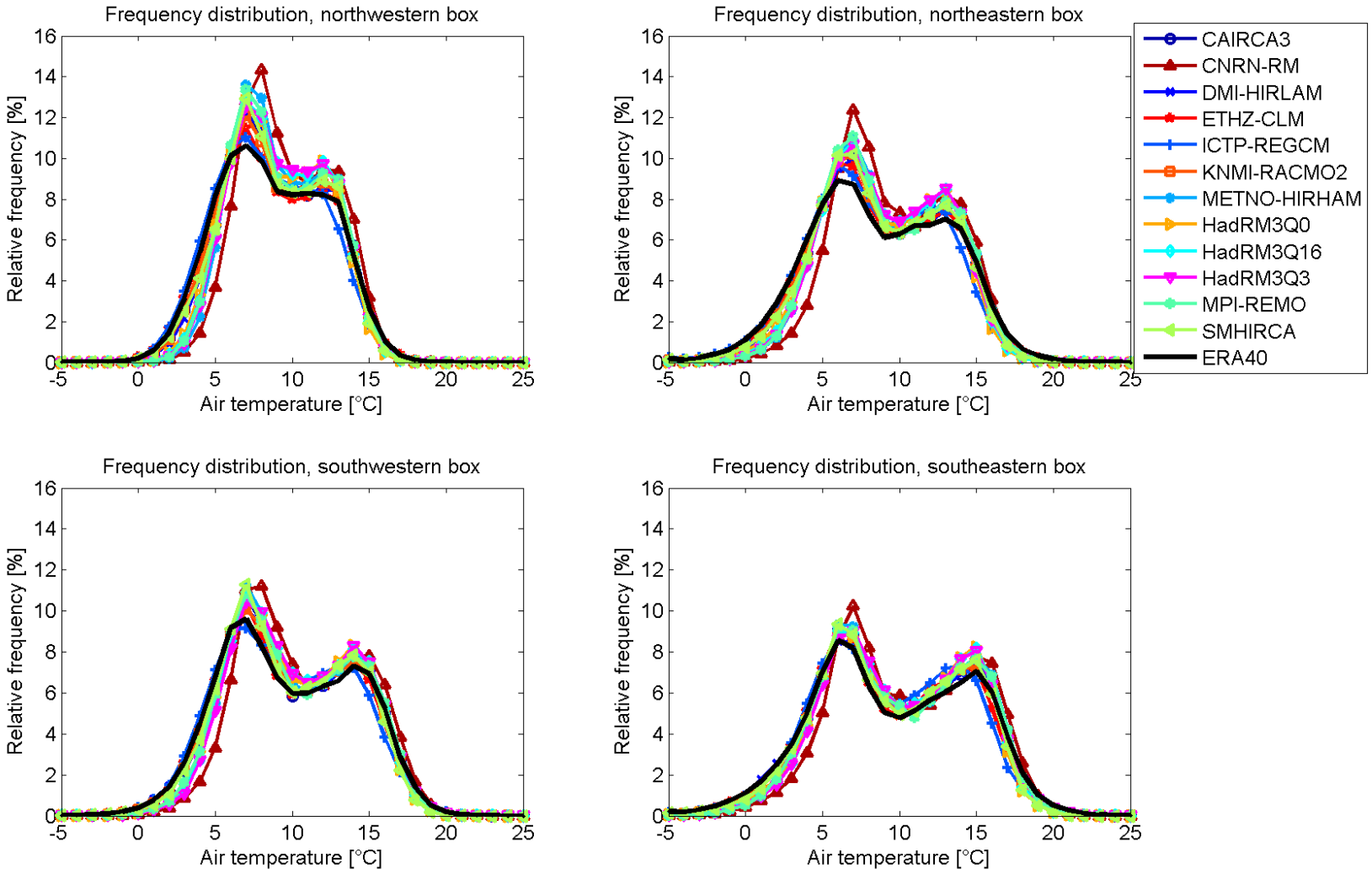

Figure 3.5.15: Frequency distributions of 2 m air temperatures [%] of the ENSEMBLES RCMs and ERA-40 in the four North Sea boxes for the period of 1971-2000

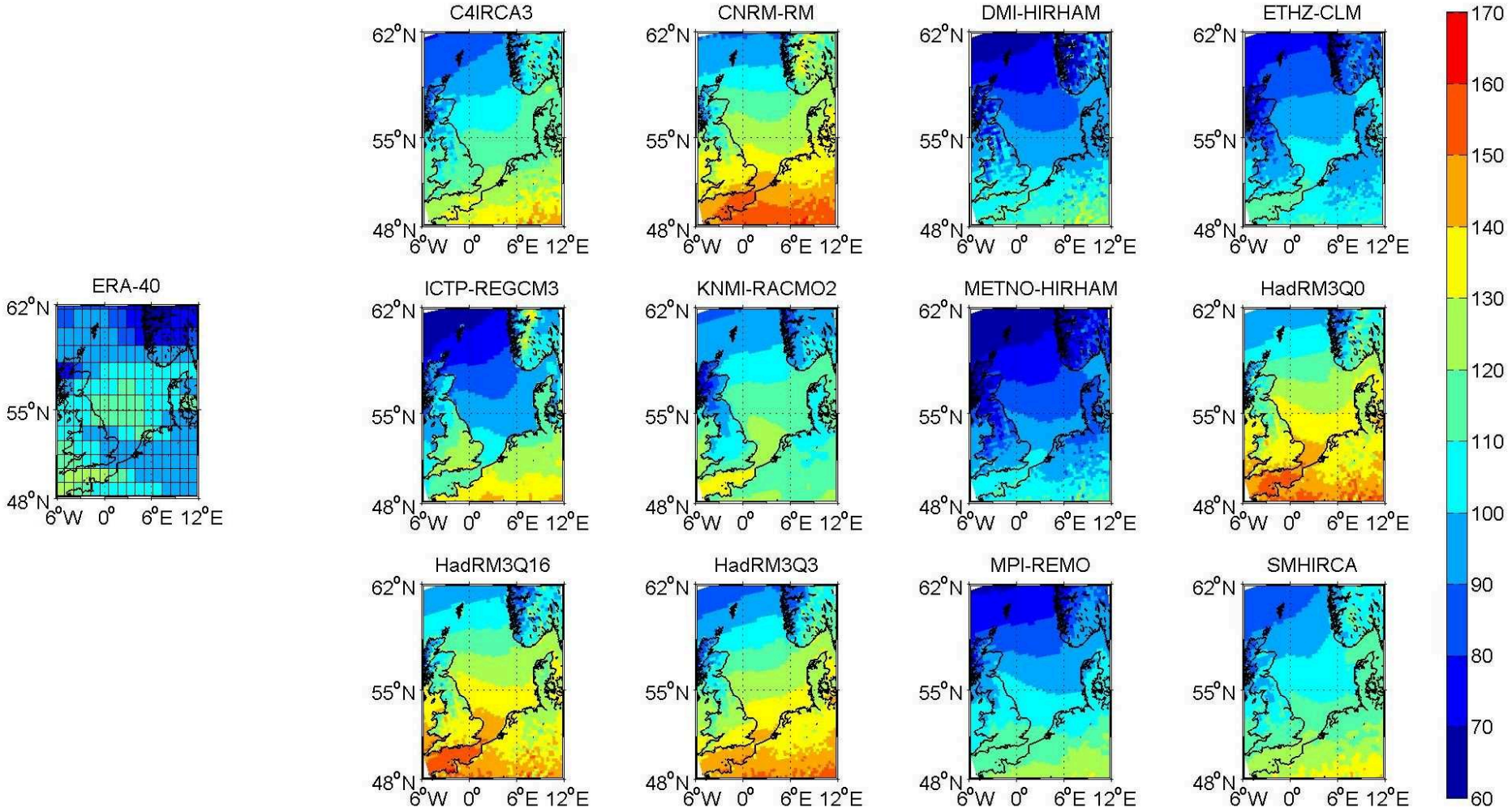

Figure 3.6.1: Mean global radiation [W/m^2] in the North Sea area for the period 1971-2000: ERA-40 (left) and the ENSEMBLES regional models (right)

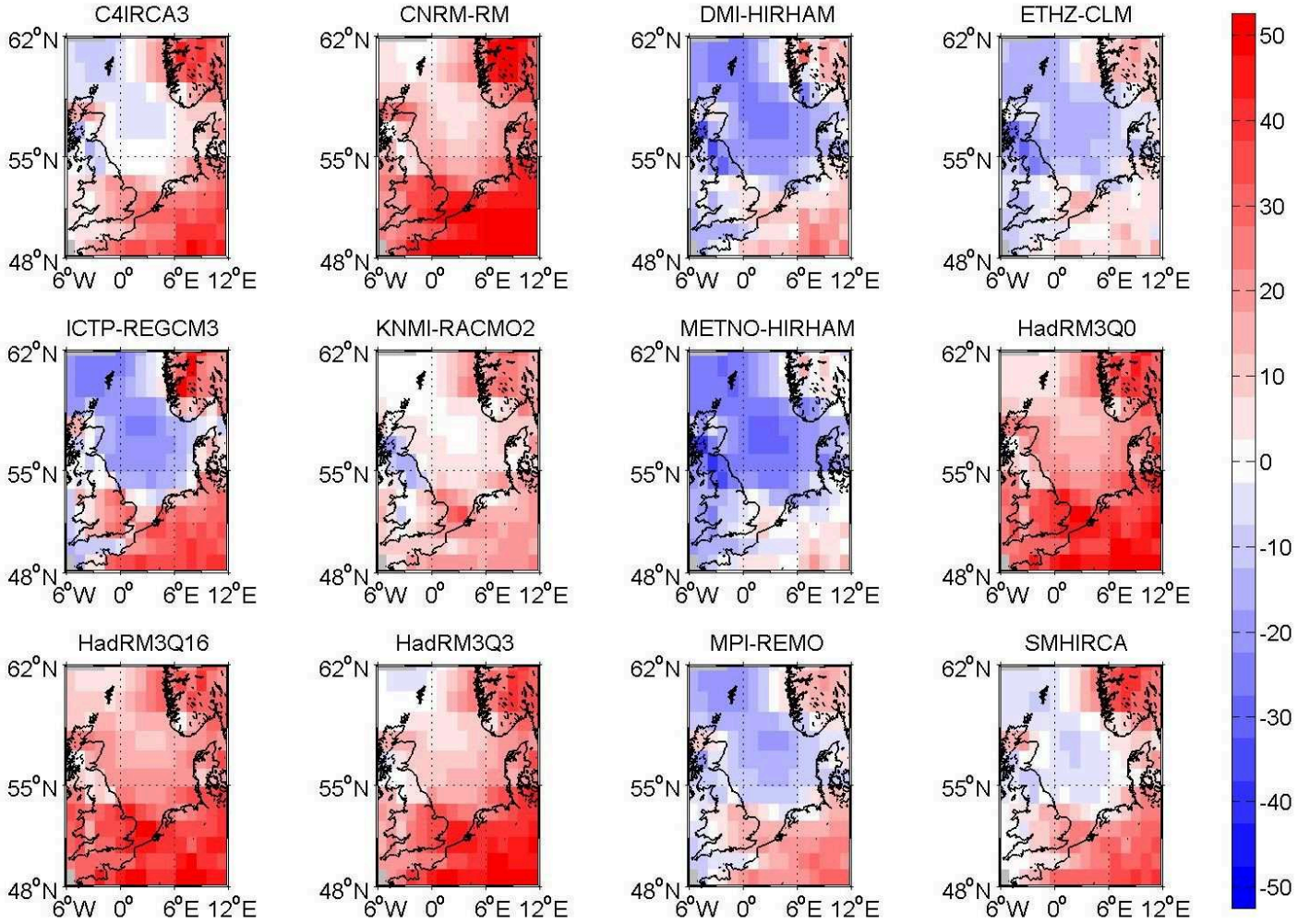

Figure 3.6.2: Differences of global radiation [W/m^2]: RCMs minus ERA-40 from Fig. 3.6.1

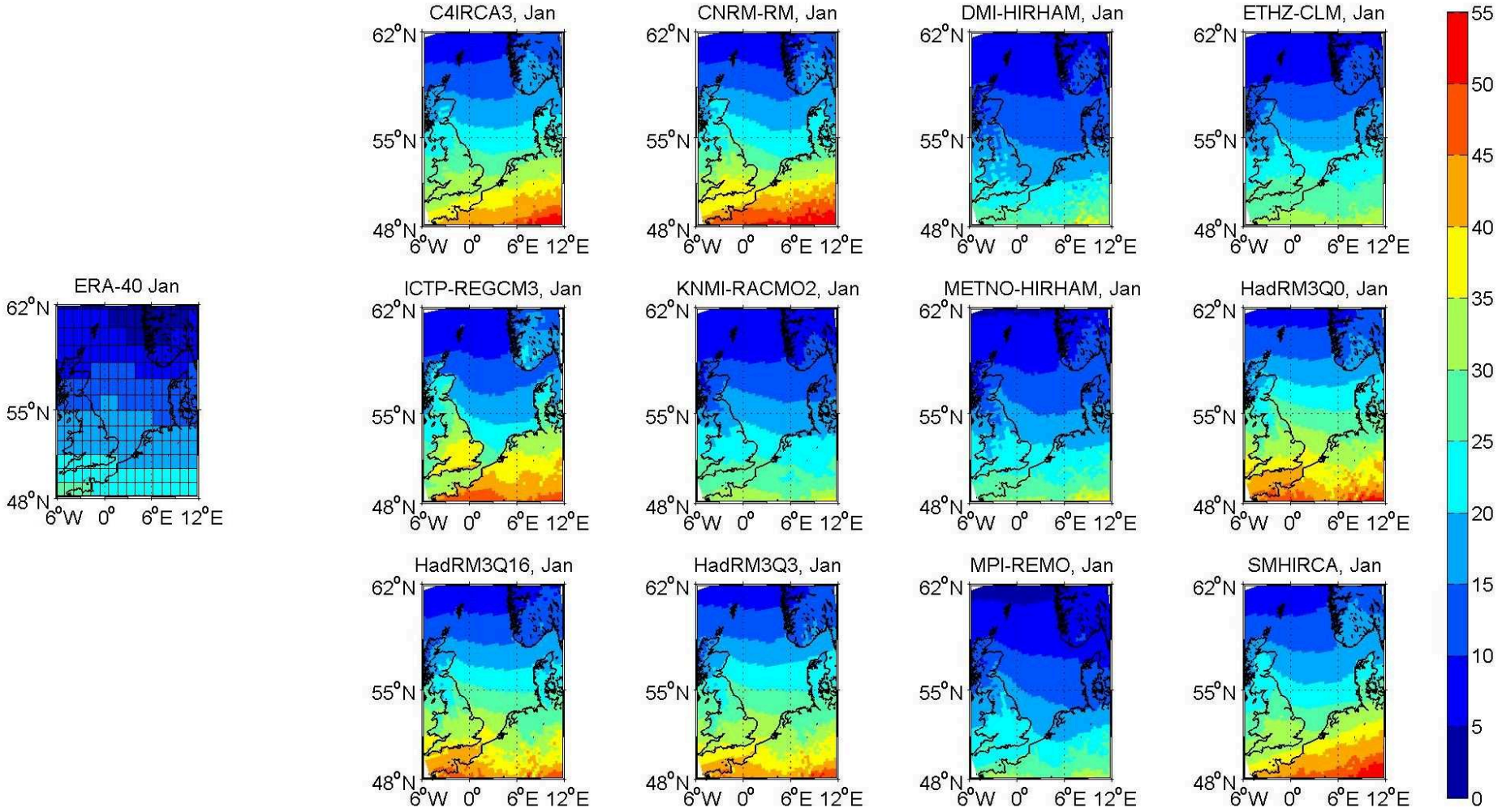

Figure 3.6.3: January mean of global radiation in [W/m^2] in the North Sea area for the period 1971-2000: ERA-40 (left) and the ENSEMBLES regional models (right)

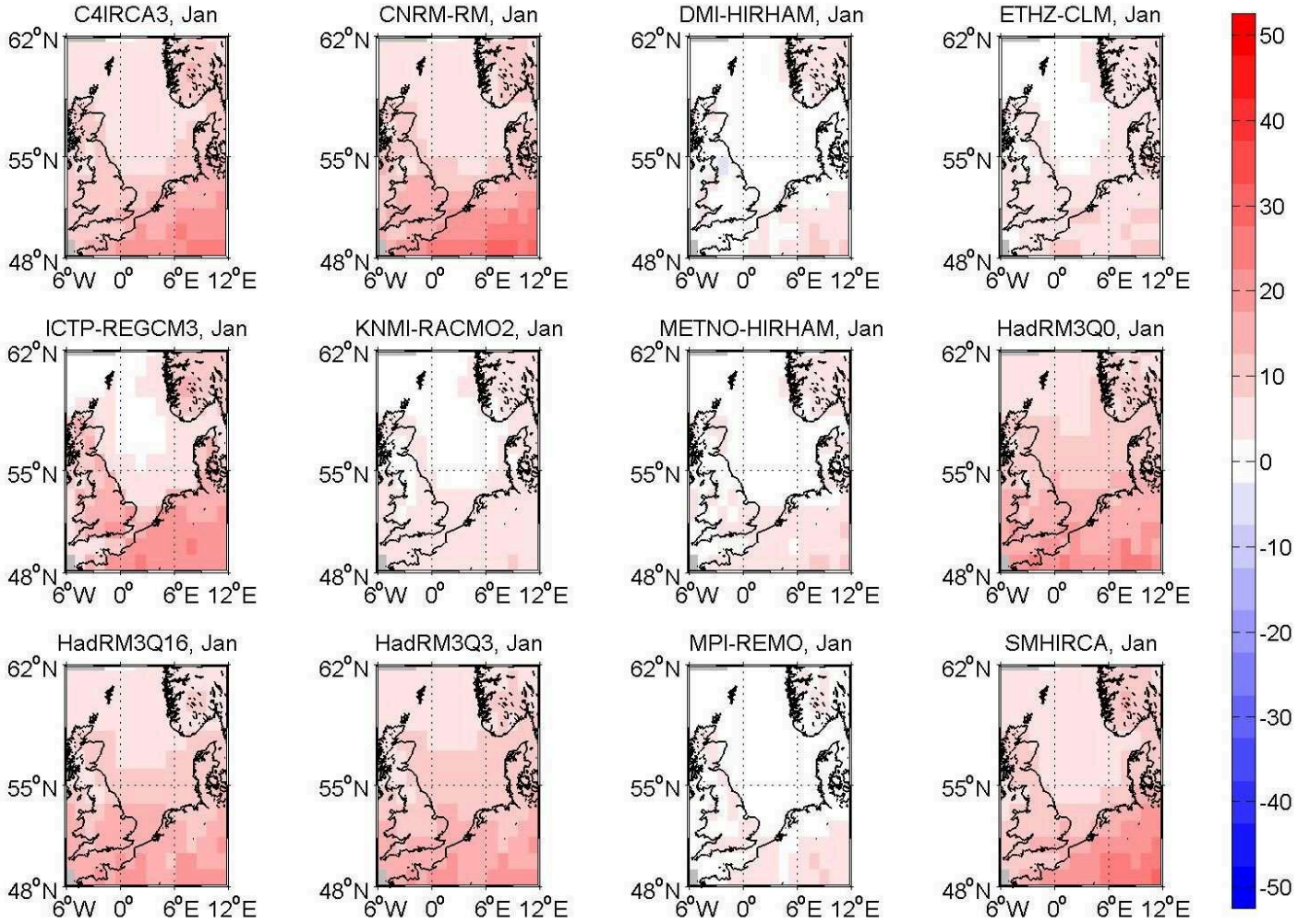

Figure 3.6.4: January differences in global radiation [W/m^2]: RCMs minus ERA-40 from Fig. 3.6.3

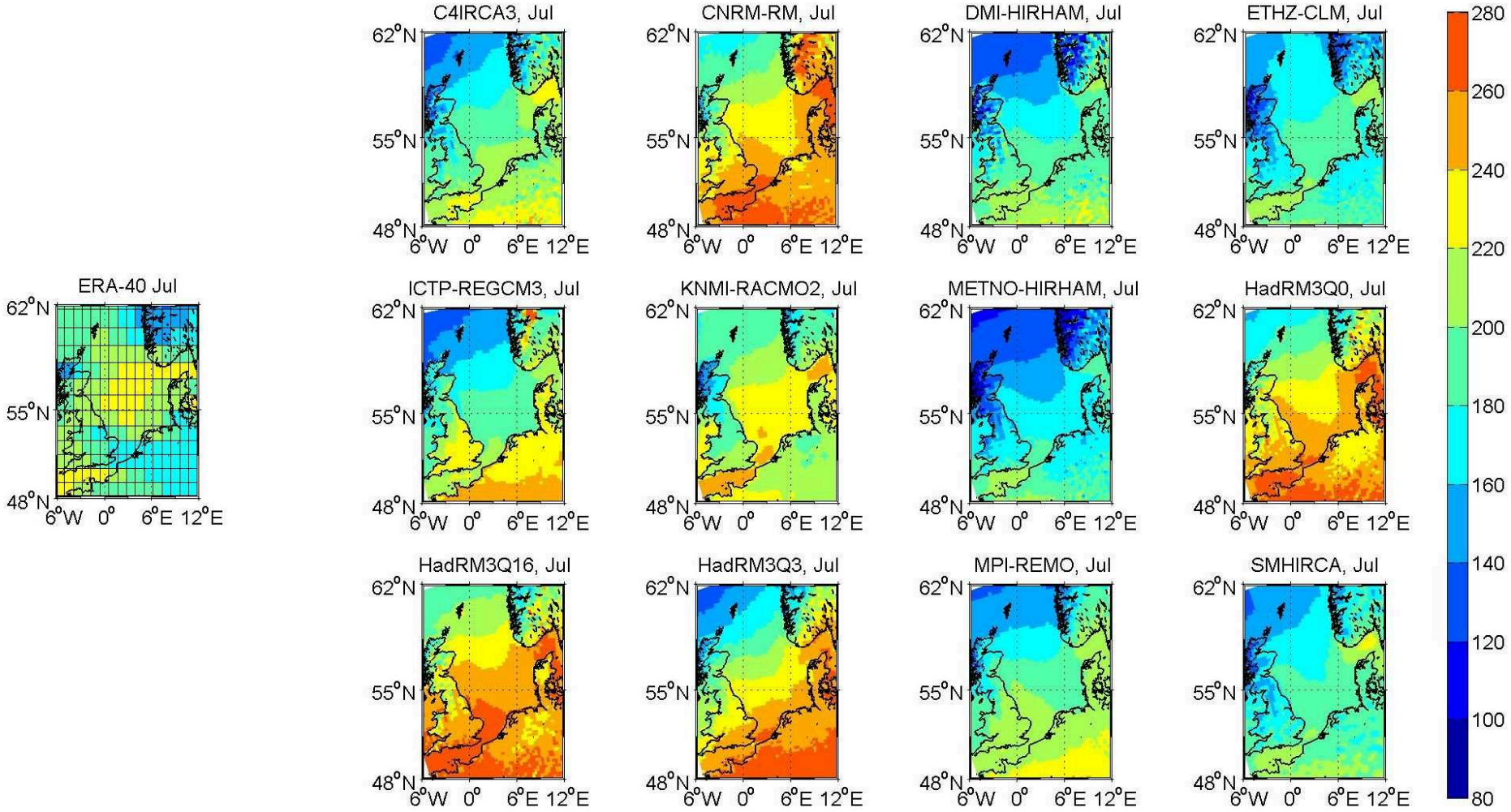

Figure 3.6.5: July mean of global radiation [W/m^2] in the North Sea area for the period 1971-2000: ERA-40 (left) and the ENSEMBLES regional models (right)

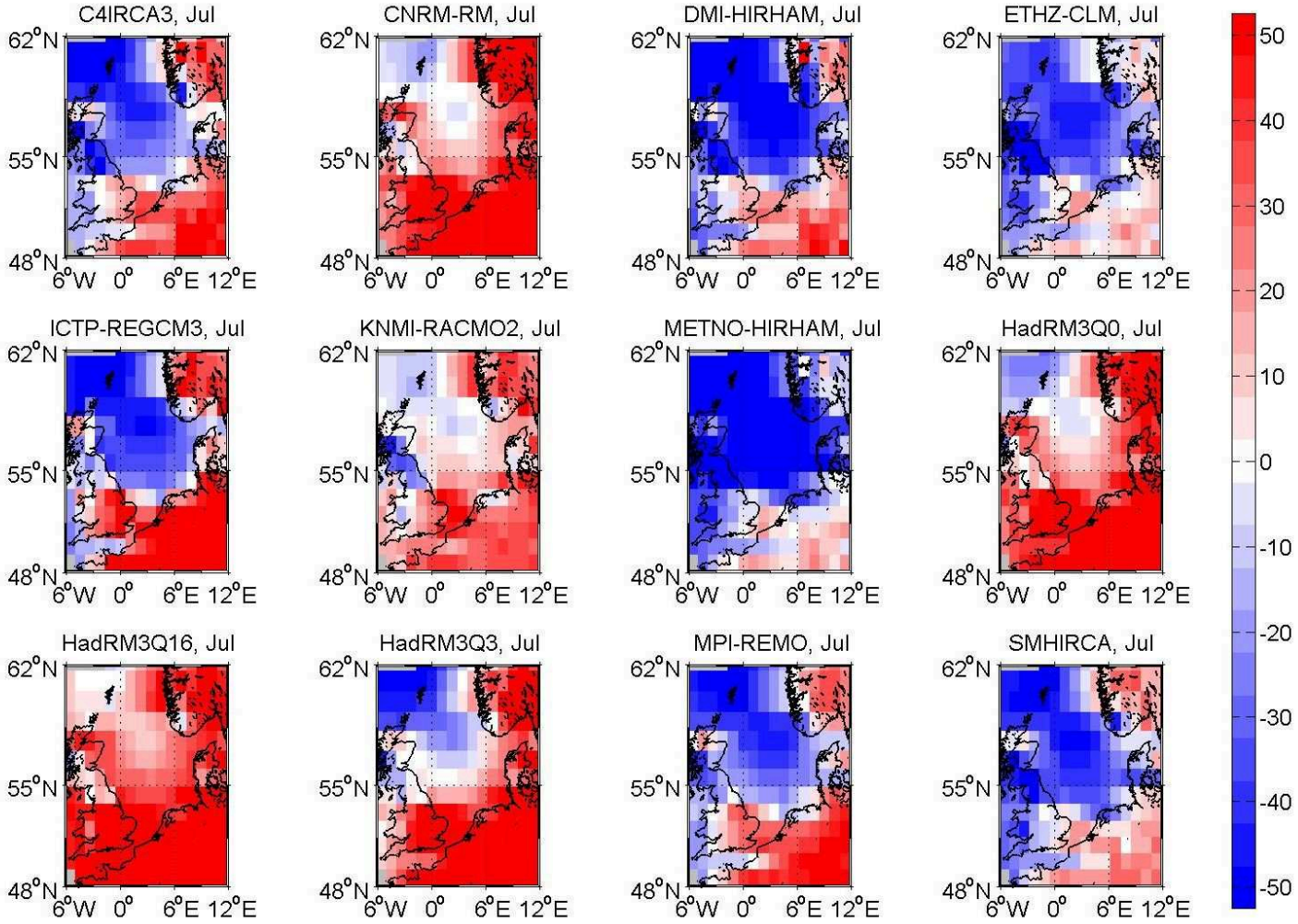

Figure 3.6.6: July differences in global radiation [W/m^2]: RCMs minus ERA-40 from Fig. 3.6.5

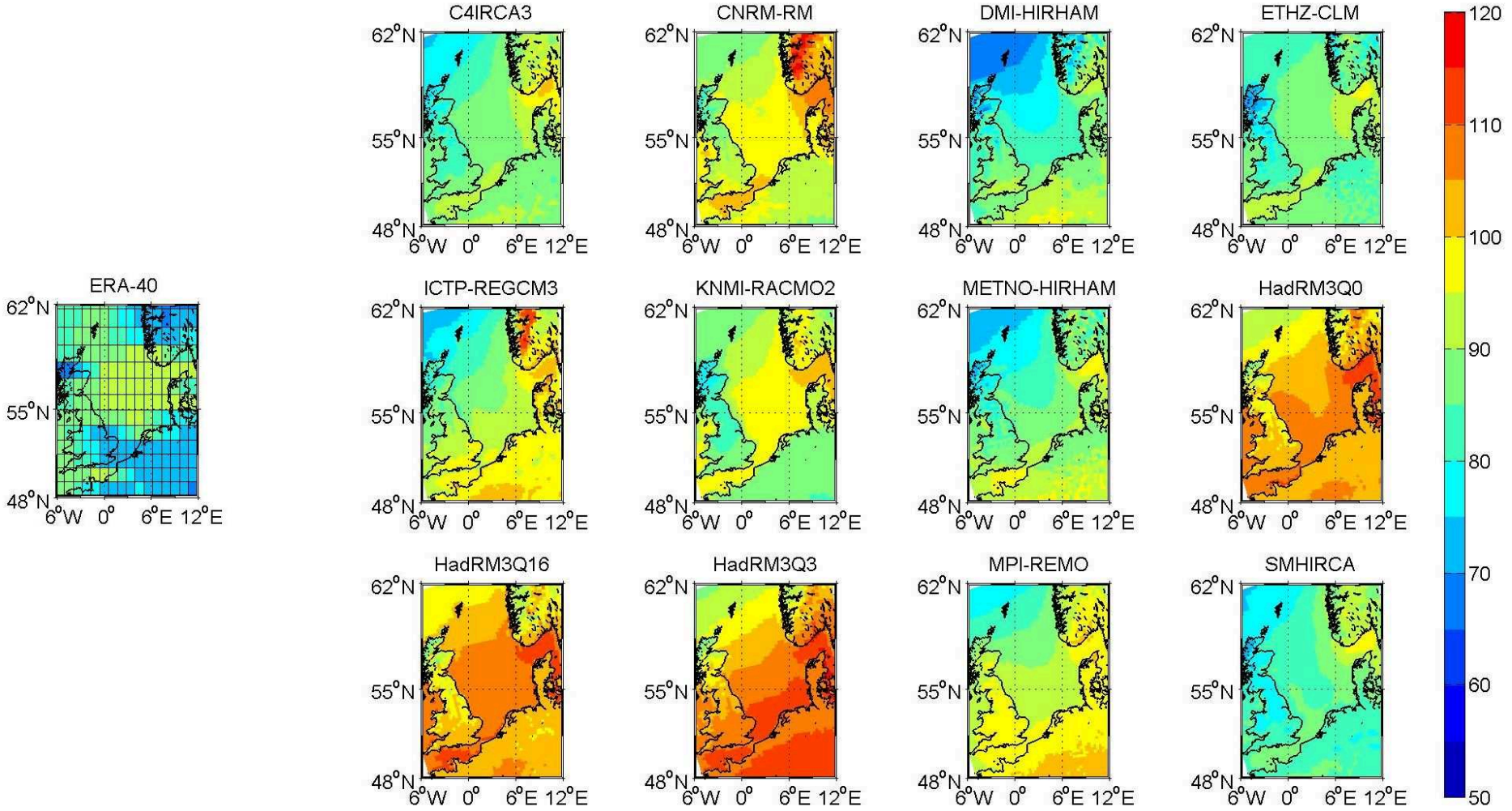

Figure 3.6.7: Standard deviation of global radiation [W/m^2] in the North Sea area for the period 1971-2000: ERA-40 (left) and the ENSEMBLES regional models (right)

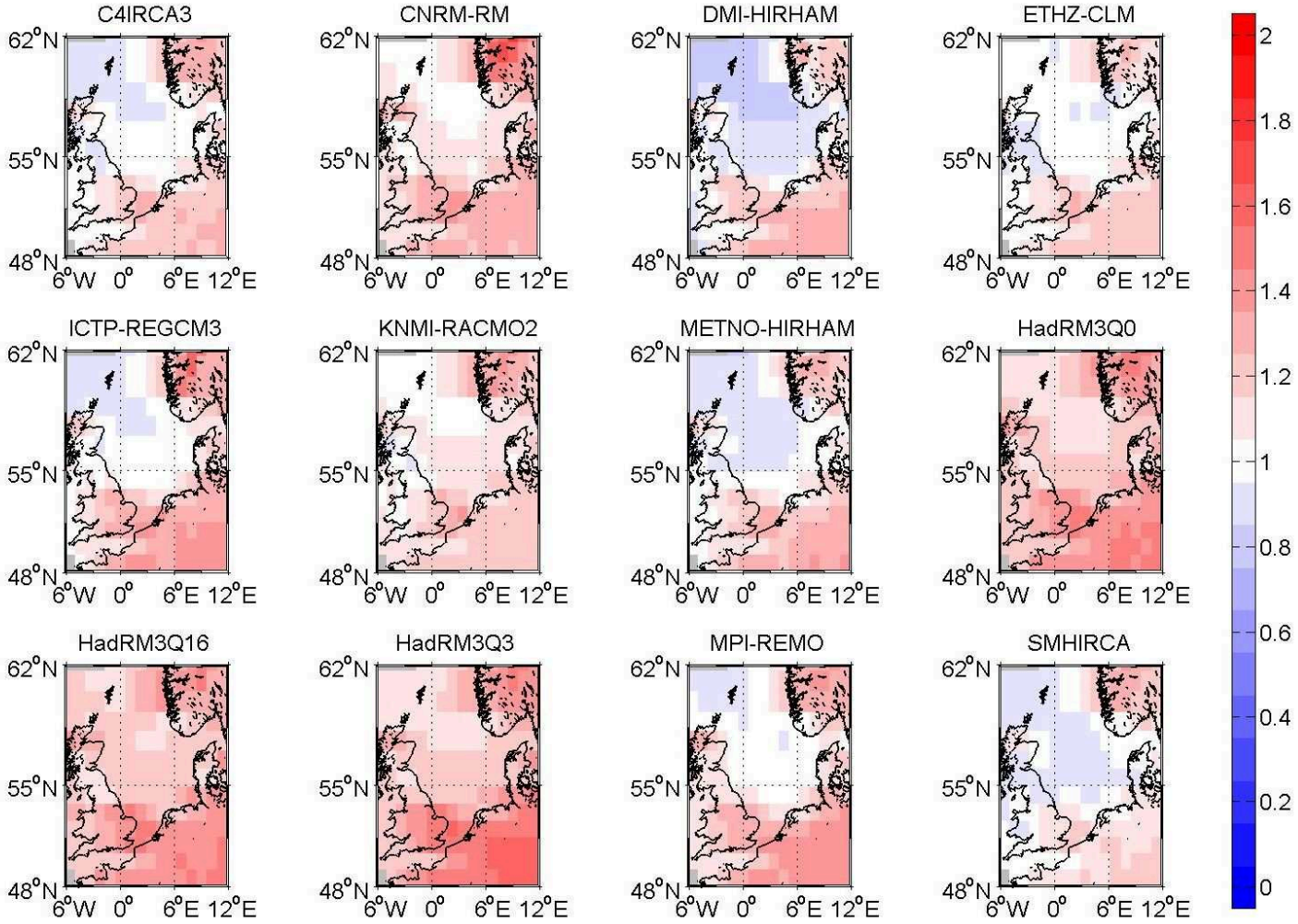

Figure 3.6.8: Ratio of standard deviations of global radiation: RCMs / ERA-40 from Fig. 3.6.7

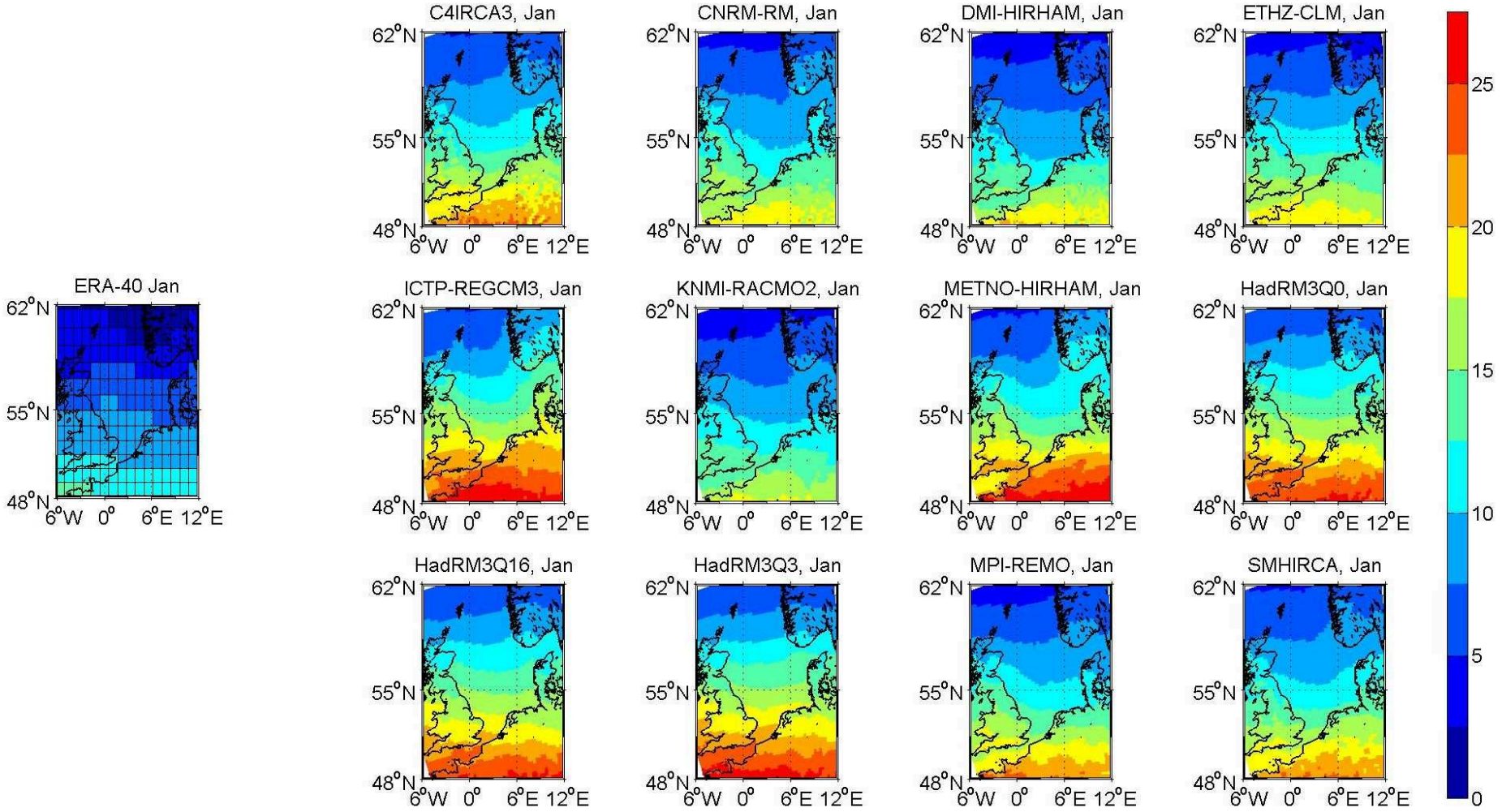

Figure 3.6.9: January standard deviation of global radiation [W/m^2] in the North Sea area for the period 1971-2000: ERA-40 (left) and the ENSEMBLES regional models (right)

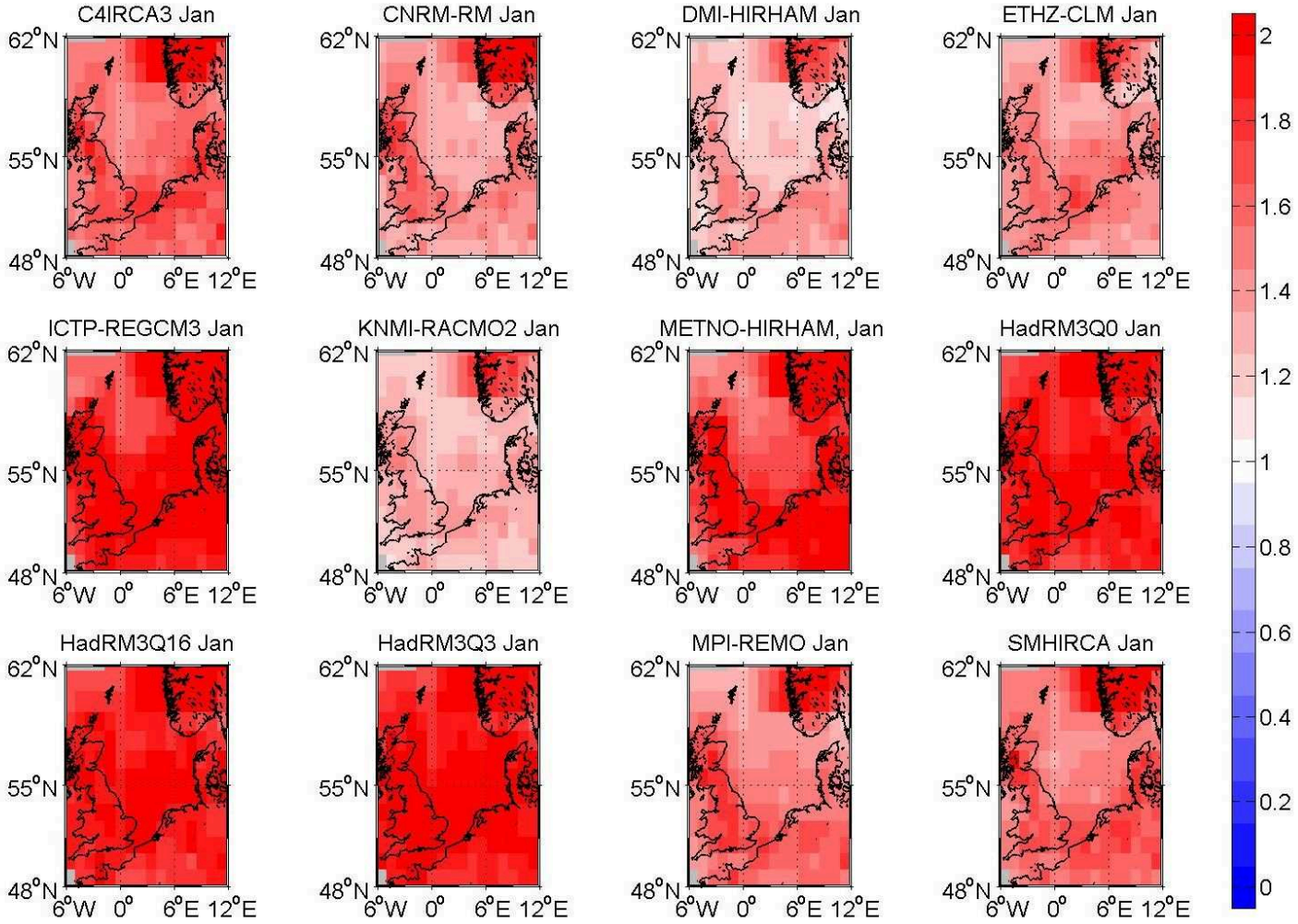

Figure 3.6.10: January ratio of standard deviations of global radiation in [W/m^2]: RCMs / ERA-40 from Fig. 3.6.9

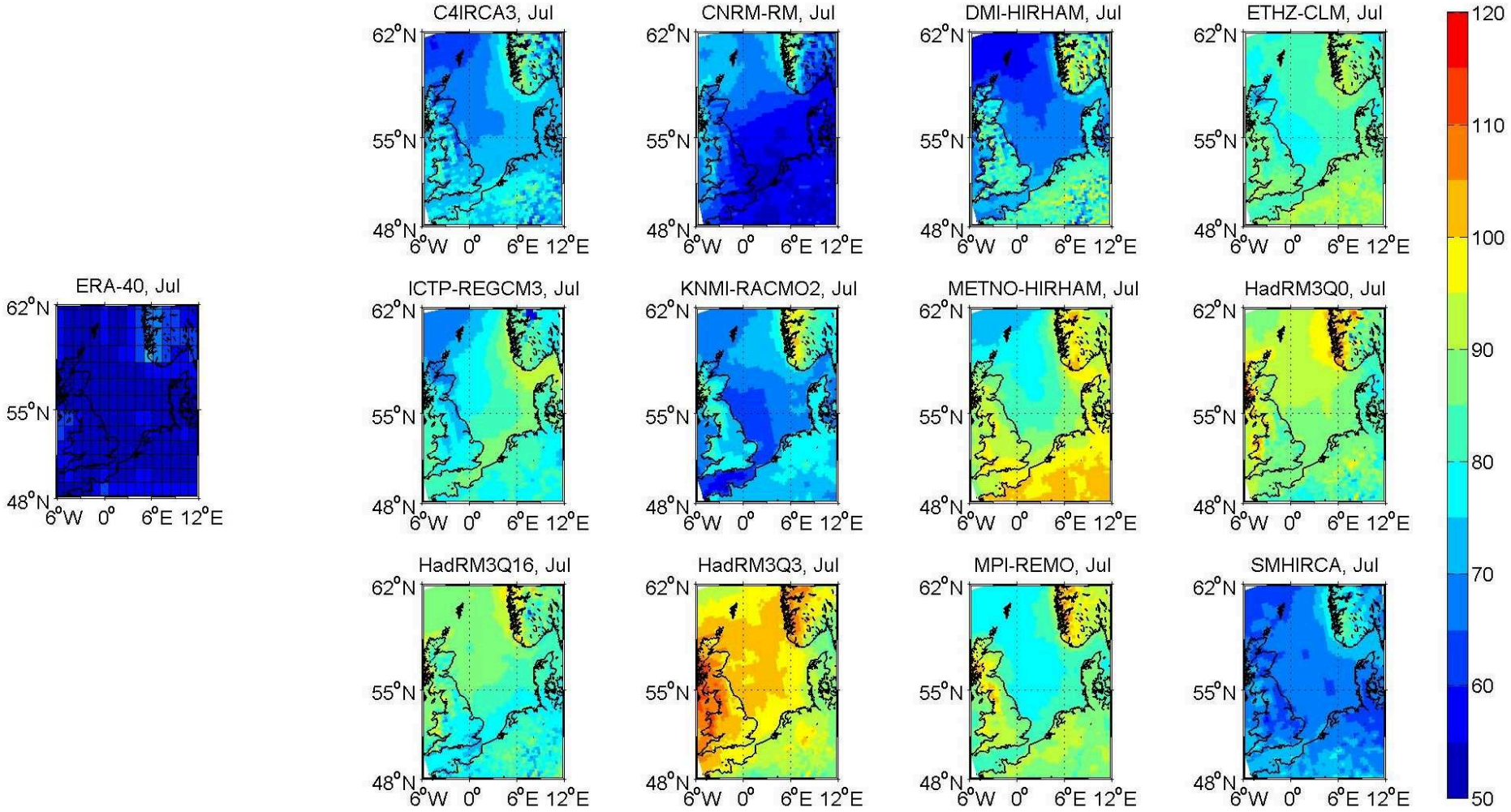

Figure 3.6.11: July standard deviation of global radiation [W/m^2] in the North Sea area for the period 1971-2000: ERA-40 (left) and the ENSEMBLES regional models (right)

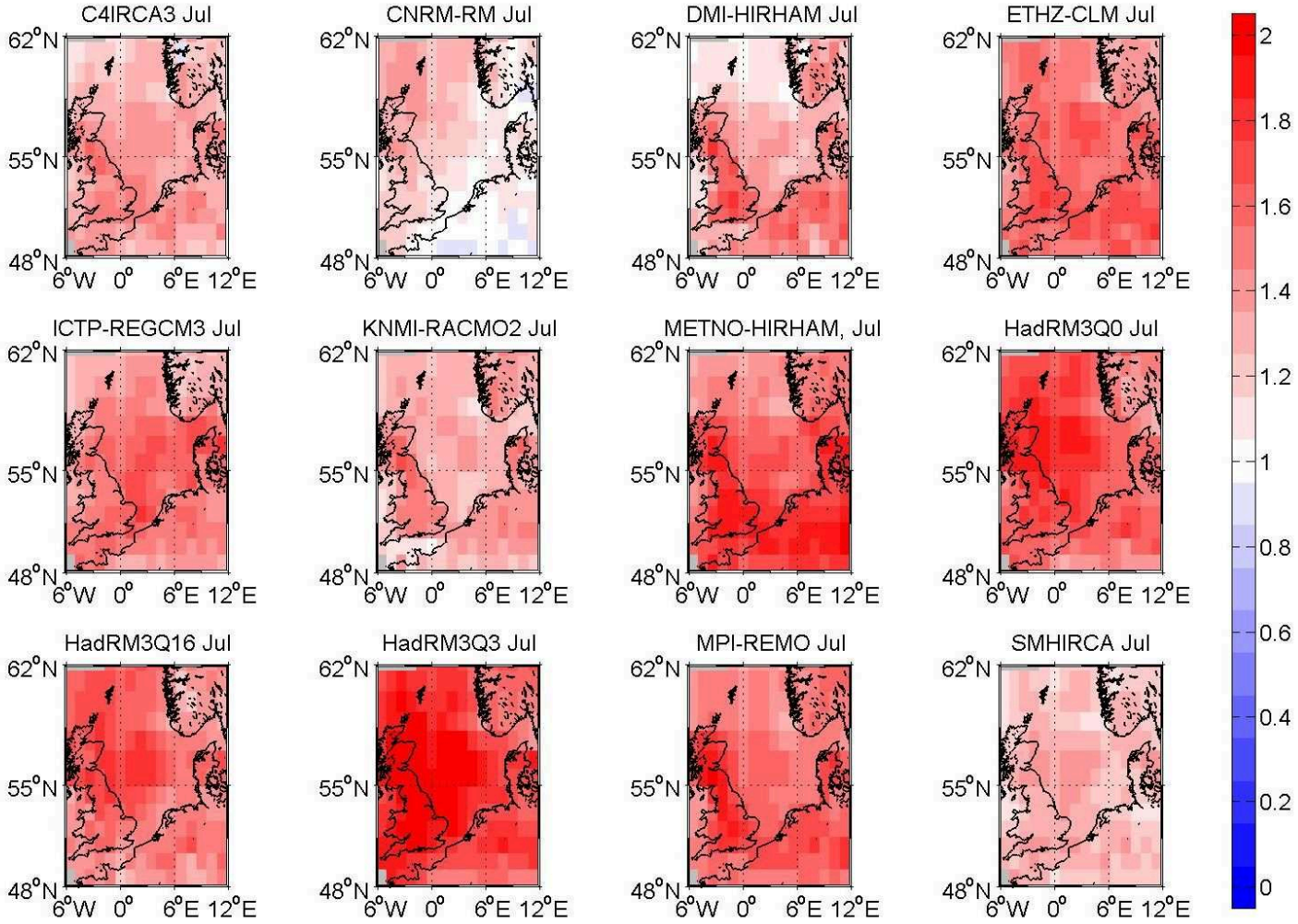

Figure 3.6.12: July ratio of standard deviations of global radiation in [W/m^2]: RCMs/ERA-40 from Fig. 3.6.11

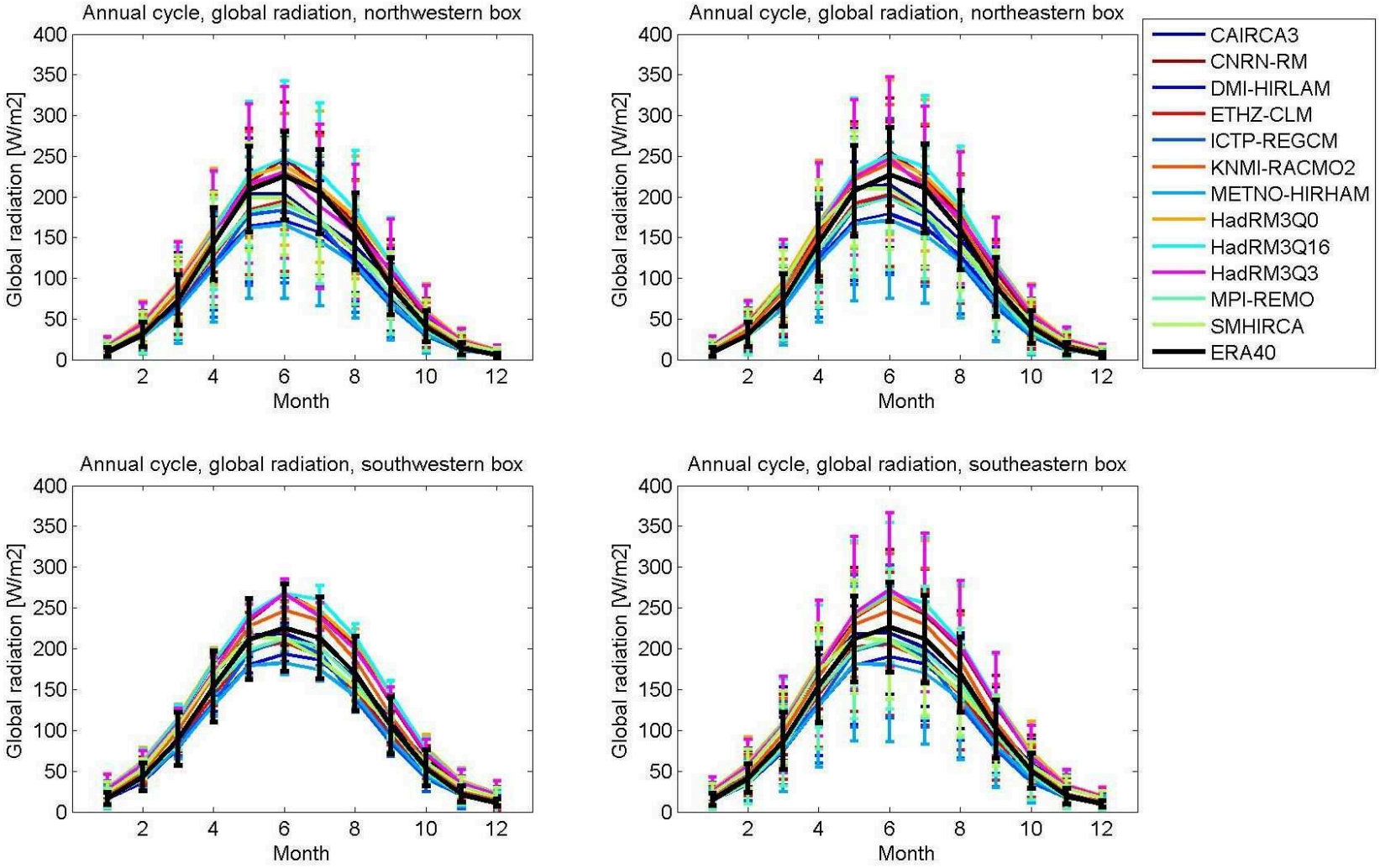

Figure 3.6.13: Annual cycles of global radiation [W/m^2] of the ENSEMBLES RCMs and ERA-40 in the four North Sea boxes for the period of 1971-2000

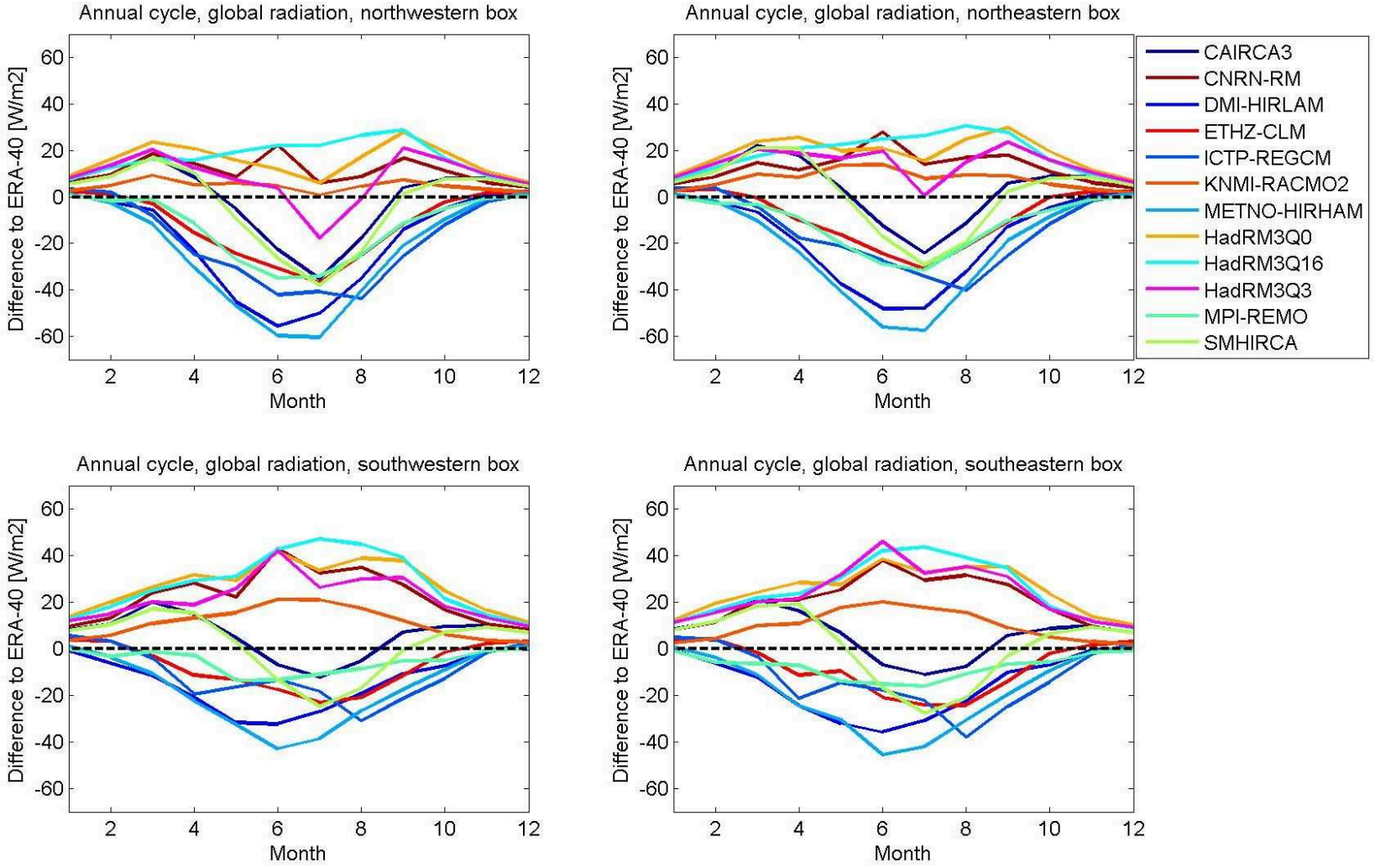

Figure 3.6.14: Difference of annual cycles of global radiation [W/m^2] of the ENSEMBLES RCMs minus ERA-40 in the four North Sea boxes for the period of 1971-2000

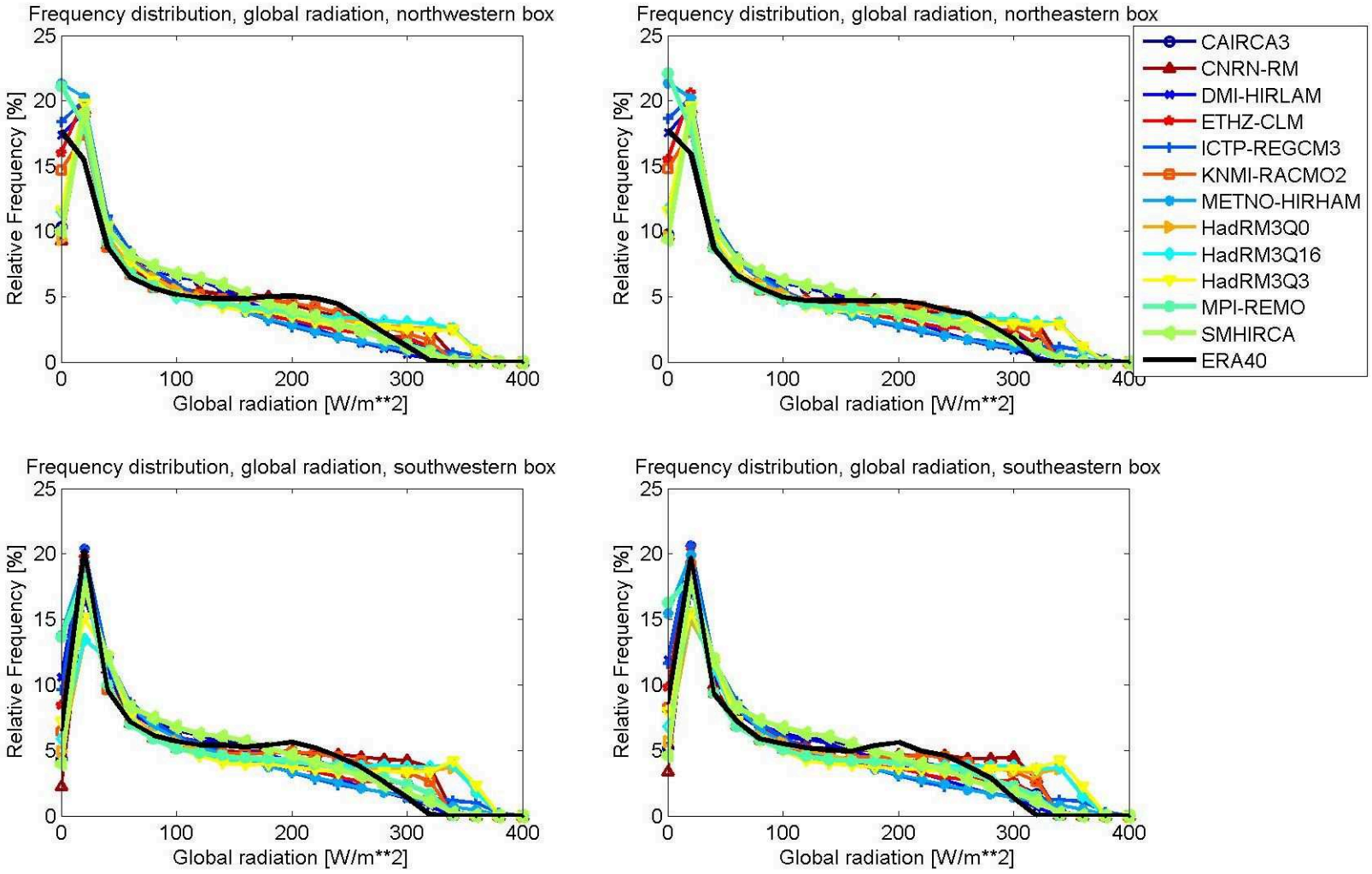

Figure 3.6.15: Frequency distribution of global radiation [W/m^2] of the ENSEMBLES RCMs and ERA-40 in the four North Sea boxes for the period of 1971-2000

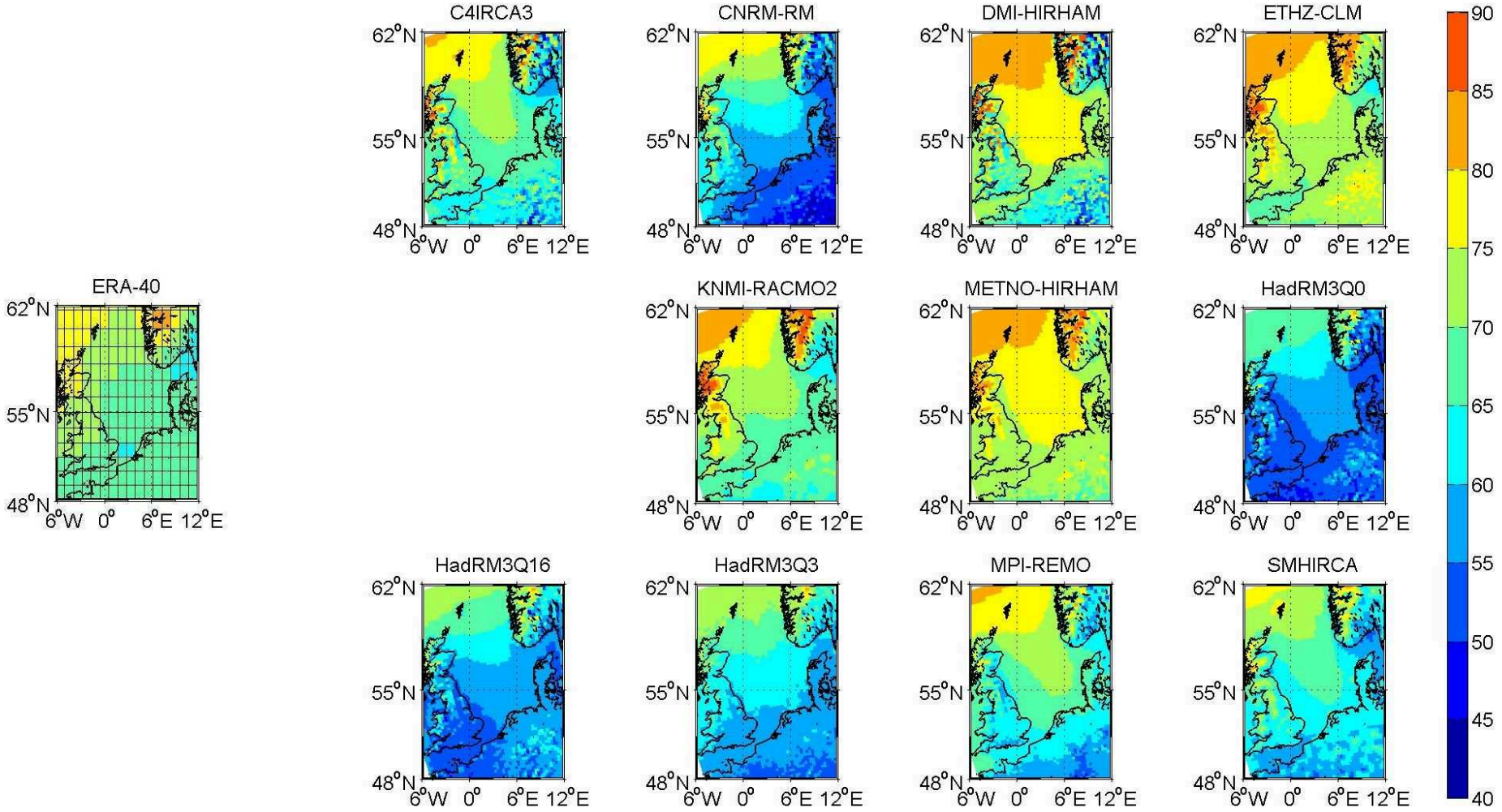

Figure 3.7.1: Mean cloud cover [%] in the North Sea area for the period 1971-2000: ERA-40 (left) and the ENSEMBLES regional models (right)

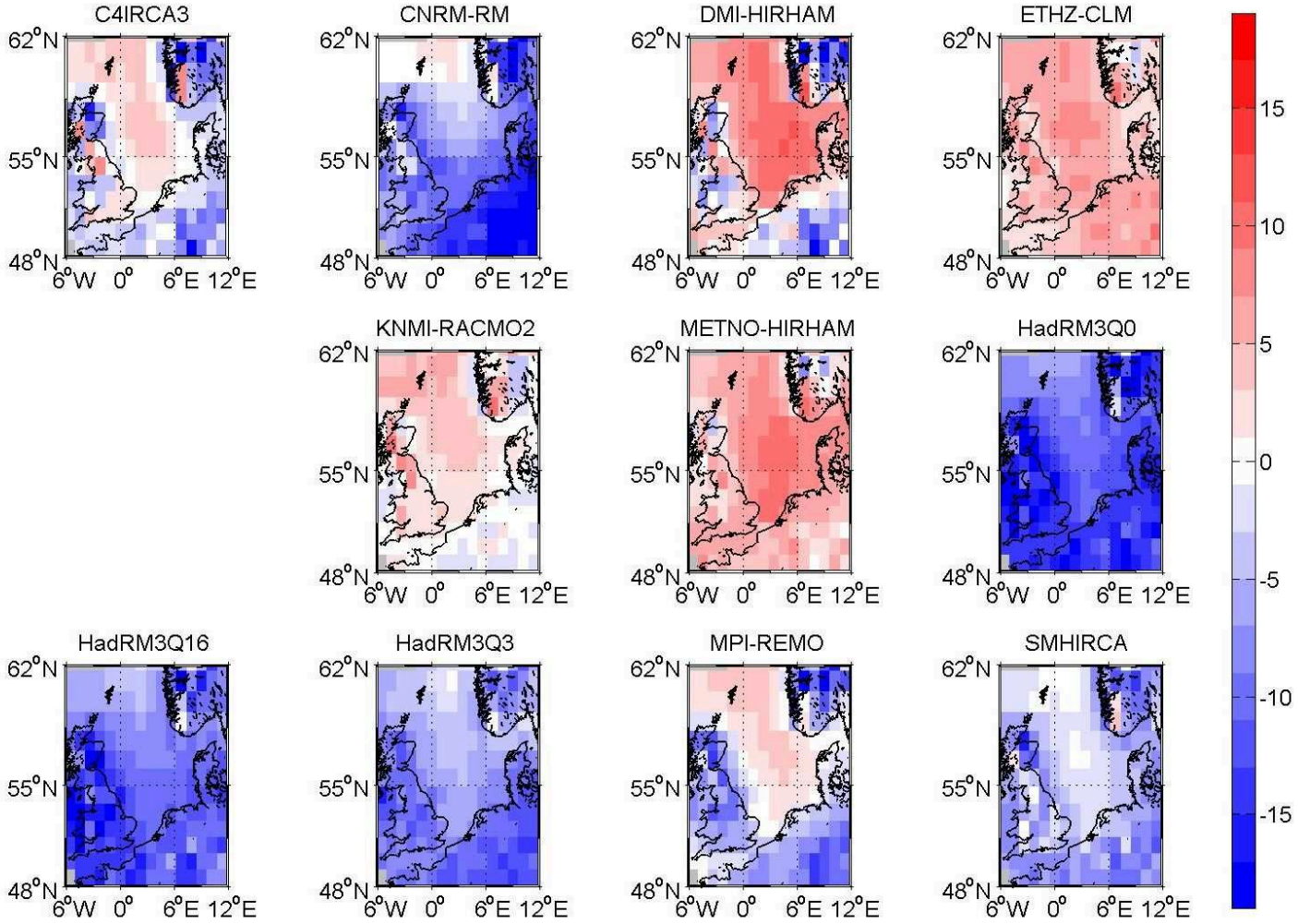

Figure 3.7.2: Differences of mean cloud cover [%]: RCMs minus ERA-40 from Fig. 3.7.1

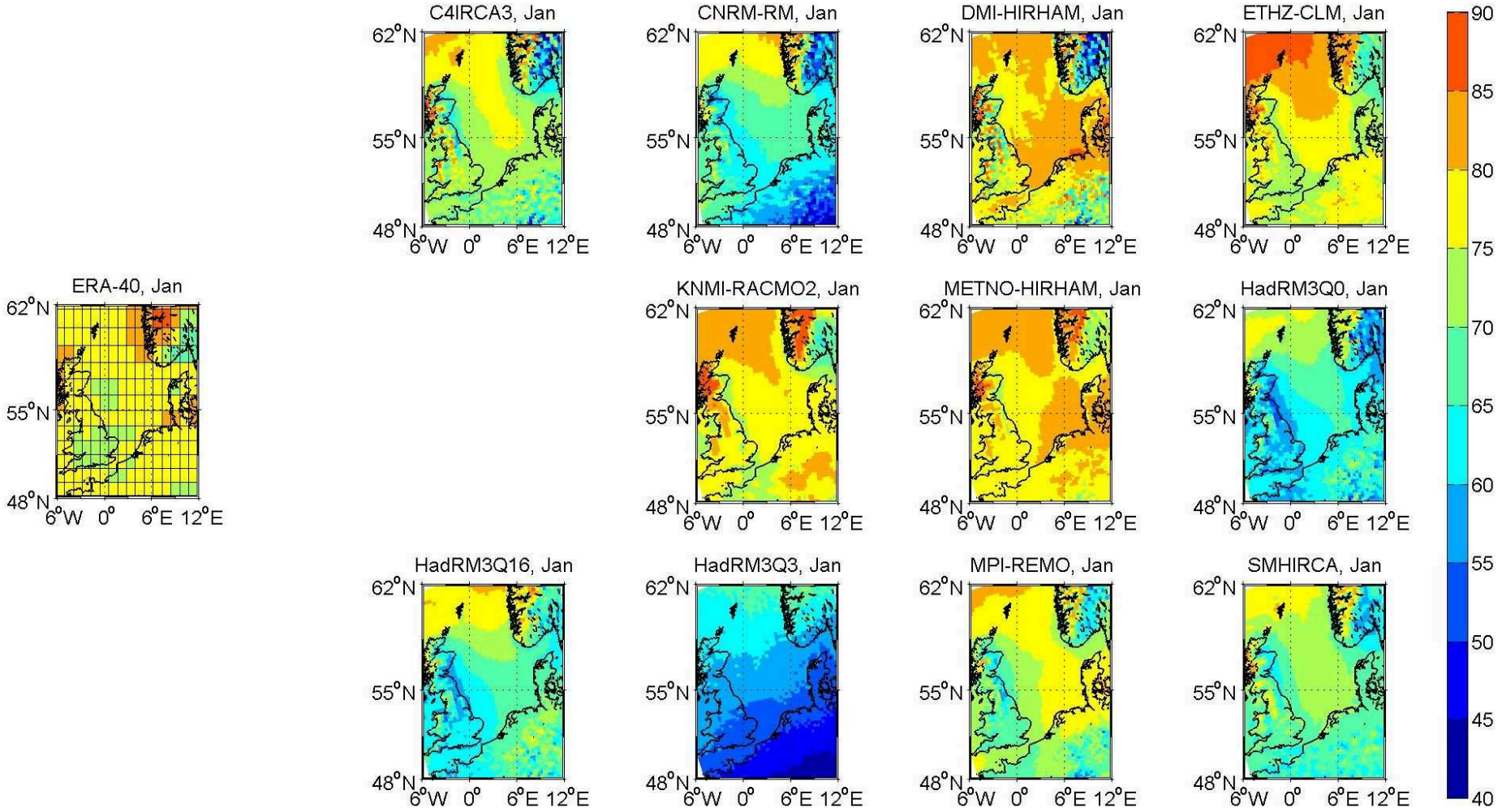

Figure 3.7.3: January mean of cloud cover [%] in the North Sea area for the period 1971-2000: ERA-40 (left) and the ENSEMBLES regional models (right)

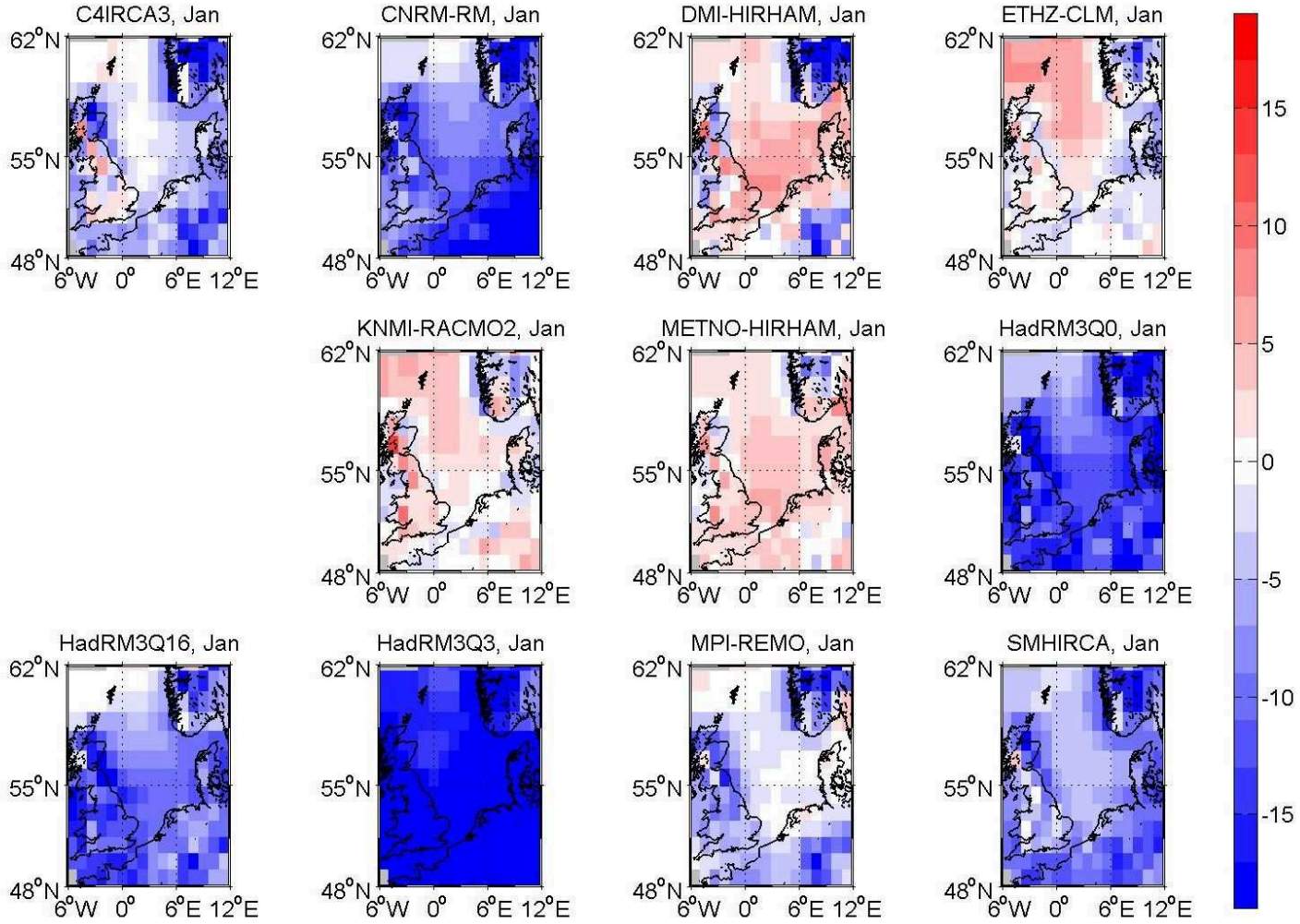

Figure 3.7.4: January differences of cloud cover in [%]: RCMs minus ERA-40 from Fig. 3.7.3

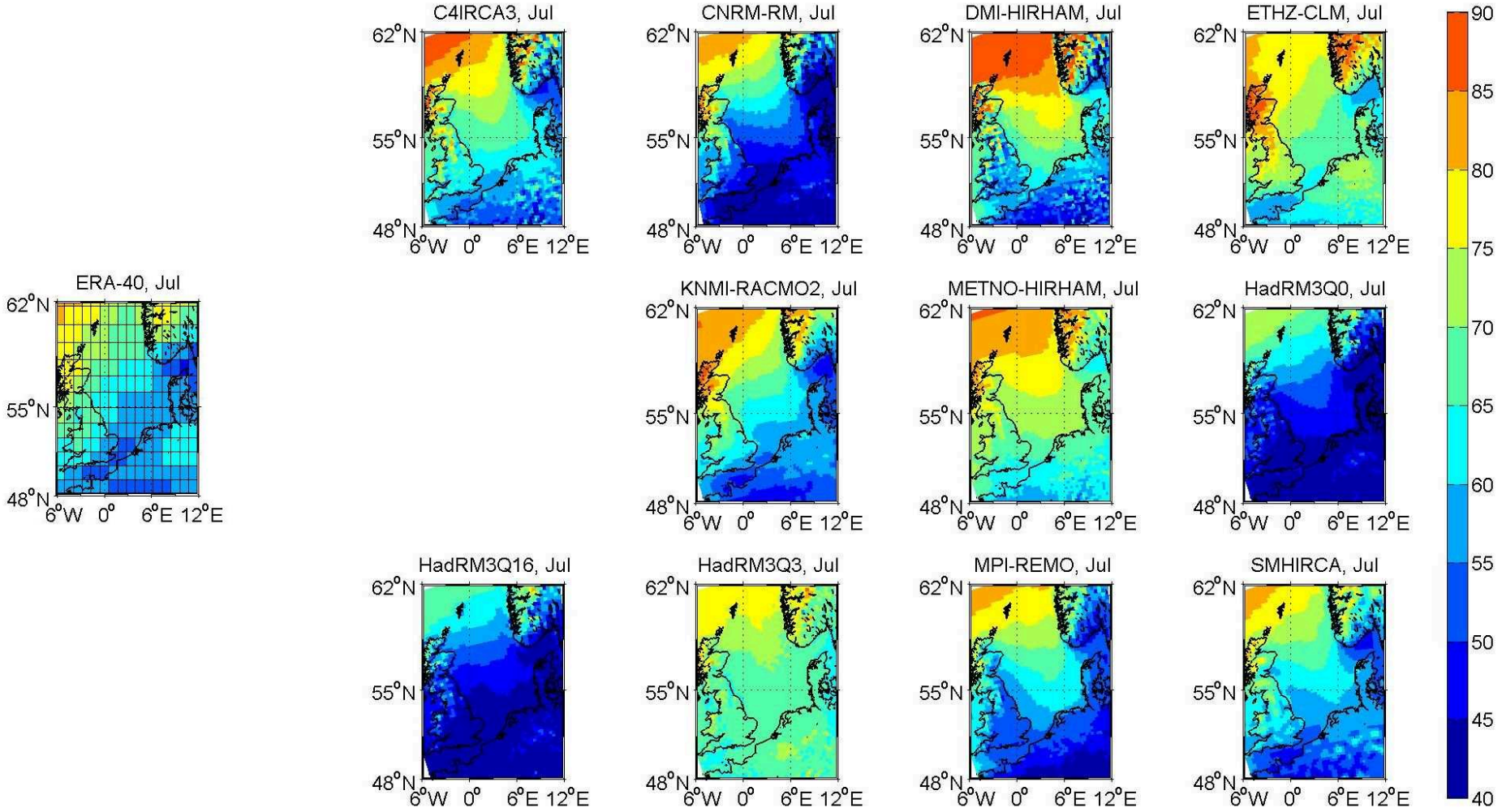

Figure 3.7.5: July mean of cloud cover [%] in the North Sea area for the period 1971-2000: ERA-40 (left) and the ENSEMBLES regional models (right)

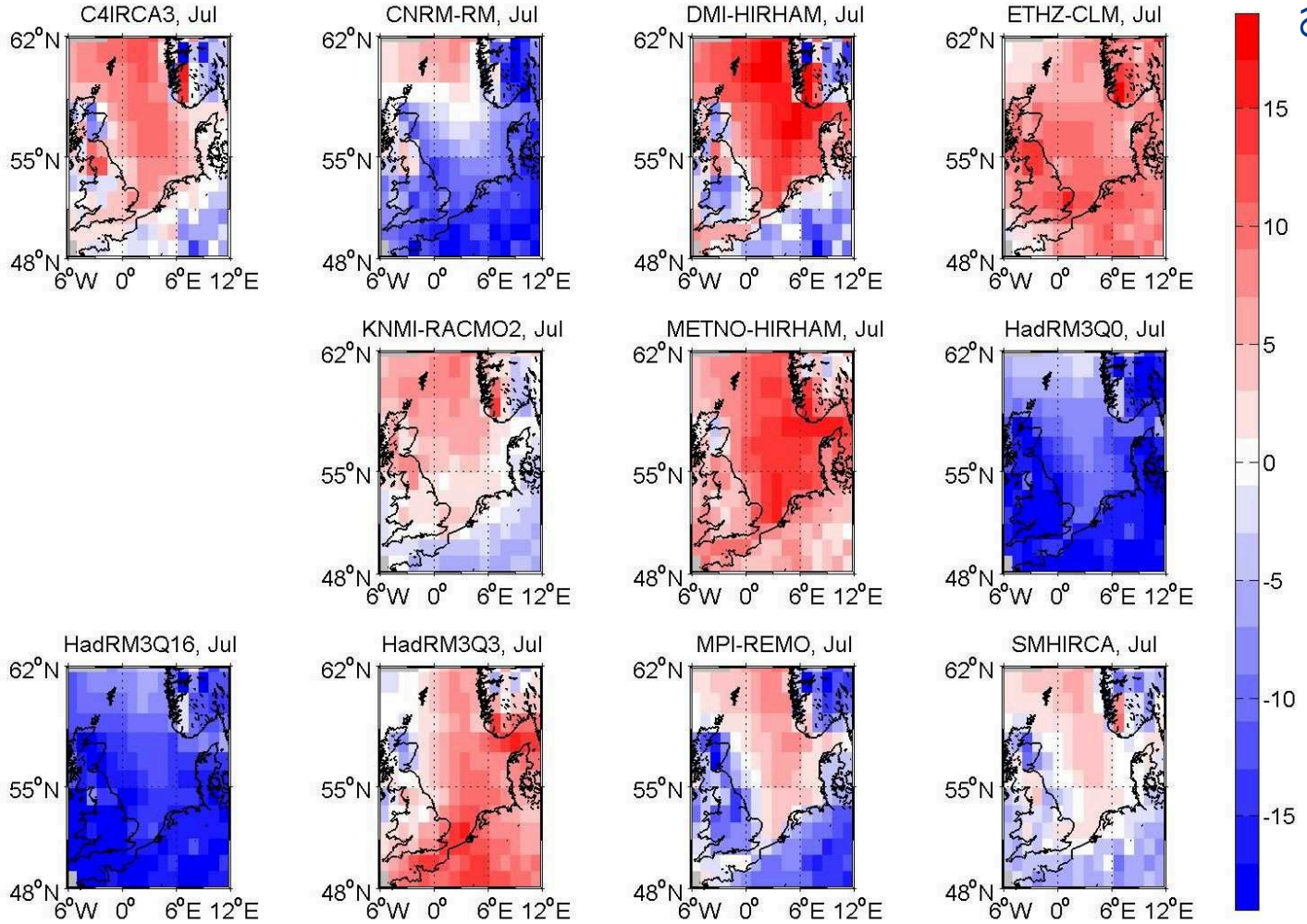

Figure 3.7.6: July differences of cloud cover [%]: RCMs minus ERA-40 from Fig. 3.7.5

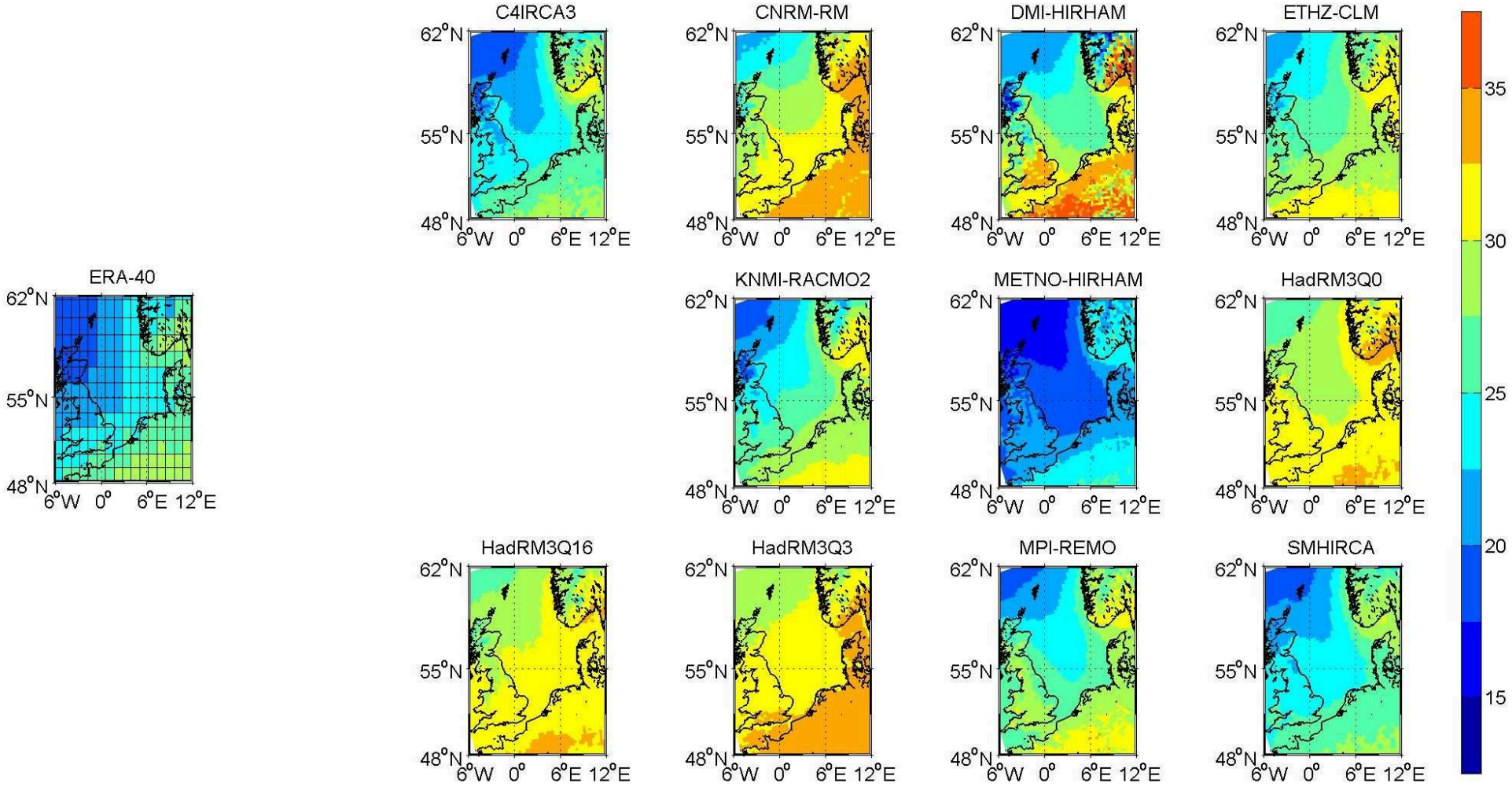

Figure 3.7.7: Standard deviation of cloud cover [%] in the North Sea area for the period 1971-2000: ERA-40 (left) and the ENSEMBLES regional models (right)

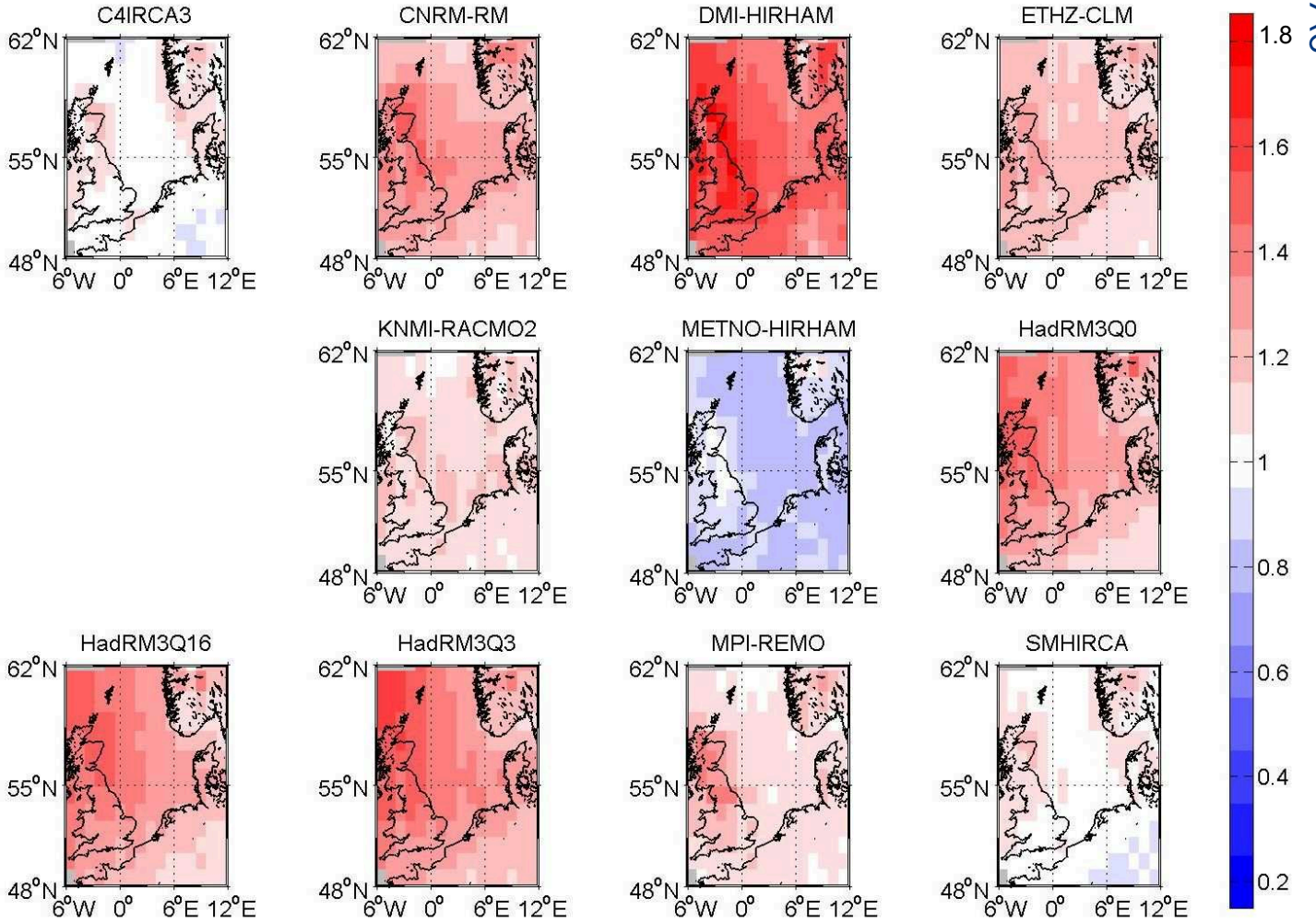

Figure 3.7.8: Ratio of standard deviations of cloud cover: RCMs / ERA-40 from Fig. 3.7.7

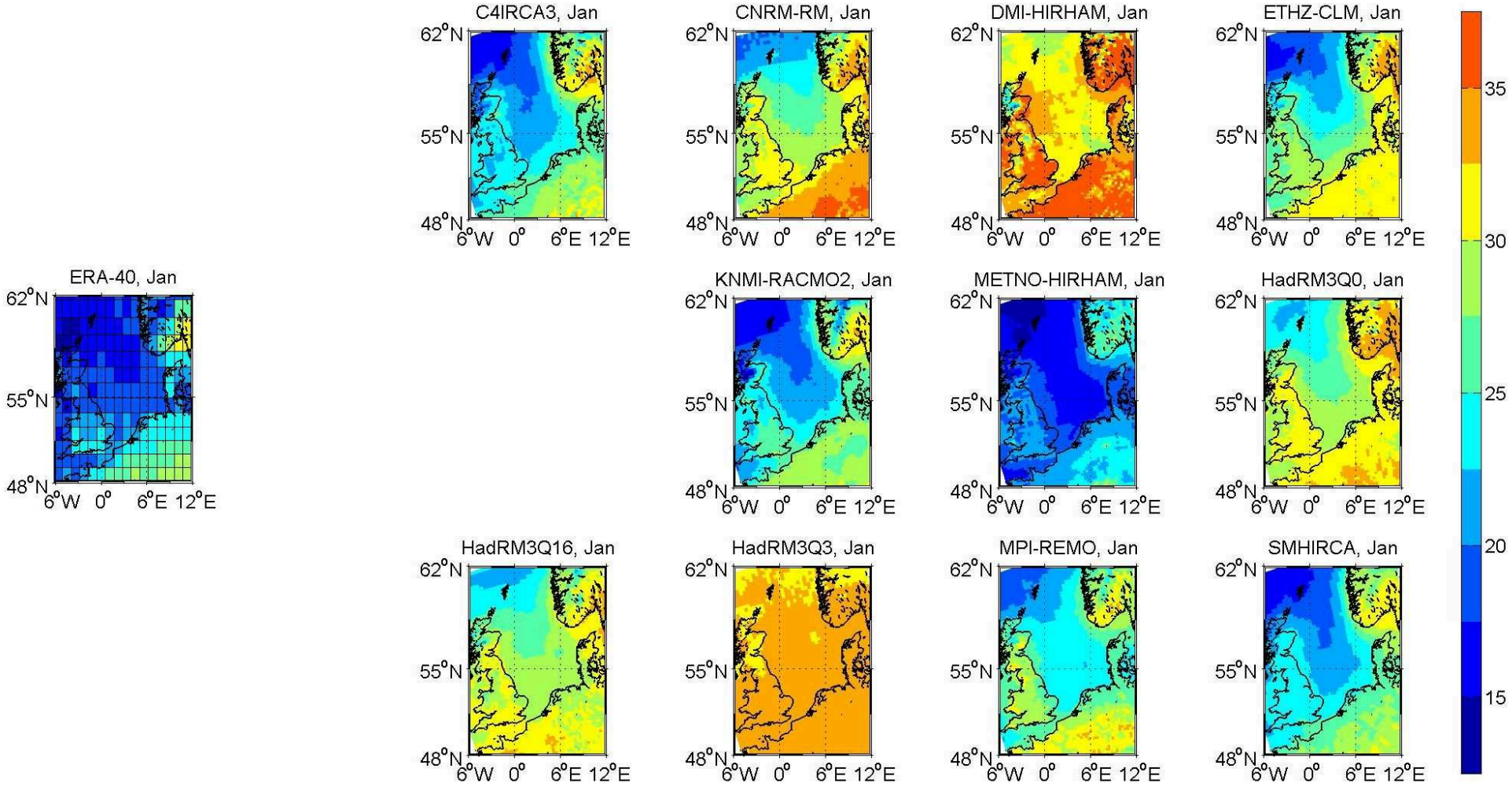

Figure 3.7.9: January standard deviation of cloud cover [%] in the North Sea area for the period 1971-2000: ERA-40 (let) and the ENSEMBLES regional models (right)

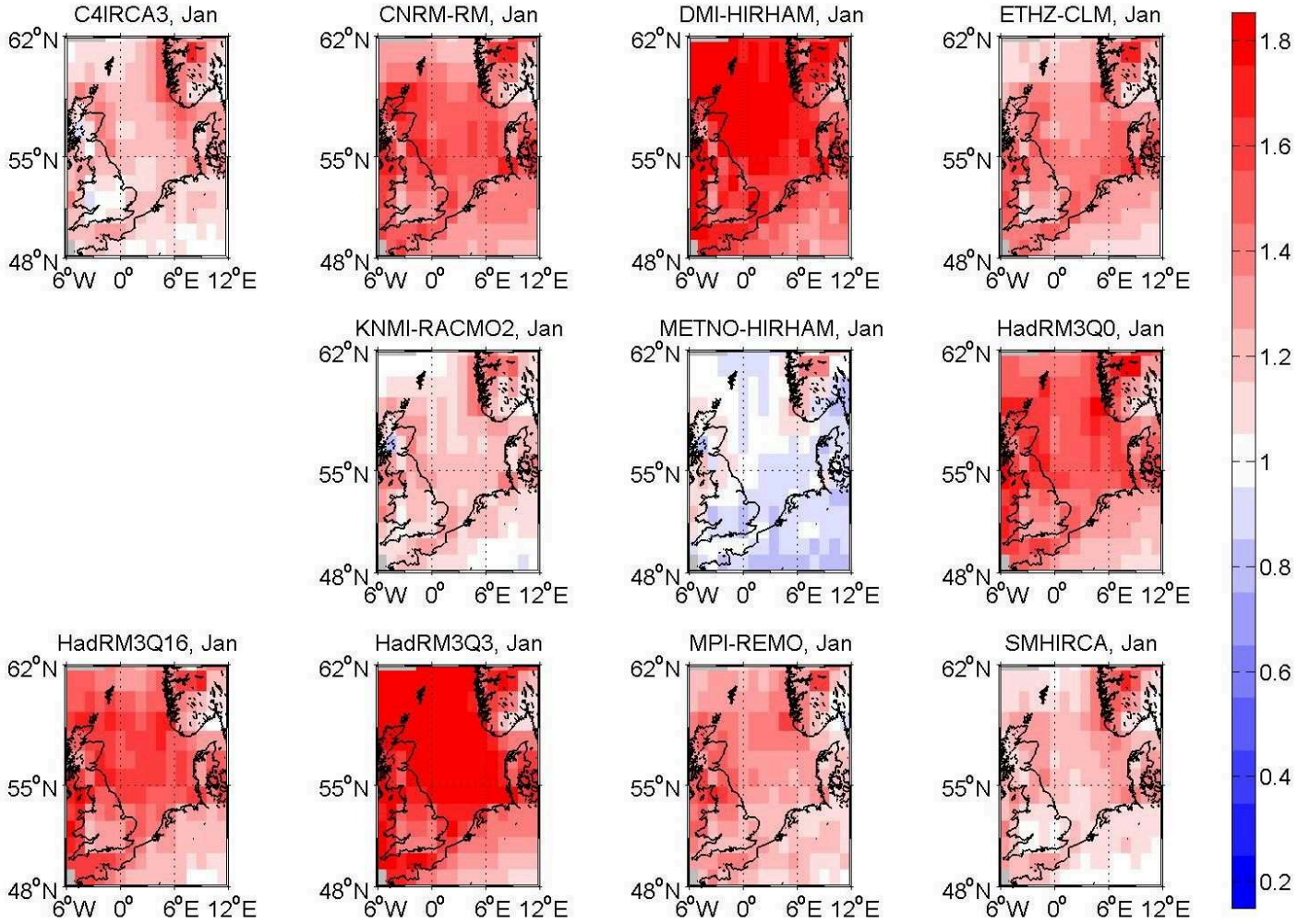

Figure 3.7.10: January ratio of standard deviations of cloud cover: RCMs / ERA-40 from Fig. 3.7.9

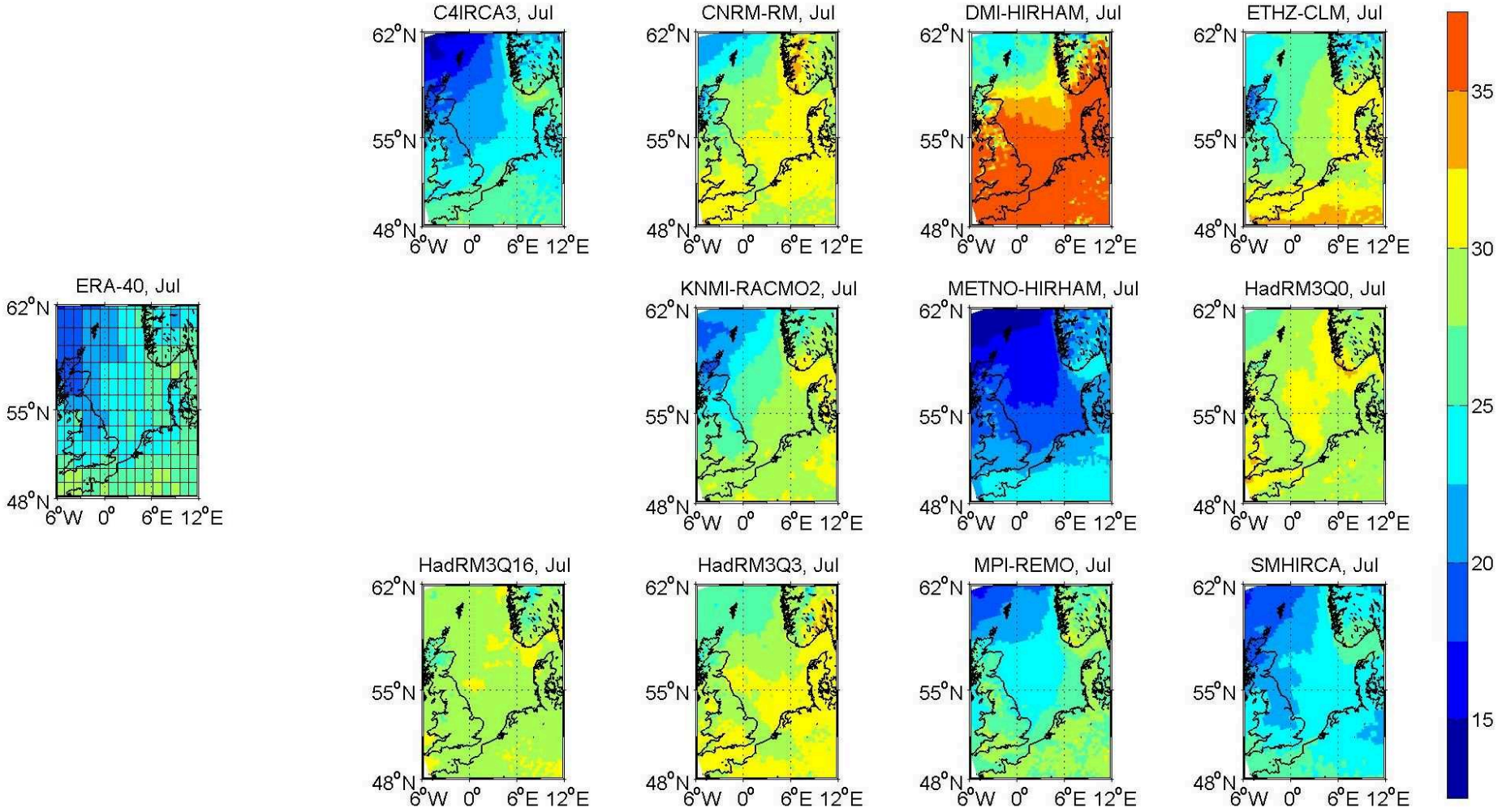

Figure 3.7.11: July standard deviation of cloud cover [%] in the North Sea area for the period 1971-2000: ERA-40 (left) and the ENSEMBLES regional models (right)

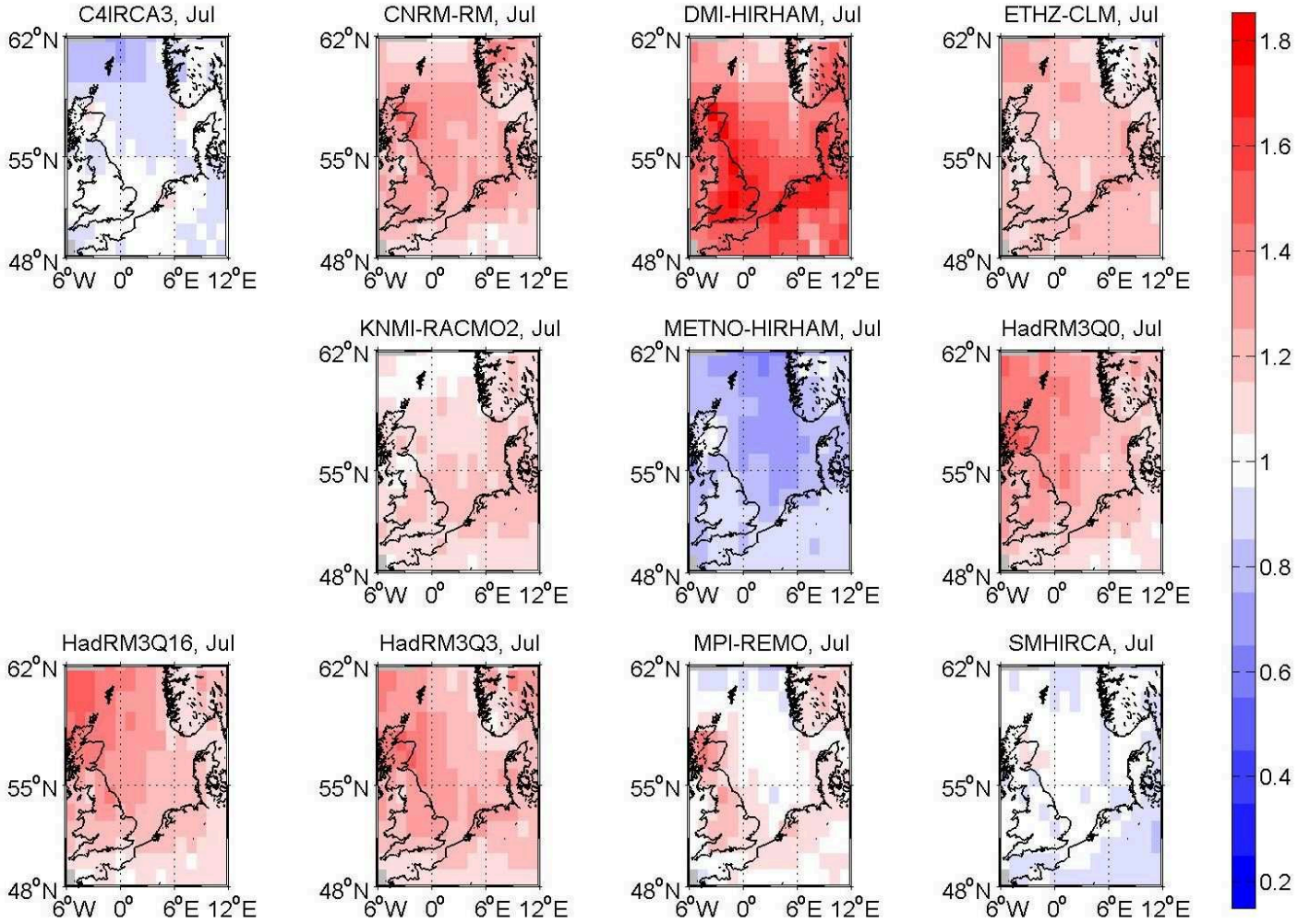

Figure 3.7.12: July ratio of standard deviations of cloud cover: RCMs / ERA-40 from Fig. 3.7.11

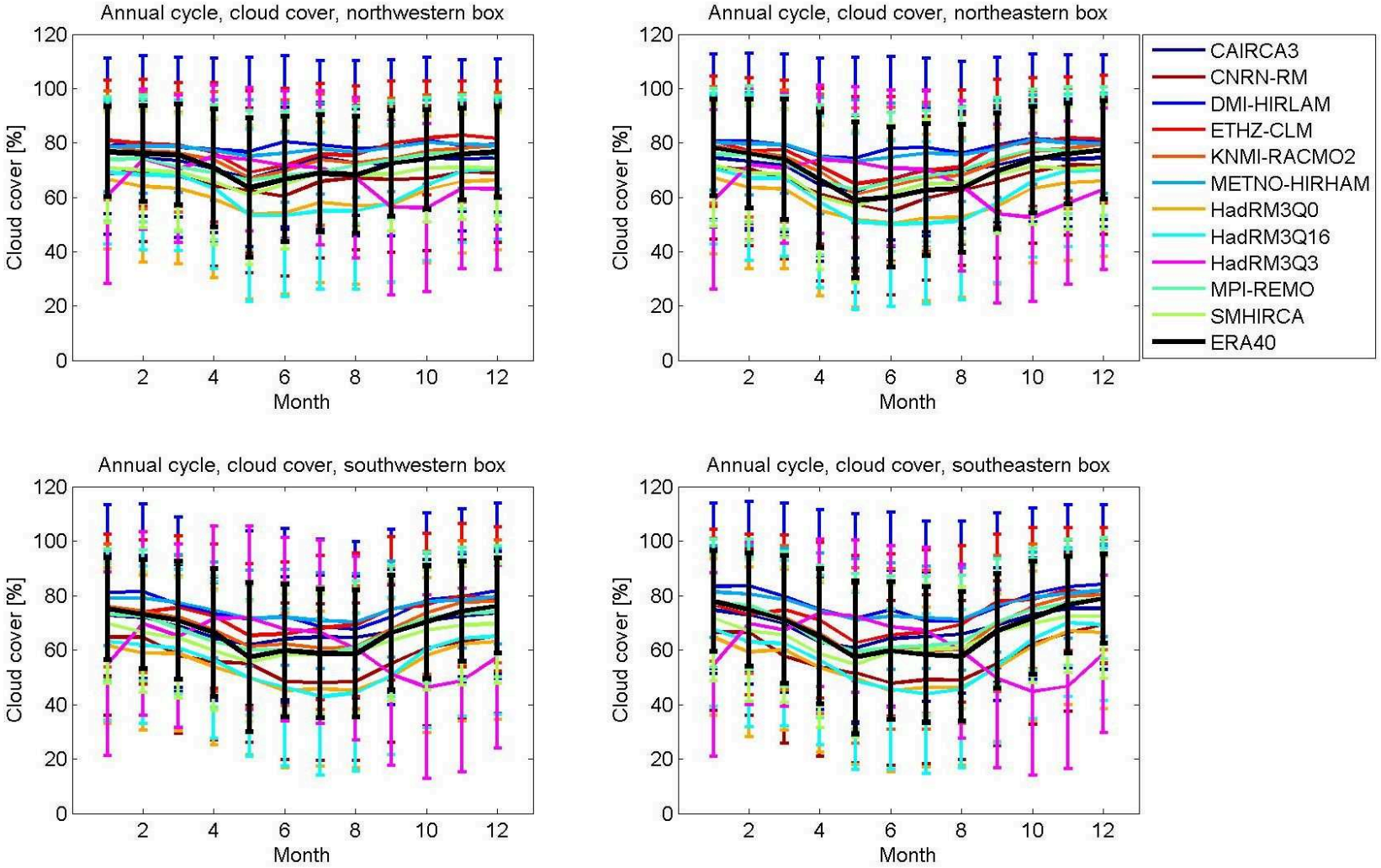

Figure 3.7.13: Annual cycles of cloud cover [%] of the ENSEMBLES RCMs and ERA-40 in the four North Sea boxes for the period of 1971-2000

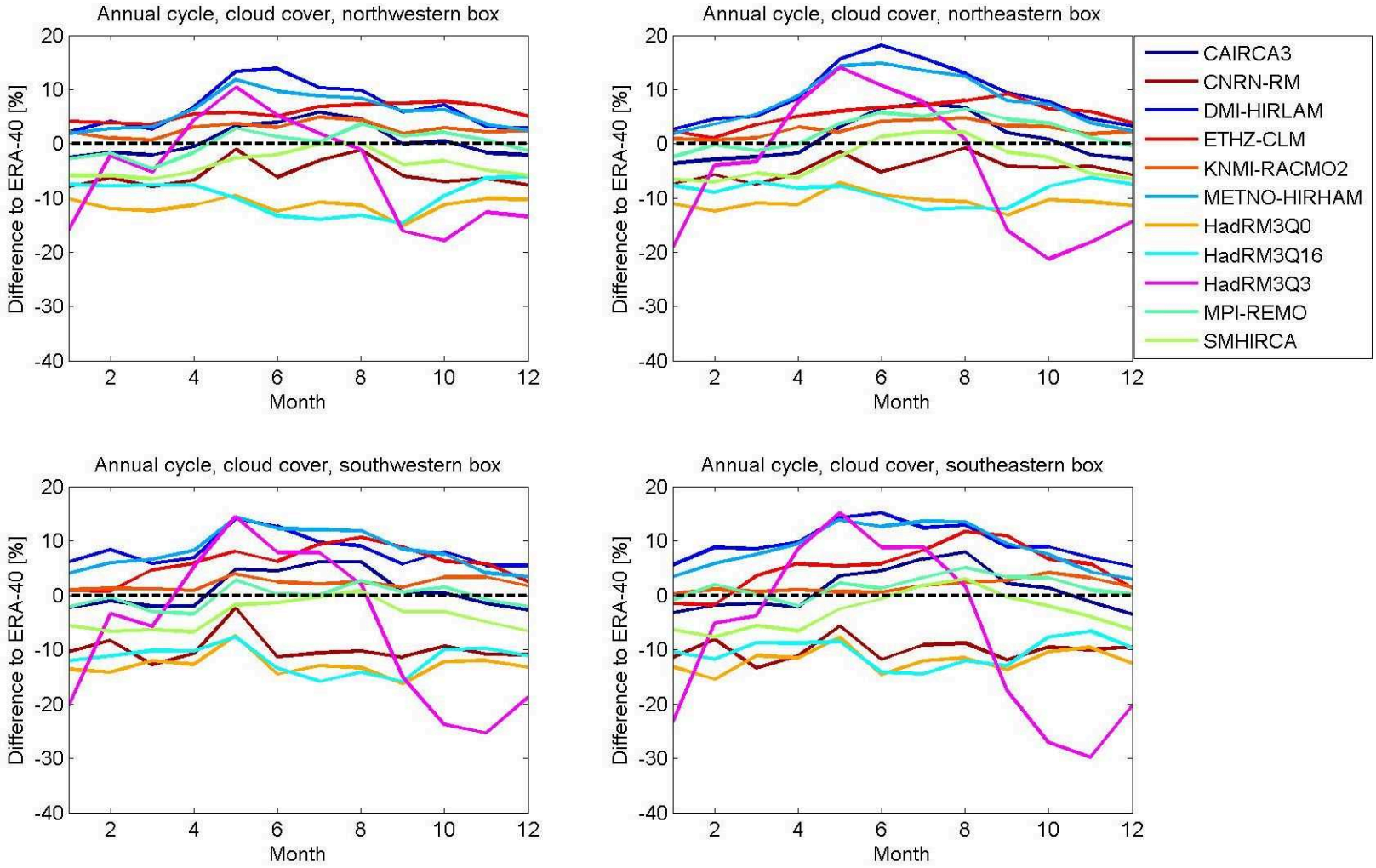

Figure 3.7.14: Difference of annual cycles of cloud cover [%] of the ENSEMBLES RCMs minus ERA-40 in the four North Sea boxes for the period of 1971-2000

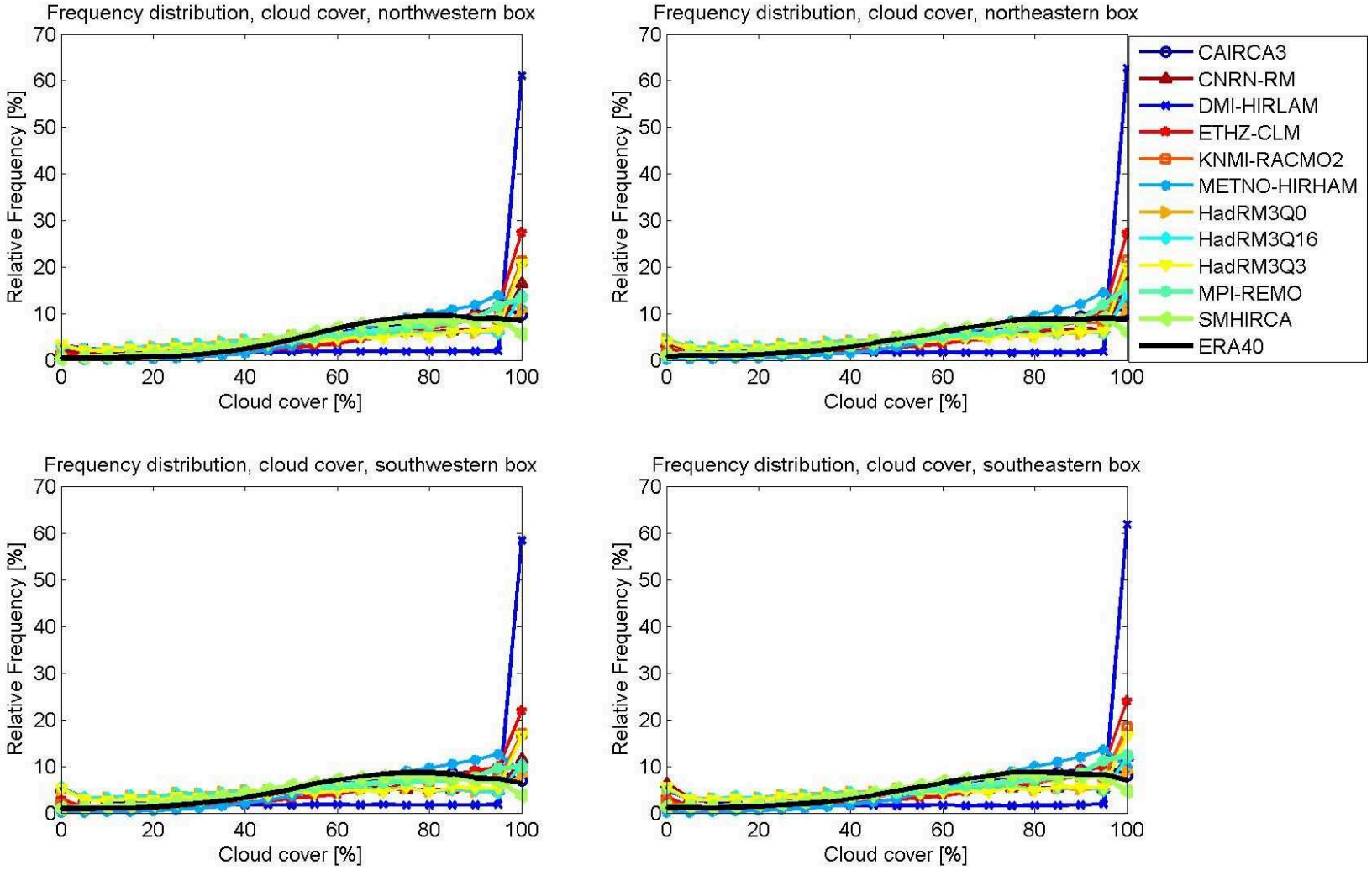

Figure 3.7.15: Frequency distribution of cloud cover [%] of the ENSEMBLES RCMs and ERA-40 in the four North Sea boxes for the period of 1971-2000

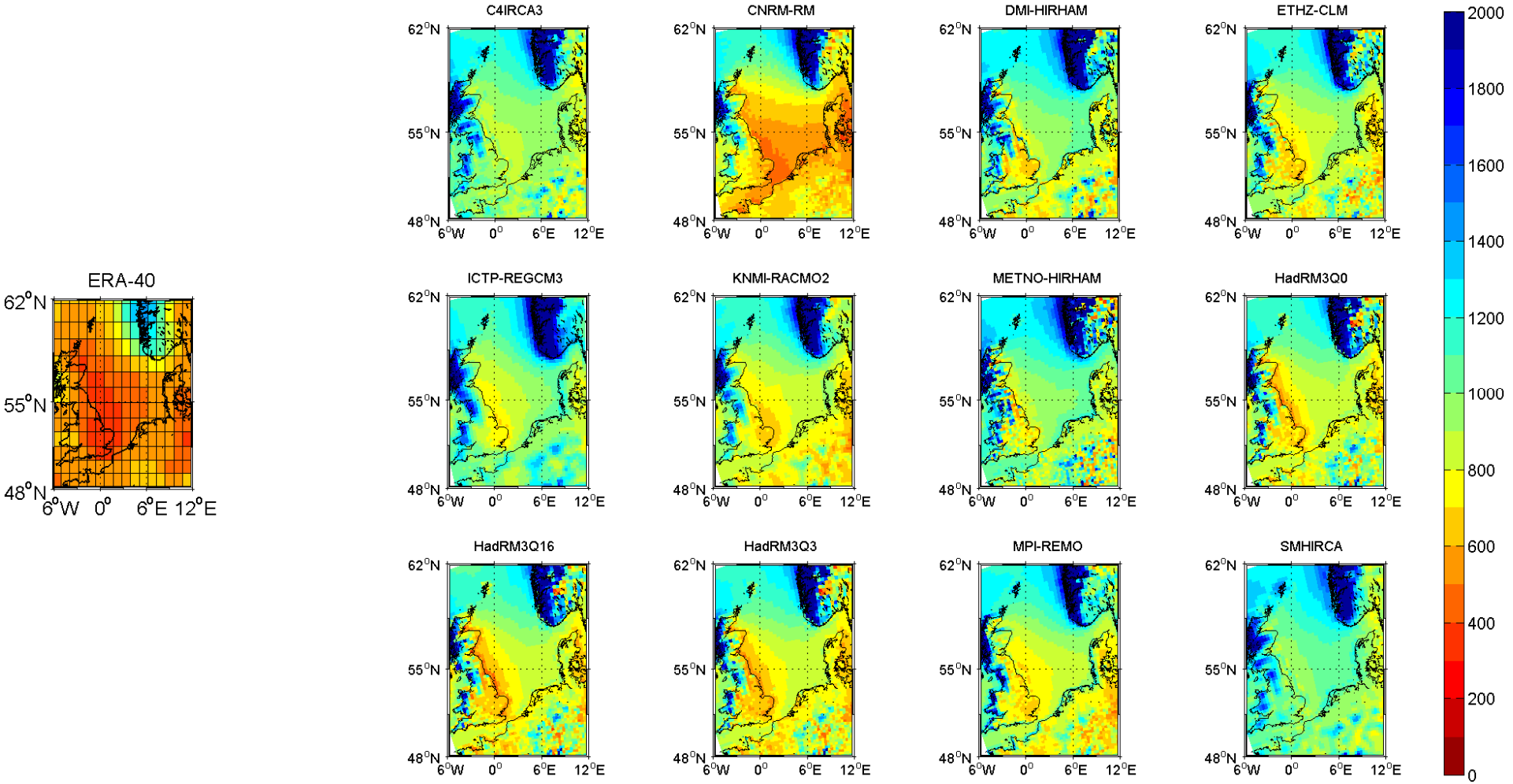

Figure 3.8.1: Mean precipitation [mm] in the North Sea area for the period 1971-2000: ERA-40 (left) and the ENSEMBLES regional models (right)

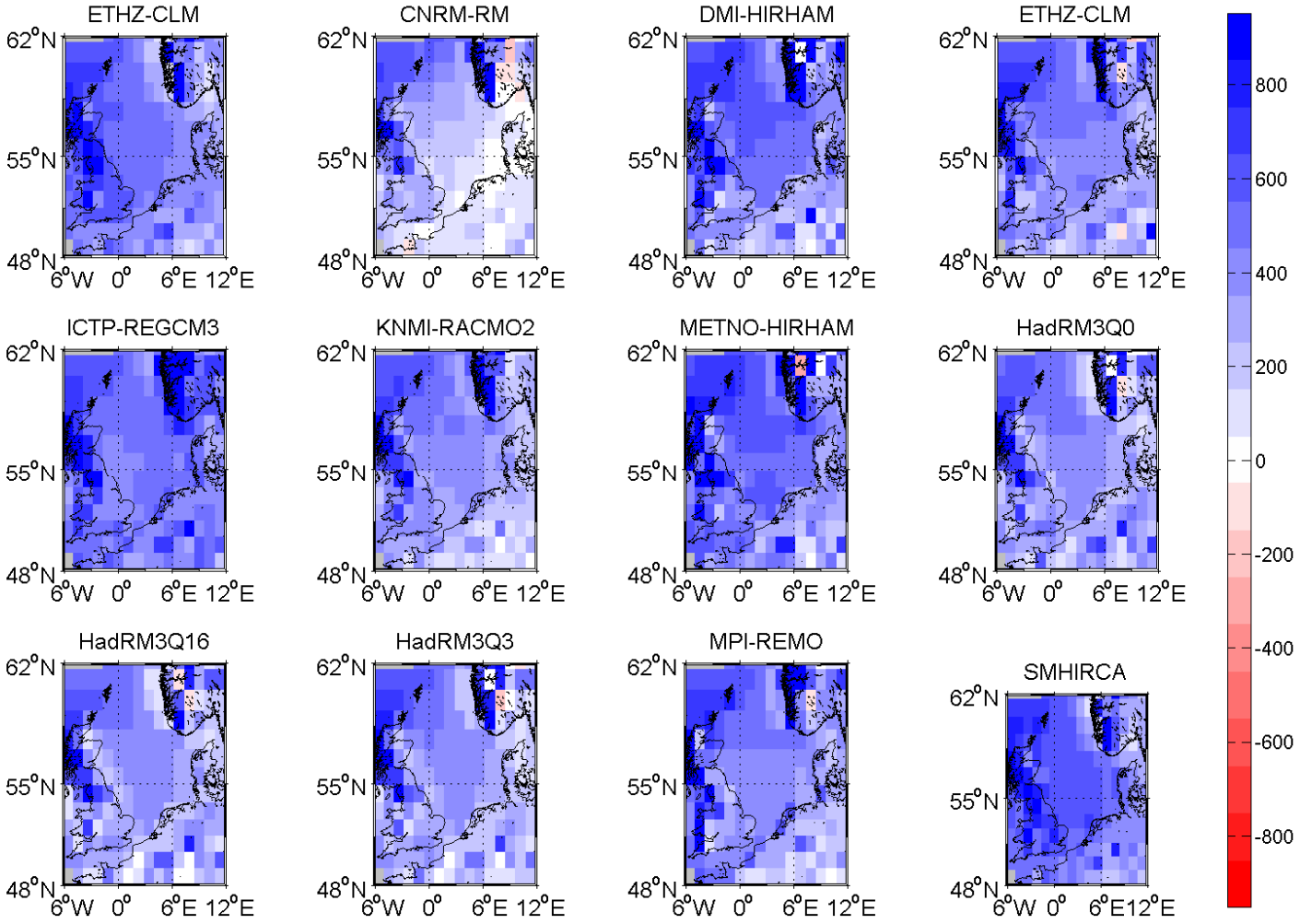

Figure 3.8.2: Differences of precipitation [mm]: RCMs minus ERA-40 from Fig. 3.8.1

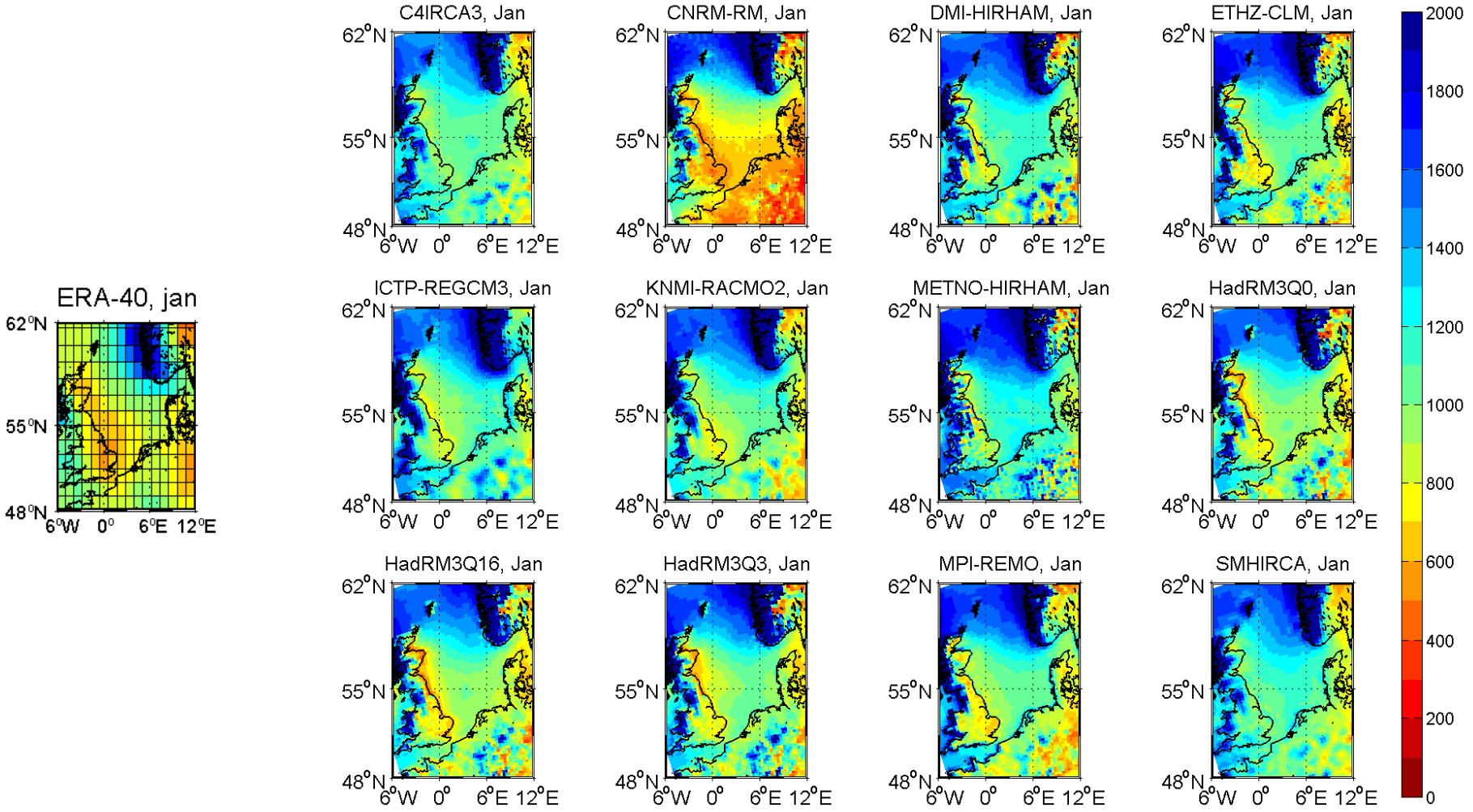

Figure 3.8.3: January mean precipitation [mm] in the North Sea area for the period 1971-2000: ERA-40 (left) and the ENSEMBLES regional models (right)

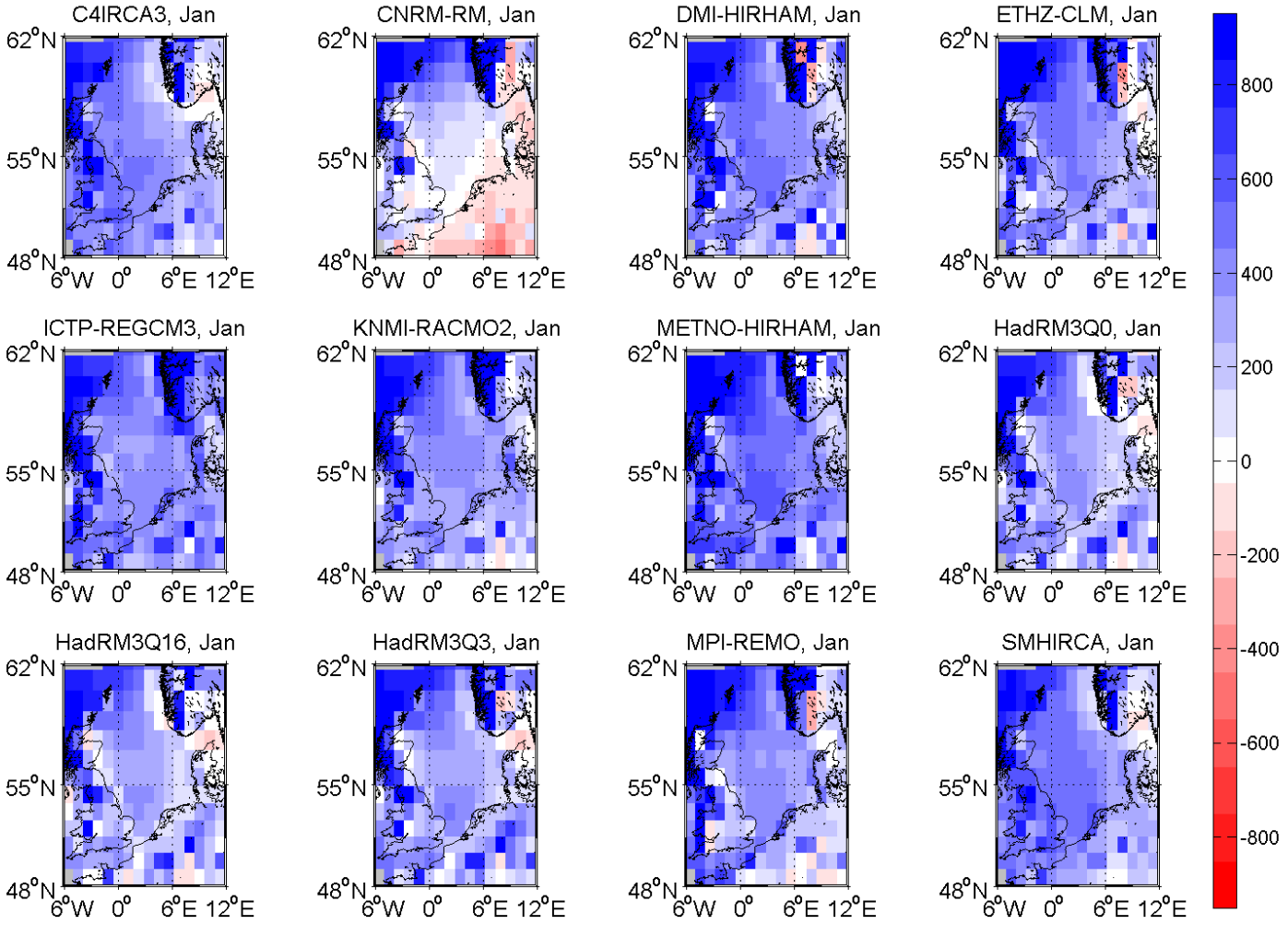

Figure 3.8.4: January differences of precipitation [mm]: RCMs minus ERA-40 from Fig. 3.8.3

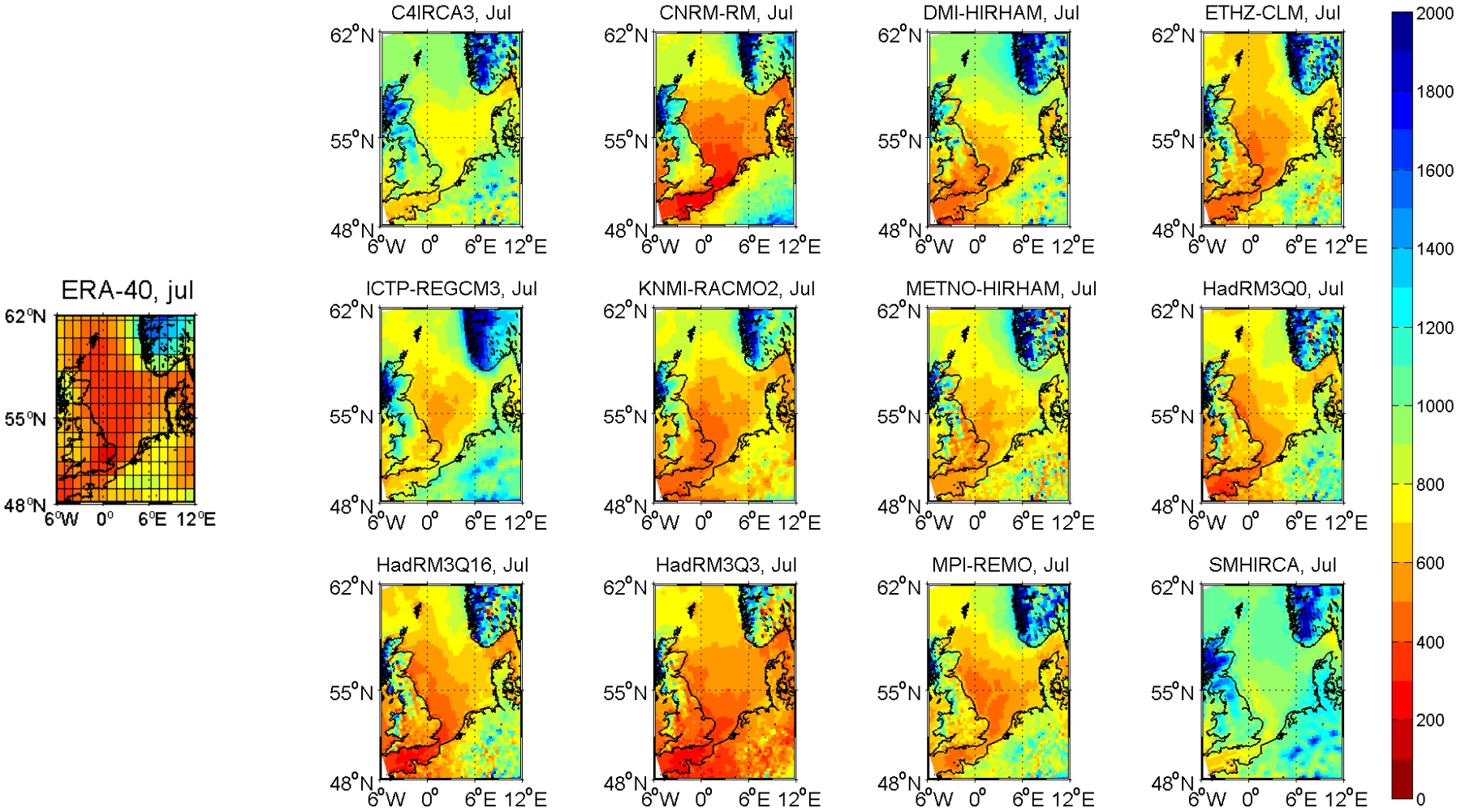

Figure 3.8.5: July mean precipitation [mm] in the North Sea area for the period 1971-2000: ERA-40 (left) and the ENSEMBLES regional models (right)

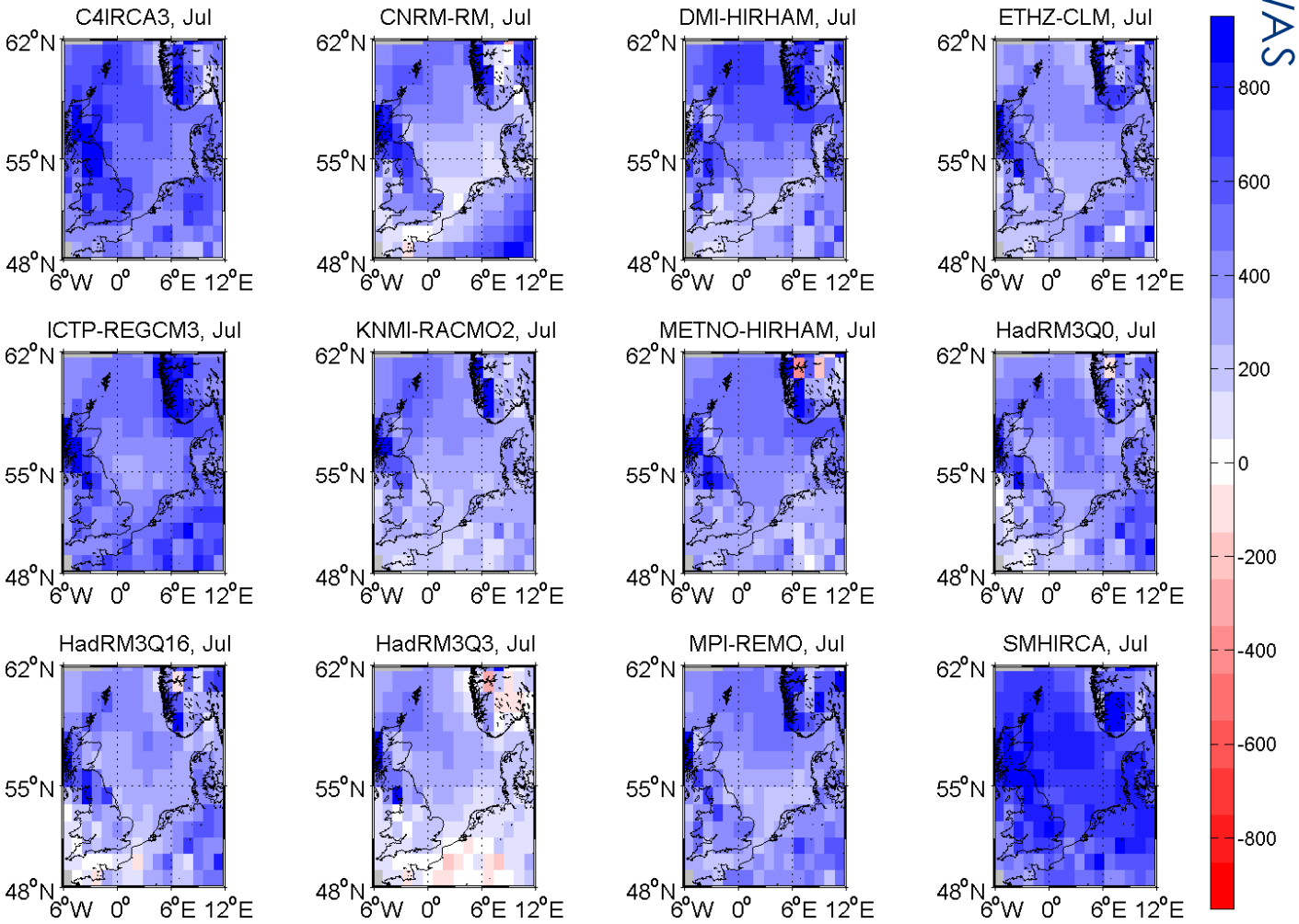

Figure 3.8.6: July differences of precipitation [mm]: RCMs minus ERA-40 from Fig. 3.8.5

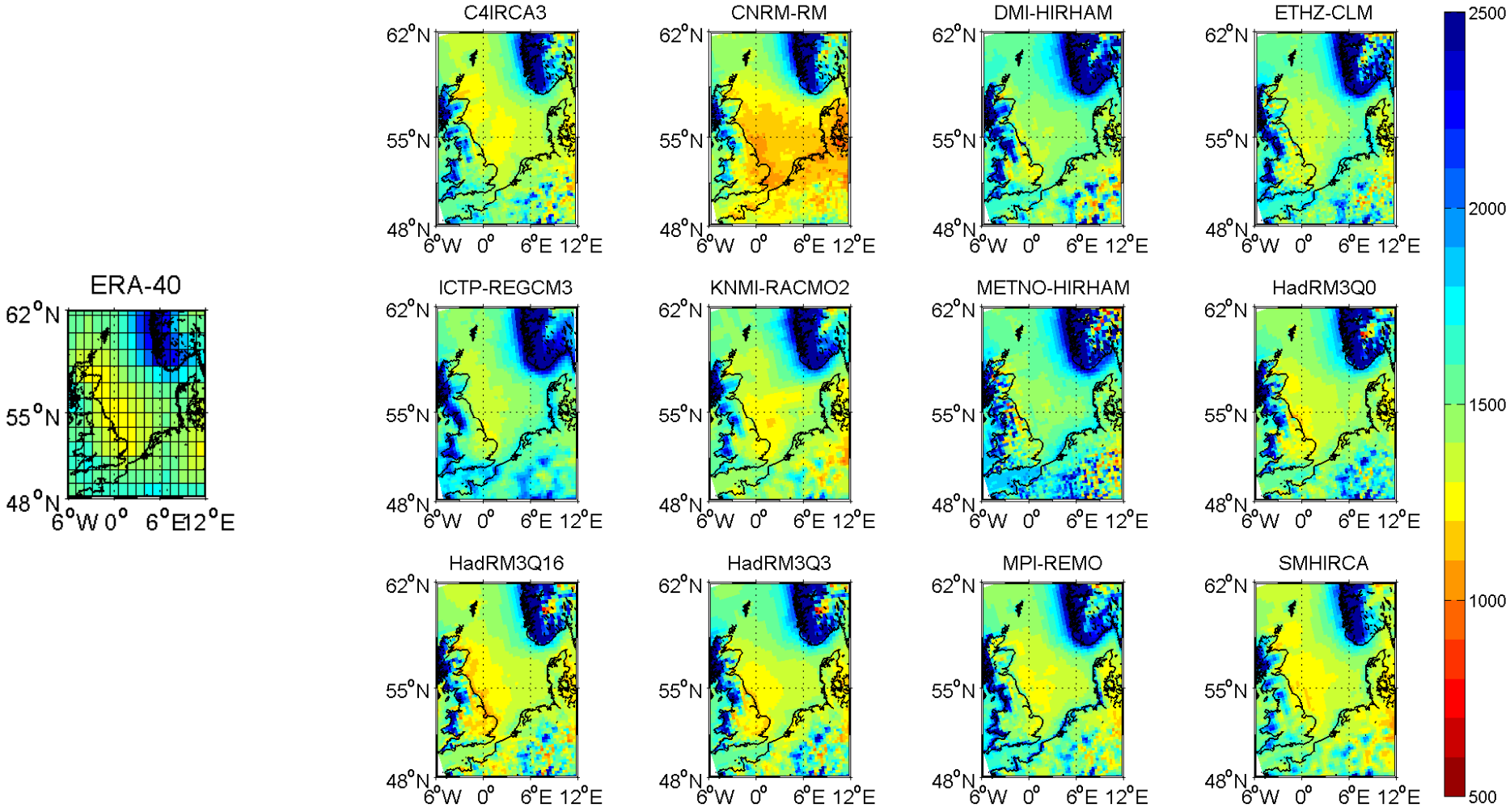

Figure 3.8.7: Standard deviation of precipitation [mm] in the North Sea area for the period 1971-2000: ERA-40 (left) and the ENSEMBLES regional models (right)

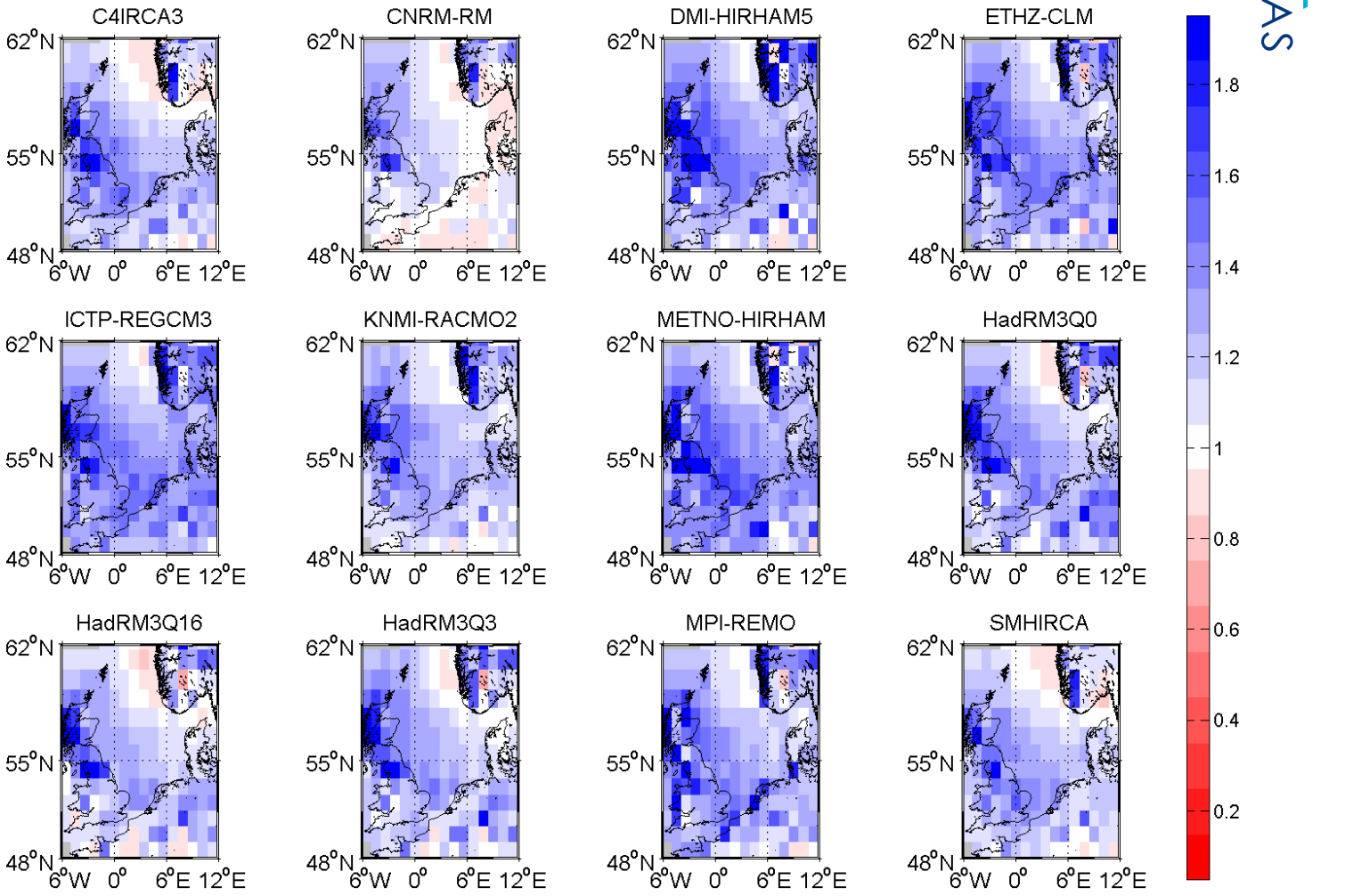

Figure 3.8.8: Ratio of standard deviations of precipitation: RCMs / ERA-40 from Fig. 3.8.7

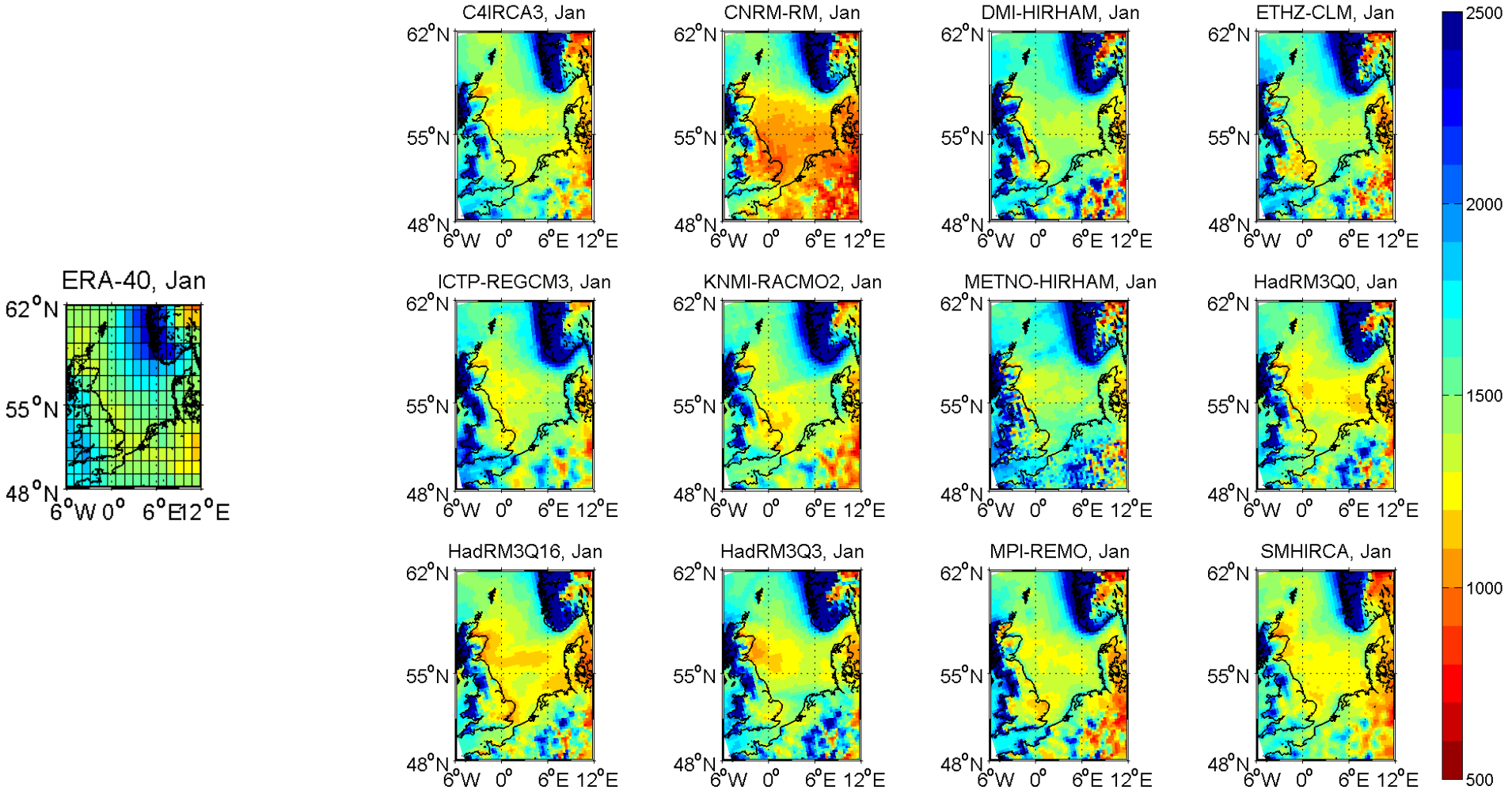

Figure 3.8.9: January standard deviation of precipitation [mm] in the North Sea area for the period 1971-2000: ERA-40 (left) and the ENSEMBLES regional models (right)

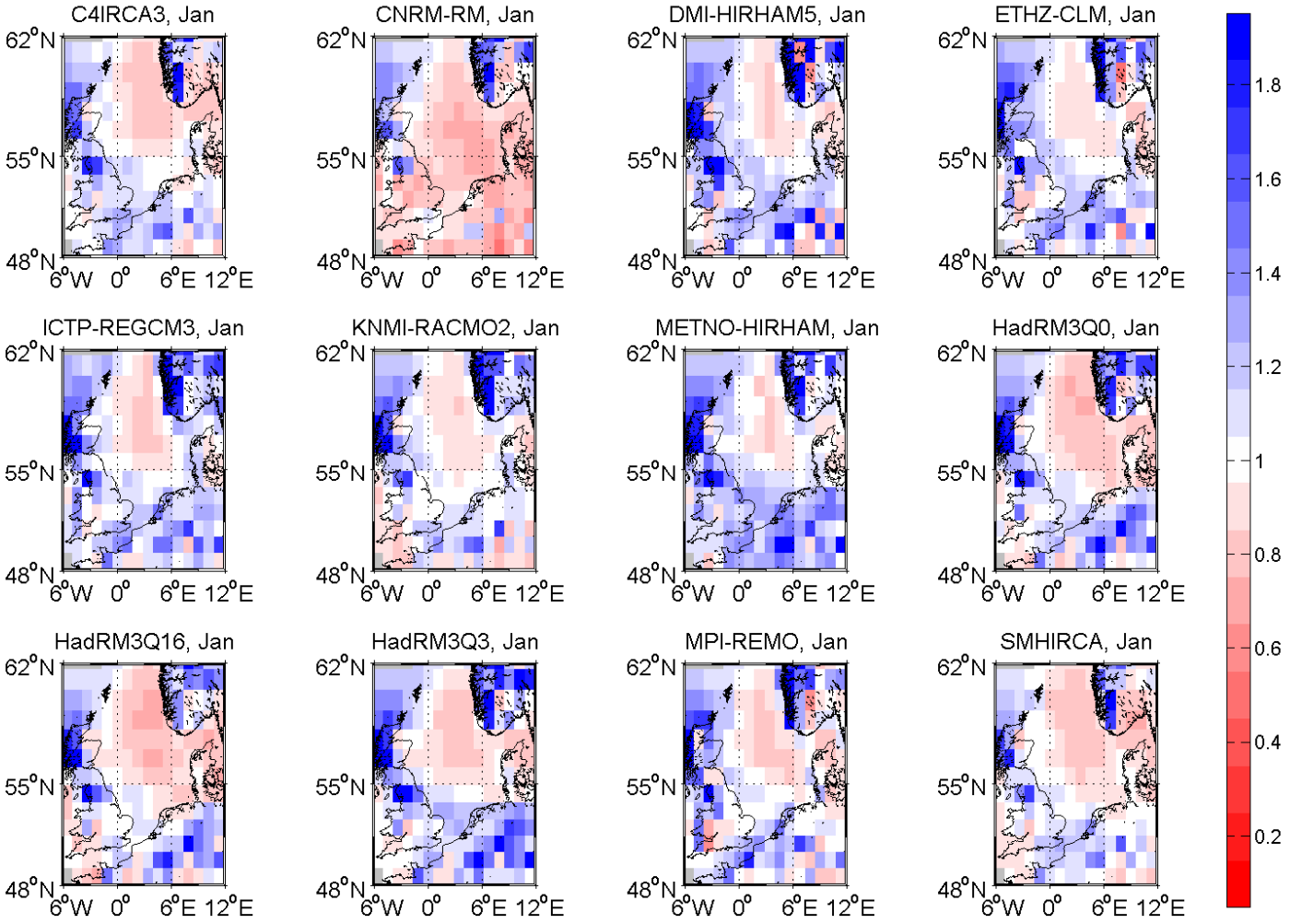

Figure 3.8.10: January ratio of standard deviations of precipitation: RCMs / ERA-40 from Fig. 3.8.9

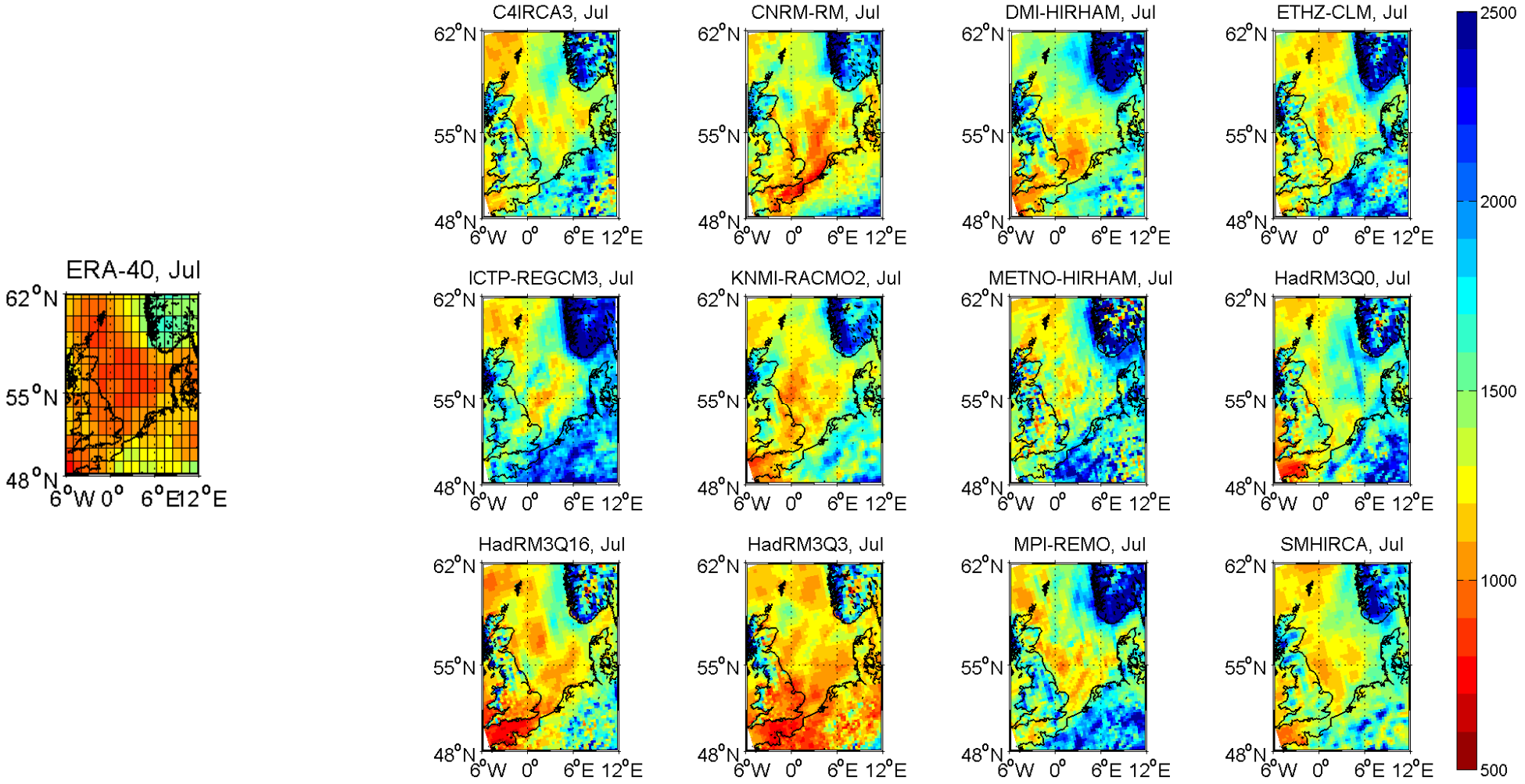

Figure 3.8.11: July standard deviation precipitation [mm] in the North Sea area for the period 1971-2000: ERA-40 (left) and the ENSEMBLES regional models (right)

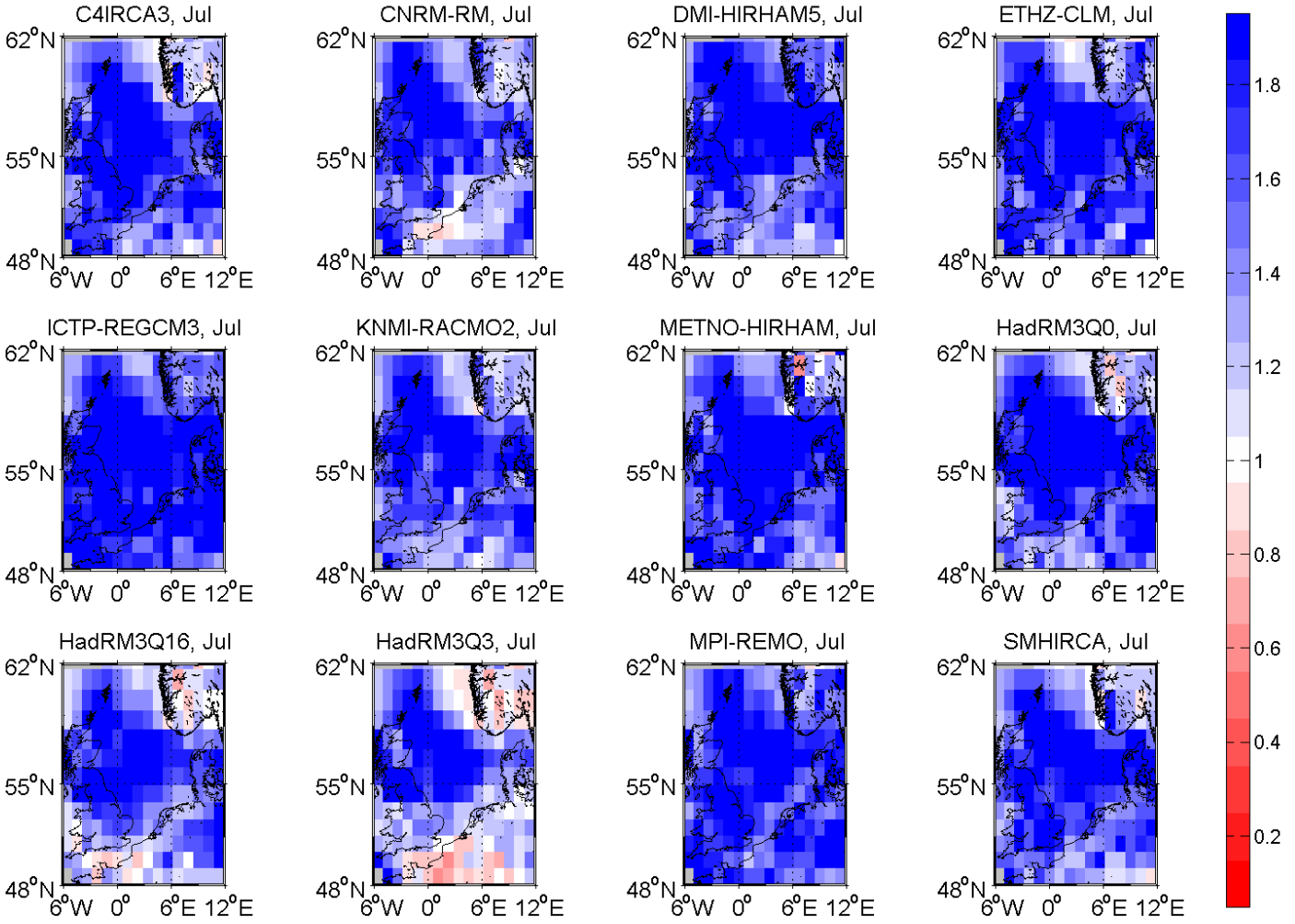

Figure 3.8.12: July ratio of standard deviations of precipitation: RCMs / ERA-40 from Fig. 3.8.11

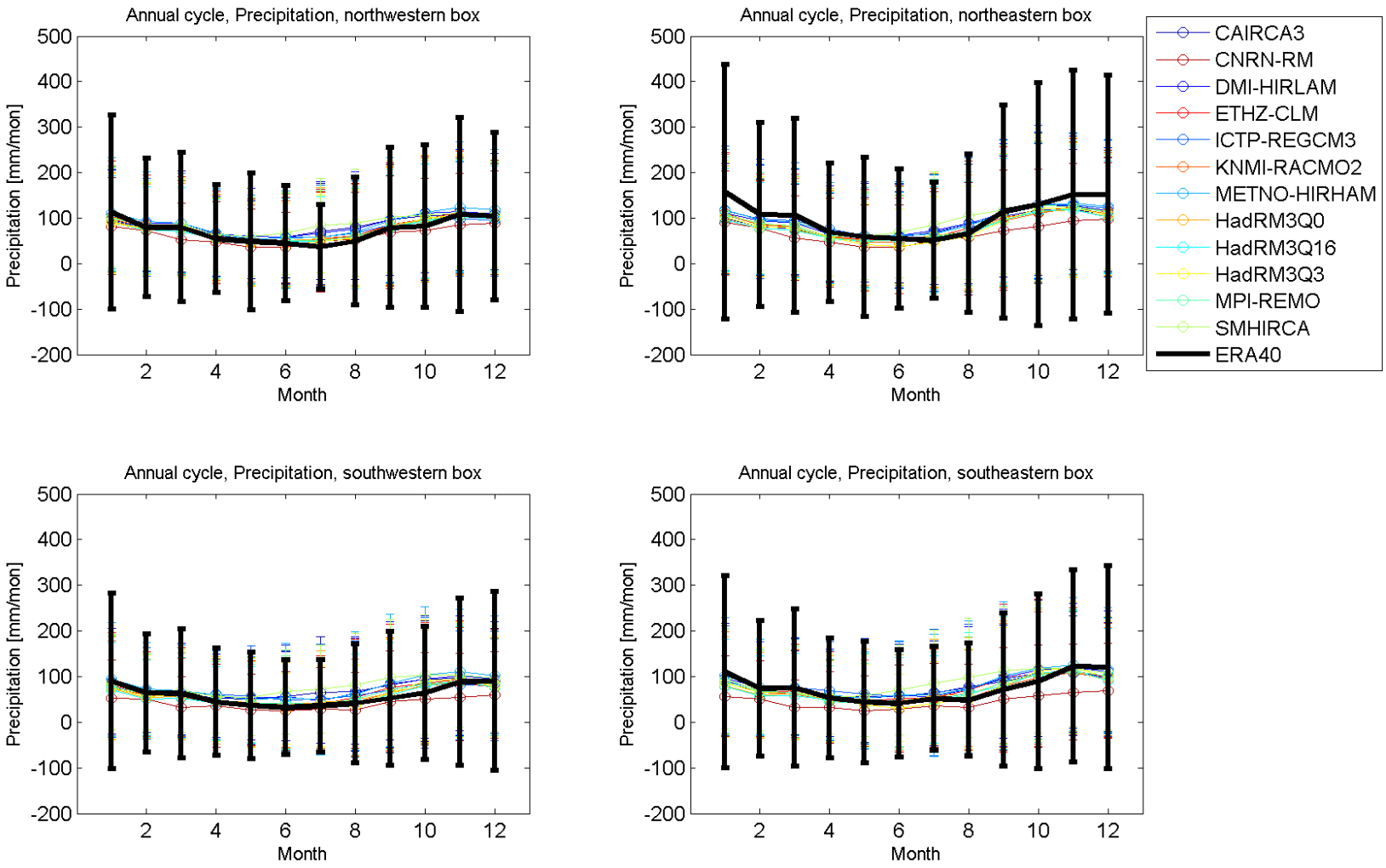

Figure 3.8.13: Annual cycles of precipitation [mm] of the ENSEMBLES RCMs and ERA-40 in the four North Sea boxes for the period of 1971-2000

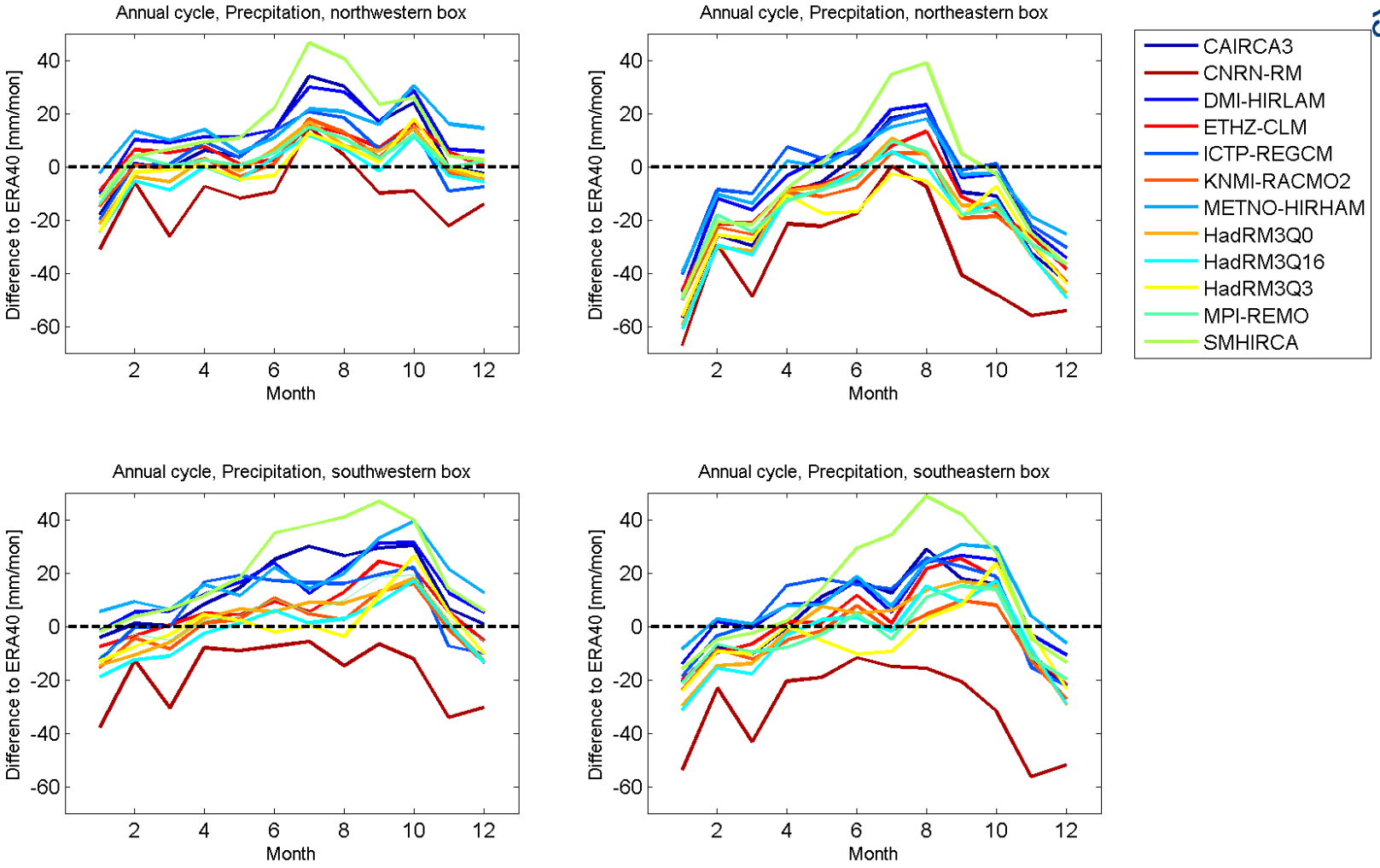

Figure 3.8.14: Difference of annual cycles of precipitation [mm] of the ENSEMBLES RCMs minus ERA-40 in the four North Sea boxes for the period of 1971-2000

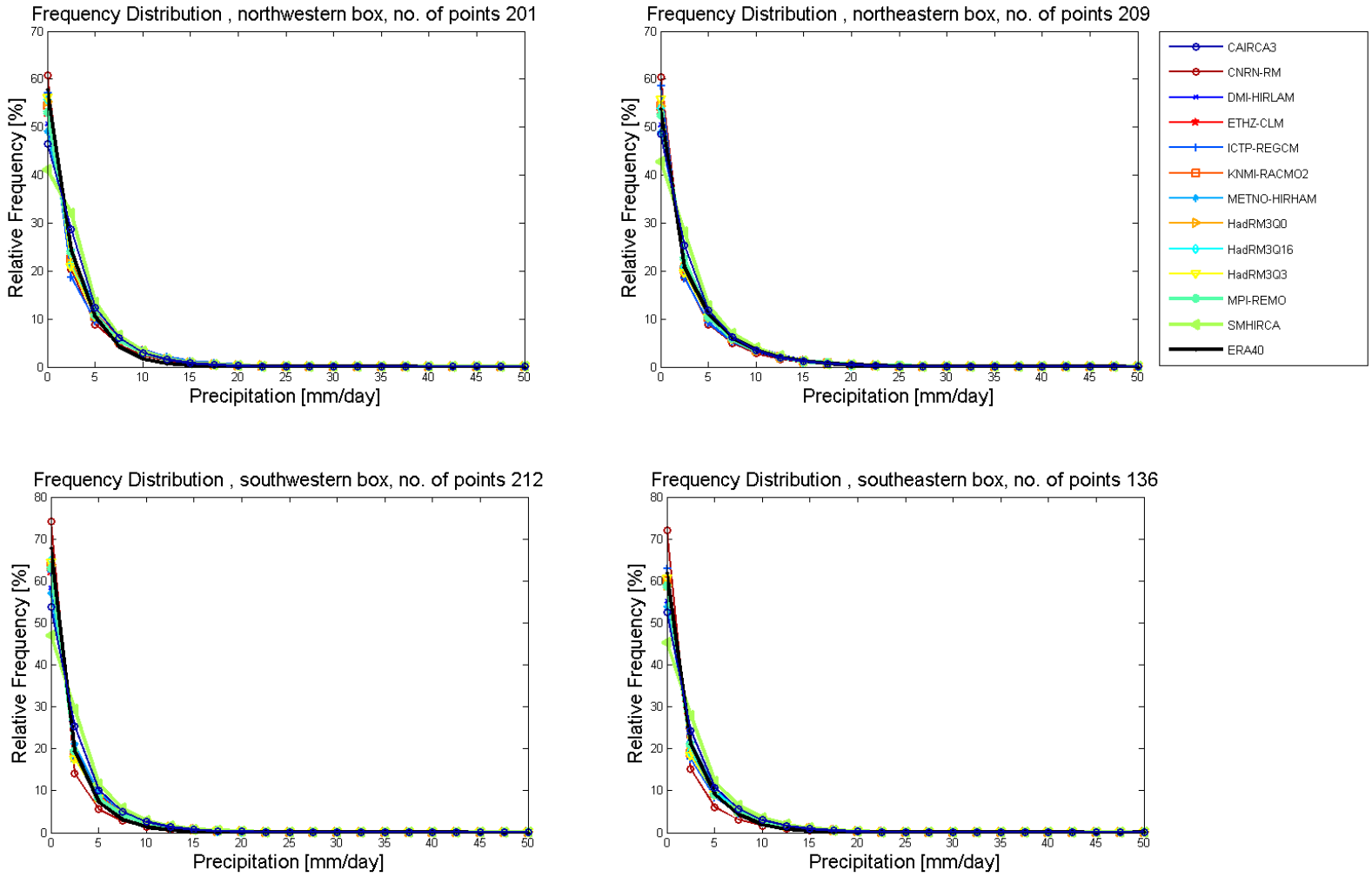

Figure 3.8.15: Frequency distribution of precipitation [mm] of the ENSEMBLES RCMs and ERA-40 in the four North Sea boxes for the period of 1971-2000

Bundesanstalt für Wasserbau
Kompetenz für die Wasserstraßen

Bundesanstalt für Wasserbau (BAW)

Kußmaulstraße 17
76187 Karlsruhe

www.baw.de
info@baw.de

Bundesamt für Seeschifffahrt und Hydrographie (BSH)

Bernhard-Nocht-Straße 78
20359 Hamburg

www.bsh.de
posteingang@bsh.de

BUNDESAMT FÜR SEESCHIFFFAHRT UND HYDROGRAPHIE

Deutscher Wetterdienst (DWD)

Frankfurter Straße 135
63067 Offenbach/Main

www.dwd.de
info@dwd.de

Bundesanstalt für Gewässerkunde (BfG)

Am Mainzer Tor 1
56068 Koblenz

www.bafg.de
posteingang@bafg.de

bfg Bundesanstalt für Gewässerkunde

IMPRESSUM

Herausgeber:
Bundesanstalt für Gewässerkunde
KLIWAS Koordination
Am Mainzer Tor 1
Postfach 20 02 53
56002 Koblenz
Tel.: 0261 / 1306-0
Fax: 0261 / 1306-5302
E-Mail: kliwas@bafg.de
Internet: http://www.kliwas.de

Redaktion: Andrea Mehling
Bundesanstalt für Gewässerkunde

Autoren: Katharina Bülow, Anette Ganske, Hartmut Heinrich, Sabine Hüttl-Kabus, Birgit Klein, Holger Klein, Jens Möller, Nils Schade (BSH), Gudrun Rosenhagen, Birger Tinz (DWD)

Layout: Christin Hantsche und Tobias Knapp, Bundesamt für Seeschifffahrt und Hydrographie - Rostock

Druck: Bundesanstalt für Gewässerkunde

DOI: 10.5675/Kliwas_21.2013_ERA40data